SBIR- 08.13-9191
release date 5/18/91 ✓

SBIR-08.13-9191
Release Date 5/18/91

NASA Contractor Report 181947

DEVELOPMENT OF MICROCHANNEL PLATES IN ADVANCED WIND-TUNNEL INSTRUMENTATION

W. Bruce Feller

GALILEO ELECTRO-OPTICS CORP.
Sturbridge, Massachusetts

Contract NAS1-18482
February 1990

(NASA-CR-181947) DEVELOPMENT OF
MICROCHANNEL PLATES IN ADVANCED
WIND-TUNNEL INSTRUMENTATION
(Galileo Electro-Optics Corp.)
151 p

N93-1571

Unclas

G3/35 0135965

National Aeronautics and
Space Administration

Langley Research Center
Hampton, Virginia 23665-5225

TABLE OF CONTENTS

LIST OF FIGURES

LIST OF TABLES

1. INTRODUCTION

1.1 MICROCHANNEL PLATES

A channel electron multiplier (CEM) is a type of radiation detector which detects and amplifies photons, electrons, ions, and neutral particles. It is essentially a hollow, nonmagnetic tube currently fabricated from a lead-doped glass, with an inner diameter of roughly 1 mm, and a length-to-diameter ratio (L/D) ranging from 40 to 100. It is similar to a discrete dynode photomultiplier tube (PMT), in that it is able to amplify extremely weak signals by 10^3 to as much as 10^8, yielding output signals which can be easily handled by auxiliary electronic equipment. Unlike a standard PMT, a channel multiplier, which is much more compact, utilizes a continuous resistive dynode along the inner channel surface rather than a series of discrete dynodes to obtain an accelerating electric field. This field acts on the secondary electrons created at the input by the incident radiation which strikes the channel wall. It then further accelerates the growing electron cascade as it moves down the channel. A high voltage is required to establish this field, and is applied through thin metallic electrodes which are deposited on opposite ends of the channel. Because the accelerating field acts throughout the channel, an amplification factor or gain of 10^8 (1 mm diameter channel) can be reached before the high space charge density near the end of the channel limits further amplification.

Parallel clusters of millions of microscopic channel multipliers can also be fused together to form a microchannel plate (MCP), a wafer-like electron multiplier able to amplify images or dispersed spectra composed of either electromagnetic radiation, charged particles, or neutrals. Upon inspection, an MCP appears as a very thin glass wafer perforated with microscopic holes, and is basically a parallel array of millions of close-packed hollow glass capillaries having internal diameters ranging from 4 to 40 microns, with each capillary being an independent, microscopic channel electron multiplier. The channel length to diameter ratios in both CEMs and MCPs range from 40 to around 120, with MCPs having thicknesses ranging from less than 0.5 mm to 5 mm, in round or rectangular formats with surface areas as high as 100 cm^2. Like CEMs, the inner channel surfaces of MCPs consist of a superficial secondary emitting layer, with an underlying semiconducting layer which replenishes the emitted electrons and which also establishes the accelerating electric field. As with the CEM, a thin metal electrode is vacuum deposited on the both sides of the MCP wafer.

MCPs are currently made using fiber optics technology. A soluble core glass rod is inserted into a glass cladding tube, and this assembly is drawn into a single glass fiber, which is cut and stacked together with other fibers into a parallel bundle. This bundle is then fused by the application of pressure and heat, and drawn down into a solid multifiber, which is once again cut and stacked into a bundle; the multifibers are then fused under vacuum. This fused boule is then sliced into thin wafers, which are ground and polished, and exposed to an acid solution which etches out the core material. A thin wafer is obtained having millions of parallel hollow microscopic channels. The channel surfaces are made semiconducting by exposure to hot hydrogen gas for several hours, which reduces the lead oxide in the glass to a form of metallic lead able to support electronic conduction. Thus, when a voltage is applied across the ends of the channels, an electric field is established, a small current flows in each channel, and the channel walls are able to support repeated electron multiplication cascades by replacing the wall charge lost in the process.

1.2 STATEMENT OF THE PROBLEM

The dynamic range of a radiation detector is one of its most important characteristics, and is the range of input flux over which the output count rate is linearly proportional to the input or signal count rate. The upper limit to dynamic range is the maximum input flux density which can be linearly amplified by the detector, and is constrained by the MCP gain falloff as well as the pulse pair resolution (PPR) and sensitivity of the pulse counting electronics. The lower limit is determined by the dark noise count rate, an irreducible background flux which occurs in the total absence of any input or signal flux.

Prior to this program, the dynamic range of MCPs was on the order of 10^8, with the lower limit being about 0.6 $cm^{-2}s^{-1}$ (counts/cm^2/sec), and the upper limit about 10^7-10^8 $cm^{-2}s^{-1}$ for single Galileo 12 micron pore MCPs, at temperatures below 70 °C.

1.2.1 HIGH INPUT FLUX LIMITATION

The inability of MCPs to linearly amplify input flux densities above this upper limit was seen as hindering the development of a new generation of scientific instruments, which would be used for high input flux applications. This concern was well illustrated in the abstract of a recent review article on detectors used for electron energy loss spectrometry (EELS): "...the possibility of eliminating the MCP and using an electron-bombarded silicon gain mechanism..." was seen as very important, due to "...the inability of present MCPs to maintain saturation gains at count rates above 1 MHz mm^{-2}" [1].

SATURATION

Figure 1 shows a typical set of curves which relate MCP input current to output current; these are called gain transfer curves. They show that linear amplification of input current occurs up to roughly 10% of the bias current which flows through the channel walls and which is determined by the bias voltage and MCP resistance [2]. Beyond this value, the MCP gain begins to drop due to saturation effects, so that the transfer curve starts to level out. Since the MCP resistance changes slightly in operation, due to the presence of a parallel resistive path (the electron cascade), and possibly due to a slight conductivity enhancement from electron bombardment, this curve never completely flattens out. This failure of linearity, or current saturation, as the output current approaches 10 to 20% of the bias current, can easily be explained by considering processes that occur on the level of an individual channel.

As a sizeable electron cascade develops towards the end of the channel, secondary electrons lost from the channel wall leave behind a positive wall charge, which must be neutralized before another electron cascade can be generated. This is accomplished by the bias current flowing down the channel from the bias voltage supply. This current also establishes the local axial electric field, which accelerates the secondary electrons released from the wall, and which is equal to the local wall current times the wall resistivity per unit length, in accordance with microscopic Ohm's law. Wall charge neutralization must occur at a rate faster than the input event rate into the channel. Otherwise, the channel will fail to recover its full gain capability between cascade pulses, and the overall detector gain will correspondingly diminish.

Positive wall charging effectively lowers the axial electric field, since the local wall current at the output end is now reduced due to the neutralization process [3]. This decreases the kinetic energy gained by secondary electrons after they are emitted, lowering their collision energies to a value equal to the first crossover potential, the energy at which the secondary yield equals unity. At output currents below roughly 10% of the standing wall current (bias current), there is a linear relationship between the output and input currents. As the output current increases, approaching this level, the local field near the input end begins to rise in order to maintain a constant applied potential, as the local field near the output end diminishes due to the diminished wall current. Once the output current reaches the 10-20% bias current level, the local field near the output is reduced to such an extent that the local gain falls below unity, and the field depletion region enlarges up the channel - effectively reducing the fraction of channel length participating in the gain process. However, as the overall gain begins to diminish, further growth of this depletion region halts, and it then begins to contract. At this point, a state of dynamic equilibrium is reached, where the charge pulse magnitude stabilizes. In practice, the upper limit of MCP dynamic range is indicated by a shift in the pulse height distribution (PHD) to lower amplitudes, indicating a falloff in gain.

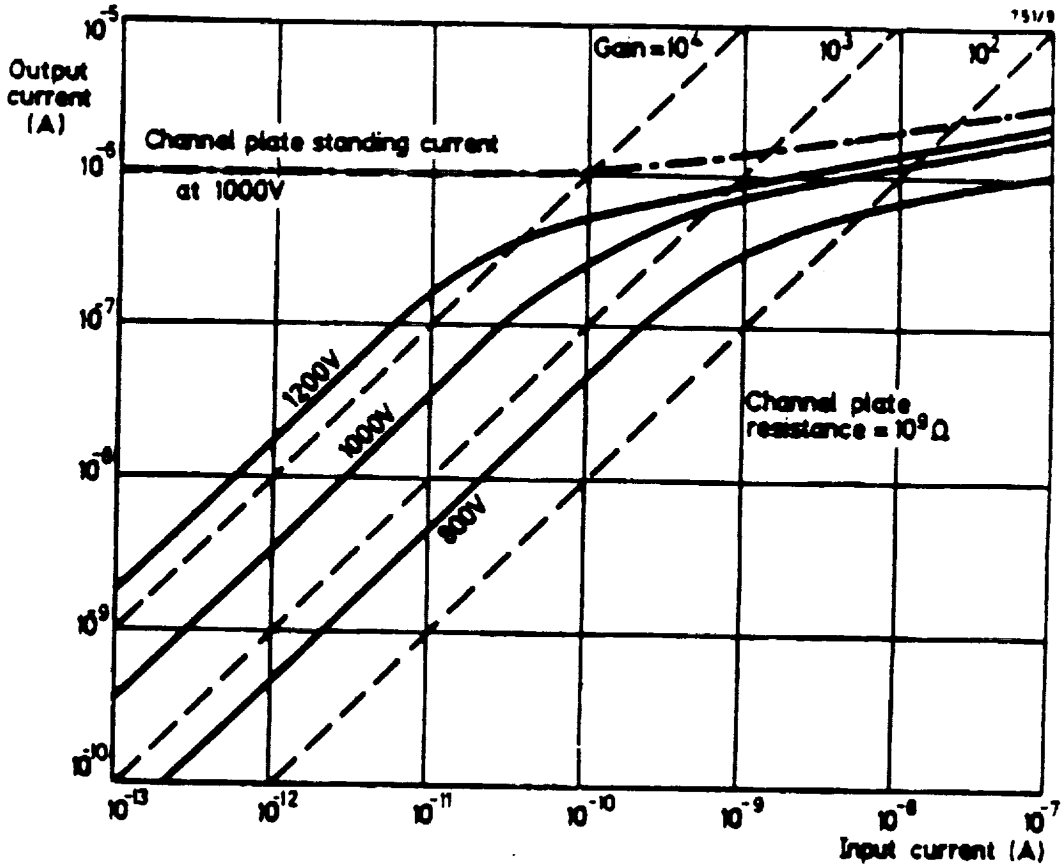

Figure 1. MCP current transfer characteristics. [from Ref. 61]

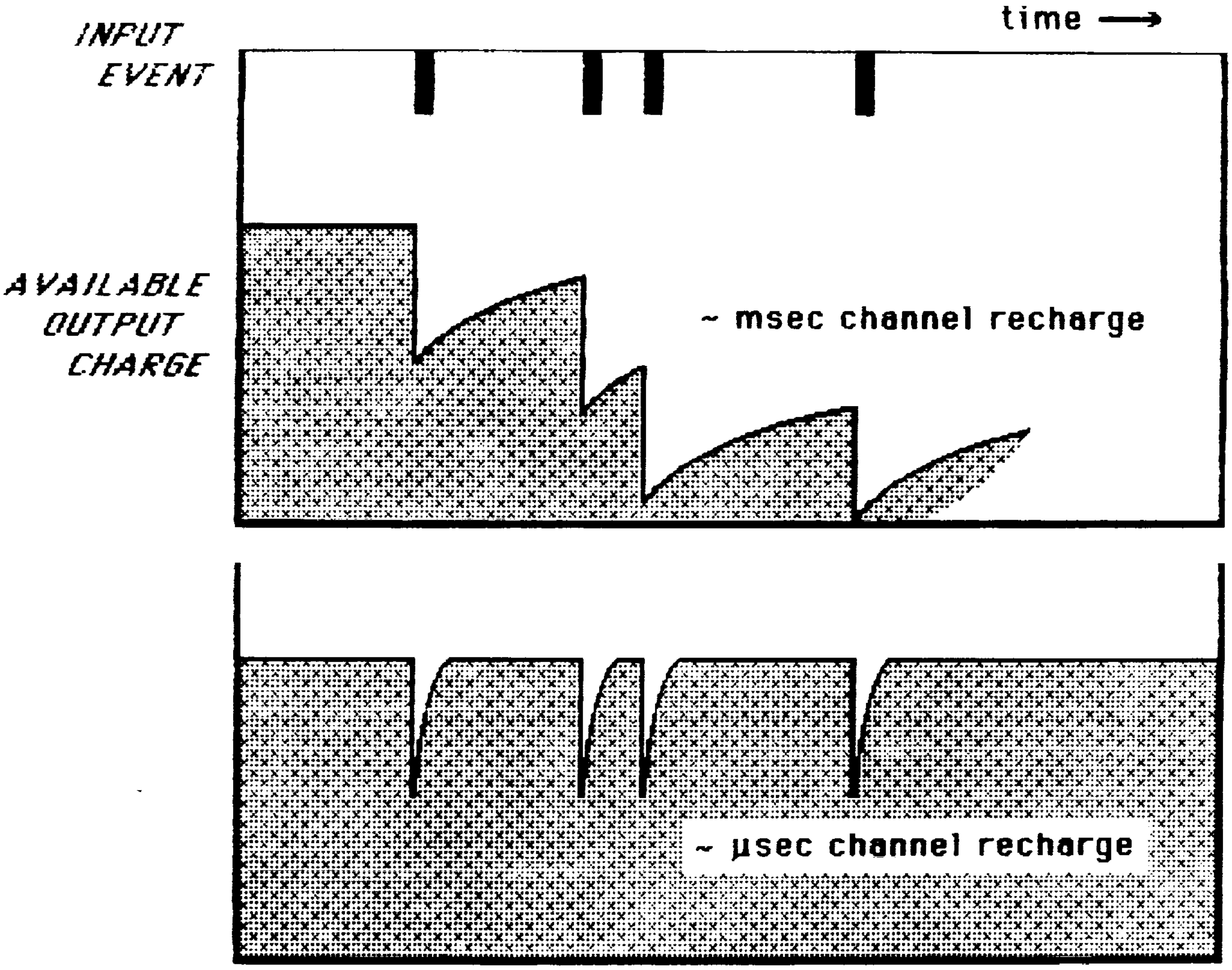

Figure 1a. MCP current saturation, as input event rate exceeds channel recharge time. [adapted from Ref. 35]

DEAD TIME

Nearly all radiation detectors require a minimum time period which must separate two input events, if they are to be recorded as separate events. In MCPs, each channel has an associated dead time due to the finite recharge time of the channel wall after an electron multiplication event occurs (with the cascade developing on a nanosecond time scale). This recharge time, typically milliseconds for standard MCP channel resistivities, can cause nonlinearities between the measured and actual count rate, resulting in loss of MCP gain and counting accuracy (i.e., as the input flux increases, an increasing percentage of input events are lost). Obviously, the input count rate statistical distribution can be severely distorted by the MCP dead time.

Another phenomenon involving MCP dead time which can distort the input signal is the variation of dead time with illumination area [4,5,6], presumably caused by interchannel capacitive coupling [7]. As the illumination spot size increases, the lateral capacitance scales with the spot circumference rather than with its area. Since the latter is proportional to the number of channels, the effective channel capacitance decreases, making less charge available per pulse. This variation in local dead time makes it difficult to accurately calibrate imaging spectrometers which operate at high count rates.

ALTERNATIVE APPROACHES

Fortunately, the maximum MCP count rate capability for linear operation can be extended in different ways.

Smaller channels

One way to increase MCP count rate capability is to fabricate MCPs using smaller diameter channels with higher packing densities. This should be viewed as a geometric effect, rather than as an effective decrease in MCP resistance (channel resistance increases directly with packing density, while the inverse holds for channel capacitance, so that RC remains constant for a fixed MCP resistance and capacitance). Since the channel recharge time remains the same as the number of channels per unit area increases, the probability is smaller that a given input event will enter a dead channel (recharging from a previous event). This will extend the maximum input flux before deterioration of detector efficiency sets in. Also, since it is less likely that neighboring channels are simultaneously activated, interchannel coupling (which increases dead time) is less likely to occur.

Achieving smaller channels is certainly useful in increasing MCP dynamic range, and Galileo has recently done significant work in this area, attaining MCP pore sizes as small as 4 microns. For example, assuming a fixed MCP resistance, the improvement using a 4 micron channel as opposed to a 12 micron channel is simply the square of the channel diameter ratio, roughly an order of magnitude. However, it is likely that the amount of possible improvement beyond this is limited. For pore sizes even smaller than 4 microns (already difficult to fabricate) the voltage levels needed to attain pulse-counting gain applied across increasingly thin and fragile wafers moves into the dielectric breakdown region. Moreover, since saturated gain scales with channel diameter [9], the noise requirements on pulse-counting electronics designed to register charge pulses of less than a hundred microvolts would be unusually stringent.

Pulsed operation

Another method used to extend the MCP linear output range is used in very high speed photography (for example, X-ray imaging of laser-produced plasmas), where shutter times of roughly a nanosecond have been achieved. Here, the MCP bias voltage is pulsed, as opposed to the photocathode-MCP bias, i.e., gating the extraction field. However, gating the cathode will not work with UV or X-ray radiation, which can pass through the cathode into the MCP and which is continuously in operation.

Rapidly pulsing the MCP bias voltage at very low duty cycles of less than 0.1% allows a very low resistance MCP to function without the danger of thermal runaway. For example, a 200 kilohm MCP dissipating 10 watts at 1000 V will rise in temperature at the rate of roughly 30-40 °C/second, so that applying an MCP bias voltage for a period of a few nanoseconds will cause virtually no Joule heating. If the tiny but finite temperature rise due to this pulse has sufficient time to return to equilibrium, subsequent pulses can follow indefinitely.

Recently, for example, a saturated Z-stack MCP composed of low resistance MCPs, which would normally have a channel recharge time approaching a few tenths of a second, has been shown to recover as quickly as 150 microseconds when gated by high voltage square pulses, with pulse widths of several nanoseconds (L. Giudicotti, Univ. Padua, private communication, 1989). Although interesting and quite useful for certain applications, this method of dynamic range extension will obviously not work for high flux applications requiring continuous, unsynchronized MCP operation.

Higher bias current

A more promising way to extend MCP dynamic range would be to find some way to dramatically increase the MCP bias current, thus dramatically increasing the 10-20% bias current value at the onset of output current saturation. This would have the attractive feature of allowing continuous d.c. operation at very high input count rates. However, increasing MCP bias current by lowering MCP runaway.

Thermal runaway

As MCP resistance diminishes (controllable through processing schedules), the bias current under high applied voltages increases. This increased current is carried by a thin (~2000 Å) semiconducting layer lining the inner channel wall. Like most semiconductors, this has a negative temperature coefficient of resistance (i.e., as temperature increases, resistance decreases). When high voltage is applied, the bias current results in Joule heating ($P = IE = V^2/R$), which must be somehow removed from the MCP since thermal equilibrium can only be reached if the net MCP heat flow is zero. As the MCP temperature increases, the resistance decreases, resulting in additional Joule heating. (Use of voltage- or current-controlled power supplies cannot prevent this without changing the MCP applied voltage, and thus gain.) If the heat is not removed quickly enough, thermal equilibrium may never be reached, and a thermal runaway condition sets in where the MCP is destroyed.

MCP heat is dissipated predominantly through radiative transfer from both MCP faces. Since the MCP is very thin, and because of the low thermal conductivity of the glass, heat conduction through the electrode connections at the rim is negligible (Figure 2). The temperature increase resulting from Joule heating can be roughly calculated using the Stefan-Boltzmann law

$$\pi^2\sigma\epsilon(T_s^4-T_a^4)/2 = V^2/R$$

where d is the MCP diameter, ϵ is the effective MCP thermal emissivity, T_s is the equilibrium MCP surface temperature (°K), T_a is the ambient temperature, and σ is Stefan's constant [10]. The right-hand expression is the Joule heat generated in the MCP by the applied voltage V across MCP resistance R. The emissivity of MCPs has never been measured directly, although semiempirical values of 0.2 for 0° bias MCPs, and 0.4 for 13° bias MCPs have been given [11]. The latter value is higher, due to the larger effective area of metal electroding resulting from electrode penetration into the angled channels (i.e., electrode penetration into a 0° bias channel is simply not as visible). The predicted equilibrium surface temperature from this simple analysis fails to take into account the changing wall resistance, and therefore underestimates the actual temperature rise; obviously an iterative analysis would be more accurate. Alternatively, one could use a semiempirical approach to find the actual thermal runaway point for a given MCP glass (without destroying the MCP). This procedure was outlined in the Phase II proposal.

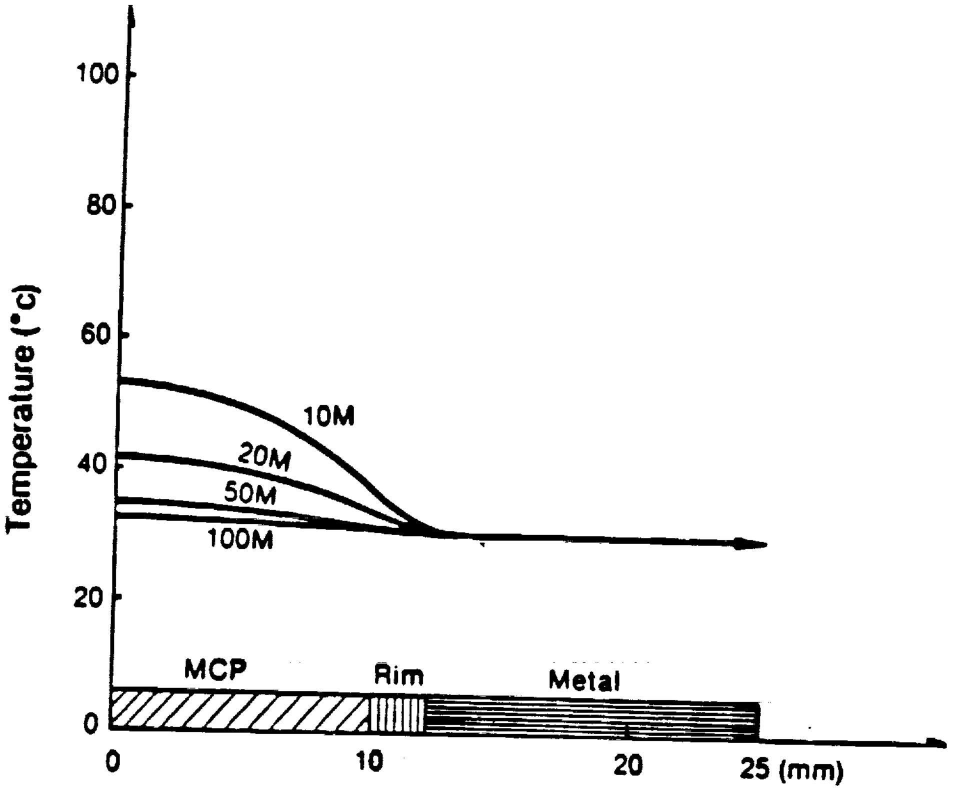

Figure 2. Temperature distribution for MCPs of various resistances. $V_{mcp} = 1$ kV. [from Ref. 62]

Low resistance MCPs

Progress has been made at Galileo in recent years in providing higher dynamic range MCPs using the high bias current approach. Galileo introduced the High Output Technology MCP, a low resistance MCP giving a dynamic range increase of two orders of magnitude, as compared with standard production military night vision plates [12]. MCPs with resistances as low as 5 megohms were able to be continuously operated without thermal runaway, mainly due to the higher temperature Galileo Long Life™ glass formulation, which allowed sustained operation at temperatures as high as 350 °C (previous MCP glasses could not go much above 200 °C). However, even at these elevated operating temperatures, where considerable amounts of heat are being radiated (from the T^4 dependence), thermal runaway would inevitably occur below about 5 megohms. Nevertheless, this advance in MCP technology has generated considerable interest for moderately high input flux applications. Many low resistance Galileo MCPs have already been installed in scientific instruments, since they are identical in format and mounting configuration with standard MCPs. Still, the requirement that the MCP temperature must rise considerably above ambient to radiate the increased heat load imposes limits on its applicability, particularly in detectors employing proximity focused photocathodes.

In many MCP applications, a photocathode is used to convert incident visible or UV photons into photoelectrons, which then become the primary input radiation to the MCP. However, photocathodes are heat sensitive, and can generate a substantial amount of thermionic dark noise at the detector output, even at room temperatures. The photocathode material has a relatively low work function, so that those electrons in the upper end of the thermal energy distribution, which also happen to be close to the surface, escape into the vacuum. This inherent thermal noise is then multiplied by the full MCP gain, and therefore cannot be distinguished from the signal. Also, the photocathode to MCP bias voltage will further lower the cathode surface potential (analogous to the Schottky effect), which only worsens the thermionic emission.

Although the successful use of the low resistance MCP had fulfilled part of the promise of the high bias current approach to MCP dynamic range, we felt that this only raised a new challenge: can MCP bias current be increased even further, while avoiding not just the thermal runaway problem, but also the MCP temperature rise problem. In this program, we attempt to solve both these problems.

1.2.2 DARK NOISE LIMITATION

When this program was first proposed, the low end of the MCP dynamic range scale was bounded by irreducible MCP background or "dark" noise. This noise was seriously limiting the sensitivity of space-based astronomical X-ray and EUV detectors, where input flux rates below 1 $cm^{-2}s^{-1}$ are often encountered, as well as the sensitivity of trace isotope mass spectrometry detectors, medical diagnostic X-ray detectors, and other ultra-low signal applications. Although other MCP noise sources had been identified, such as "hot spots" due to field emitting debris on the MCP input, field emission from mounting hardware, and outgassing, these were all controllable using appropriate cleaning and preconditioning techniques. However, even when these noise sources were eliminated, there remained a low gain exponential tail which required careful setting of discriminator levels, which degraded the signal-to-noise ratio for very low event rates (~1 $cm^{-2}s^{-1}$) to essentially unusable levels.

At the time of the Phase II proposal, it was not at all clear what the true cause of MCP dark noise was, although several mechanisms had been proposed. Indeed, it was not known if it could even be reduced.

1.3 PHASE II TECHNICAL OBJECTIVES

The overall objective of this program was to greatly enhance MCP dynamic range, by enhancing the input count rate capability to well above 10^9 $cm^{-2}s^{-1}$, and by increasing the signal-to-noise ratio for very low-level input signals (Figure 3). At the time of the Phase II proposal, the best approach was felt to be the development of a two-layer "sandwich" MCP capable of high temperature (150 °C), high current operation, with reduced dark noise. By doing this, the previous current saturation limit would be greatly increased, through increasing the MCP bias current while avoiding thermal runaway - the bane of all previous high current MCPs. At the low end, provided that thermionic emission was not a factor, the solution of the dark noise problem would involve investigating a number of postulated causes, including field emission from channel walls as well as radioisotope decay.

To achieve the necessary degree of thermal control with an MCP having a negative temperature coefficient of resistance, a temperature-controlled electrostatic image inverting tube was proposed having a multianode electrical readout. A specialized power supply with two independent outputs would be required to supply controlled currents to the two MCP layers. The temperature control system would be linked to the power supply circuitry for purposes of feedback control. The dynamic range of the device would then be characterized, with life tests of low noise sandwich MCP's carried out at elevated operating temperatures.

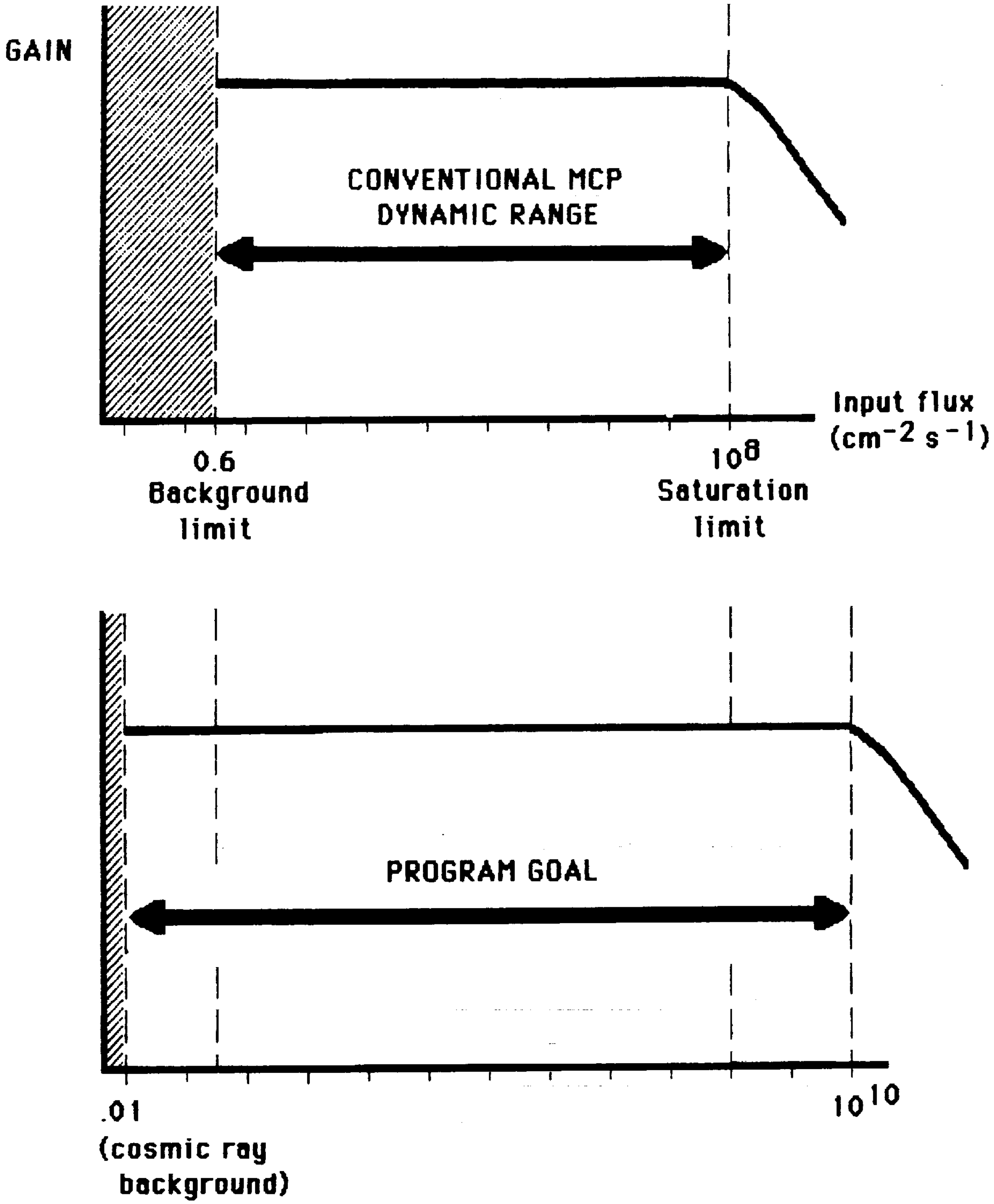

Figure 3. MCP dynamic range.

The statement of work was later clarified, with a number of general milestones: to determine the source of MCP dark noise, and find out how it could be reduced; to develop and fabricate a high current sandwich MCP, having a channel recharge time approaching 10 microseconds (instead of the usual recharge time of up to tens of milliseconds); to develop and fabricate the power supply and thermal control system; to develop a high-speed multianode electrical readout; to develop and fabricate a device enclosure; and finally, to conduct tests.

After the program was underway, a better approach to the high-end problem soon evolved which dispensed with the need for a complex thermal control/power supply system and a laminated MCP, which would allow room temperature MCP operation at very high currents. This approach will be described in detail in the sections that follow.

2. PROCEDURES AND RESULTS

We will present the dark noise reduction results first, since the bulk of this work occurred during the earlier parts of the program.

2.1 DARK NOISE REDUCTION

In some applications, the residual background of MCPs has diminished their effectiveness as detectors at very low input count rates (Figure 4). For several years, a variety of possible noise sources had been discussed [13-16]. However, unambiguous determination of the underlying source had proved elusive. As with conventional discrete dynode multipliers, mechanisms that had been considered included intrinsic radioactivity in MCP glass, thermionic emission, residual gas ions, field emission from hardware, as well as cosmic ray events. In addition, field emission from asperities or microcracks in the MCP channel walls was often considered a major contributor [14-15]. Until as recently as 1987, there was no clear-cut evidence for the predominance of any one of the postulated MCP noise mechanisms, with results obtained by different investigators often contradictory. Earlier attempts to fabricate low noise MCPs at Galileo and elsewhere gave discouraging results, and the lack of consensus on the chief source of MCP dark noise halted further progress.

The two most likely candidates causing MCP background noise were thought to be field emission from channel wall defects, and radioisotopes in the matrix glass. A survey of the literature suggested that field emission was the more probable cause, although the data was inconsistent. Consequently, a decision was made at the start of Phase II to study the field emission hypothesis first. If the results of the study turned out to be negative, attention would then focus on radioisotope decay.

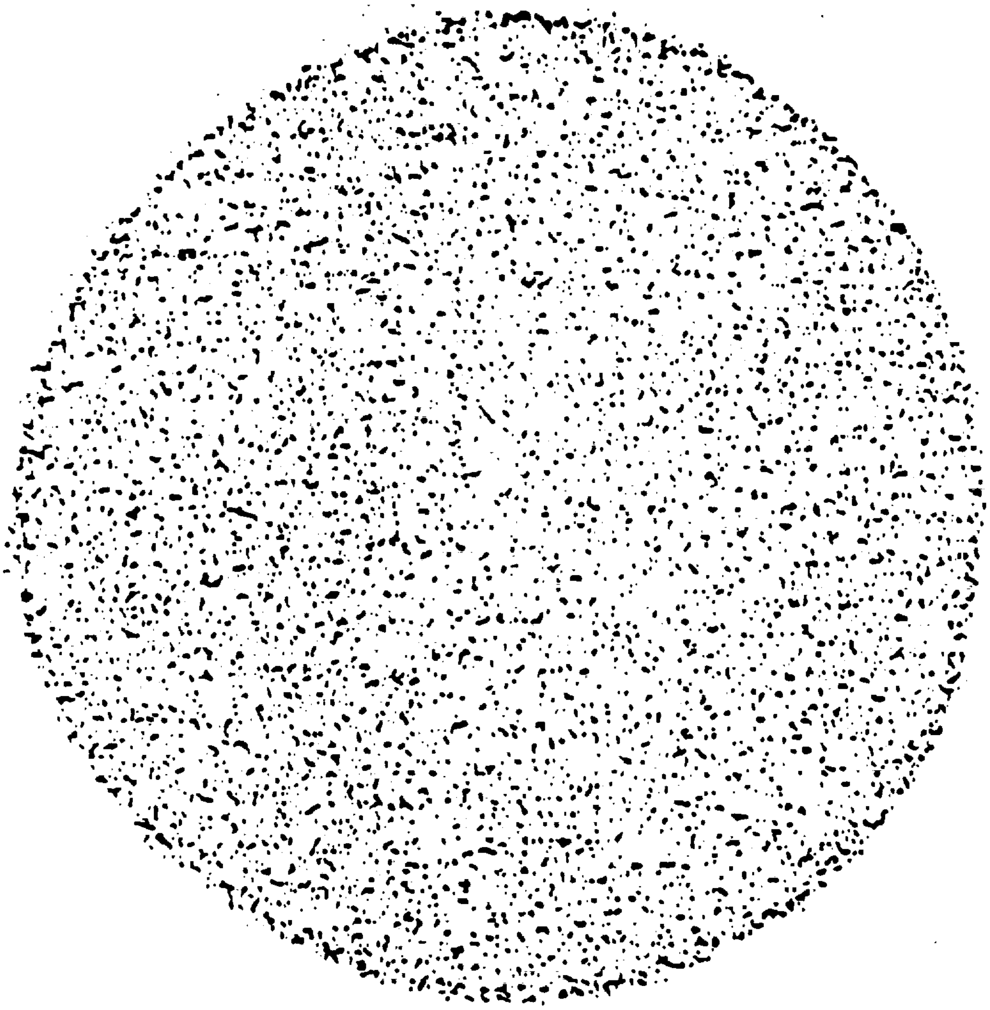

Image of microchannel plate background events for a microchannel plate Z stack (12.5µm pores, 240:1 total L/D, 50mm aperture), illustrating the overall background uniformity.

Figure 4. [from Ref. 21]

2.1.1 FIELD EMISSION DUE TO MICROCRACKING

The application of an electric field to a surface being struck by impacting energetic particles, resulting in secondary electron emission, facilitates the emission process by lowering the effective work function. For field strengths $< 10^4$ V cm^{-1}, the enhancement to zero-field electron emission is called the Schottky effect. For stronger fields, quantum mechanical tunneling begins to dominate when the surface barrier becomes sufficiently thin. When this occurs, electron emission is spontaneous, not requiring an impacting primary event. This process is called field emission.

Since the MCP background noise pulse height distribution (PHD) has the form of a negative exponential (Figure 5), even at MCP voltages high enough to give input signals a peaked PHD, a noise source uniformly distributed along the channel is indicated: those events originating inside the channel below the input plane would not be amplified enough to achieve saturated gain levels. If the noise source were field emission, the most plausible cause would be defects or microcracks along the inner channel surface. Sharp edges with tip radii on the order of 10-100 Å would give rise to local fields far more intense than the nominal bias field of 10^4 V cm^{-1}. If negative ions were adsorbed on these surfaces, these local fields would then be within the range of field emission, in a process similar to that occurring in a field emission microscope (as described by the Fowler-Nordheim equation [17]).

HIGH RESOLUTION SEM MICROGRAPHS

To see if microcracking were actually occurring along channel walls, a high resolution (30 Å) SEM study of an actual MCP channel was undertaken at Photometrics, Inc., Woburn, MA. A standard production Long Life™ MCP, which has been shown to have a relatively high dark count of 0.7 $cm^{-2}s^{-1}$ [18] was fractured, and channel walls were exposed. No microcracks or asperities were seen, even at the highest achievable magnifications. Although charging phenomena due to the superficial siliceous layer made imaging below 100 Å quite difficult, there was no indication of anything less than a featureless and uniform channel wall.

2.1.2 RADIOISOTOPES

The concept of reducing MCP background noise ("dark noise") by fabricating MCP's from radioisotope-free glass is not new, and has been discussed in the scientific literature for several years (Figure 6). The first known published mention of internal MCP glass radioactivity as a possible background noise source was in a paper by Henry et al. [14] in 1977. (Their measurements, however, suggested that field emission from channel wall defects was the most likely cause of MCP dark noise.) Radioisotope

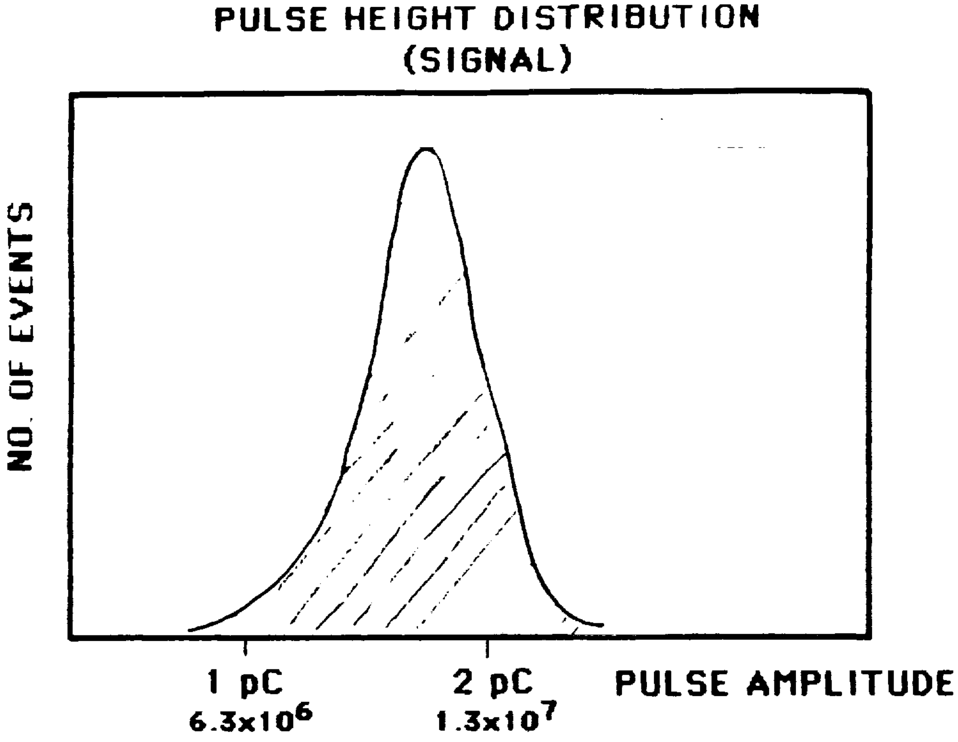

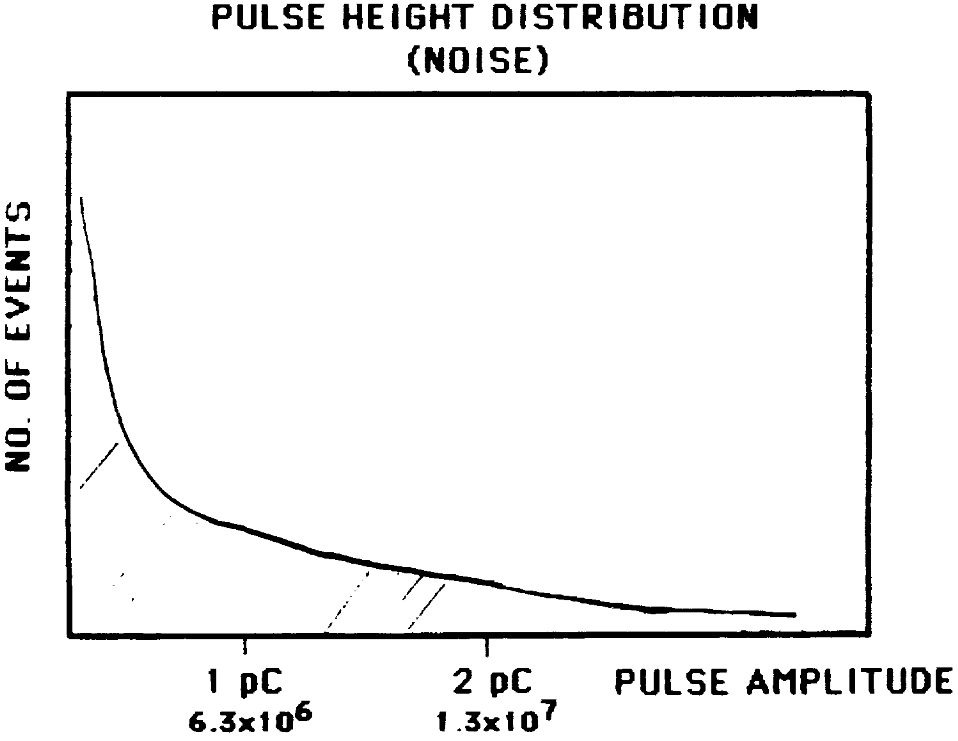

Figure 5. Comparison of signal and noise pulse height distributions.

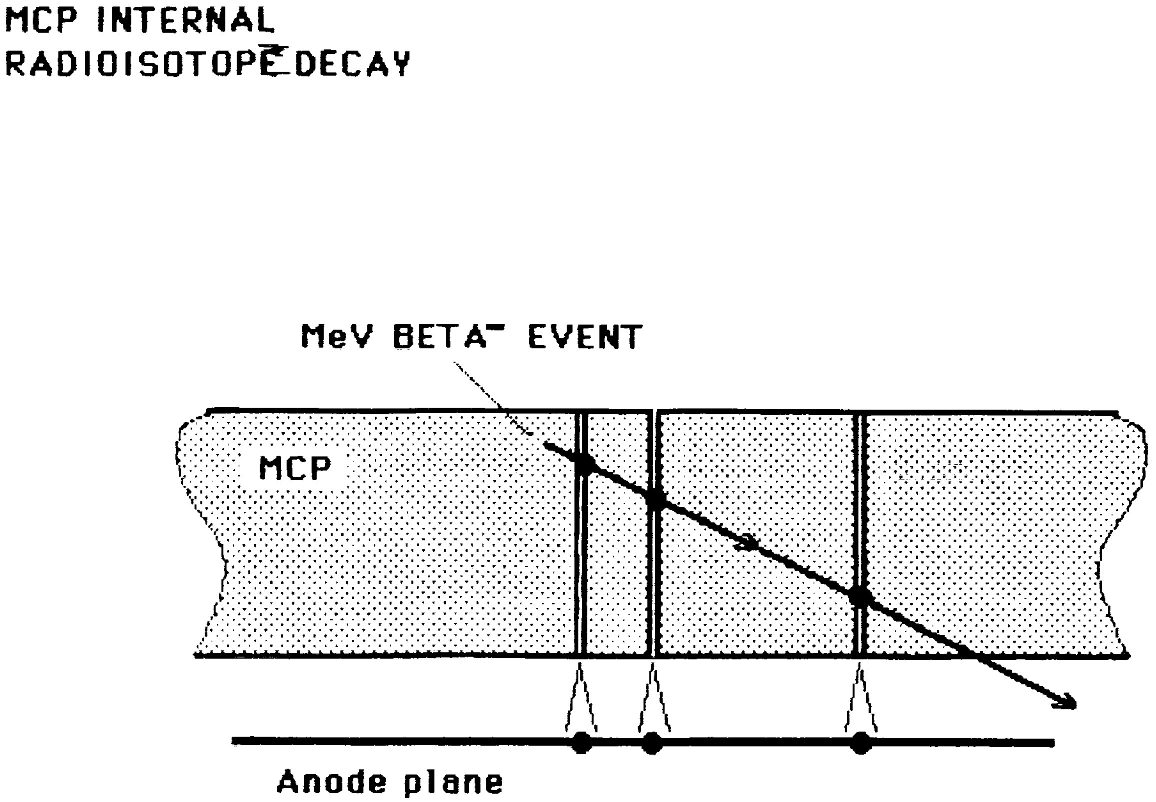

Figure 6. MeV beta particle traversing MCP active area. [from Ref. 20]

activity was again mentioned as a possible dark noise source in the initial 1984 proposal for this program (C. Tosswill, NASA SBIR Proposal #8139191, June 1984).

In 1985, the first published calculations giving strong prima facie evidence for the radioactivity model were given by Fraser et al. [19]. Assuming that MCP glasses contain around 5 wt% of potassium, a count rate due to ^{40}K decay was estimated which roughly agreed with experimental data. Pb isotope contamination was also mentioned as a possible additional noise source (but of considerably lesser importance than the alkali radioisotopes). Fraser et al. [20] followed with a publication in 1987 which comprehensively and rigorously studied the background noise problem. This study showed, with a high degree of confidence, that ^{40}K was the dominant noise source in well-outgassed, hotspot-free MCP's fabricated from MCP glass containing 6.5 wt% potassium from Mullard (Philips Components Ltd. Mitcham, Surrey, UK), with no heavier alkalis. Corroborating evidence for the deleterious effect of ^{40}K was presented by Siegmund later that year [21]. A subsequent paper by the Leicester group [18], which studied MCP's made from Long Life™ glass, concluded that ^{87}Rb was the dominant source of radiation in this potassium-free material, further supporting the internal radioactivity noise model. At the end of the paper it was stated that "...investigation of MCP's manufactured from potassium- and rubidium-free glasses will be of very great interest."

LOW NOISE GLASS DEVELOPMENT

During the first quarter of the program, we became aware of these findings on radioisotope activity. We then immediately set out to develop a new MCP glass formulation with 1) low intrinsic background noise, 2) superior gain stability, 3) stable high temperature operation, and 4) strip current stability equivalent to the best prior art MCP material. Moreover, we would have to do this using Galileo's standard manufacturing processes, if timely results were to be achieved. After carefully choosing the amount of each glass constituent, based on estimates of the constituent's influence on glass properties, a precise glass formulation was arrived at [64]. Work on a test melt then started.

A 20 kg batch was prepared from high purity raw materials and melted in a six liter induction heated platinum crucible to prepare cylindrical glass castings. The castings were then extruded into tubes which were used to prepare the low noise MCP wafers, using the standard Galileo MCP production process described in Sect. 1.1. The core glass was an acid soluble glass of different composition than the low noise cladding glass, but with matched properties such as viscosity, thermal expansion, and transition and softening temperatures, so that no changes to the standard MCP production process were needed. Also, no efforts to improve channel surface quality were made (to reduce possible field emission).

After the MCPs were fabricated, they were tested at Galileo for gain and strip current, and found to perform about the same as standard Long Life™ MCPs. A lifetest carried out on a sample plate (to 3 C cm^{-2} accumulated output charge) showed that gain stability under prolonged electron bombardment was equal to or better than standard Long Life™ plates.

LOW NOISE MCP TESTING

We then sent the first group of low noise MCPs to two groups of X-ray astronomers, at the University of California-Berkeley and to the Leicester group, for thorough dark noise testing. (Since MCP dark noise is a major concern in X-ray astronomy imaging detectors, these groups were highly motivated to study this problem.) The Berkeley group received the plates first, due to shipping delays to Leicester. Their results were discouraging, and showed that the MCPs behaved quite poorly; they noted no improvement in dark noise characteristics. However, it was later discovered that the plates had been damaged, invalidating the test results. In marked contrast, the Leicester group one month later reported that the MCPs were the quietest plates ever tested, and in all other performance characteristics, behaved almost identically with standard Long Life™ MCPs.

Two groups of low noise MCPs were eventually fabricated and tested, and the test results were published. (A third group of low noise MCPs is currently being fabricated, but test results on these will not be available for inclusion in this report.) The remaining text in this section is a condensation of one of these papers [22], with the present writer being the principal author.

Dark Noise Figures

MCP background measurements can be presented in two ways. One way is to plot the background event rate as a function of the counting threshold d, with the latter specified as a fraction of the model (most probable) detector gain G_c. Due to the negative exponential noise pulse height distribution, one can then extrapolate to the zero charge threshold and use the limiting value of the noise event rate $N_n(0)$ as a comparative measure of MCP background.

Another method, perhaps more useful in specifying actual detector performance, is to give the observed detector background under optimized conditions of detector signal-to-noise. Optimization can be achieved by first deriving a signal to noise index S(d) according to procedures outlined in Ref. 24. One then sets the counting threshold to correspond with the peak of the S(d) curve (Figure 7). The background event rate $N_n(d)$ will be the noise

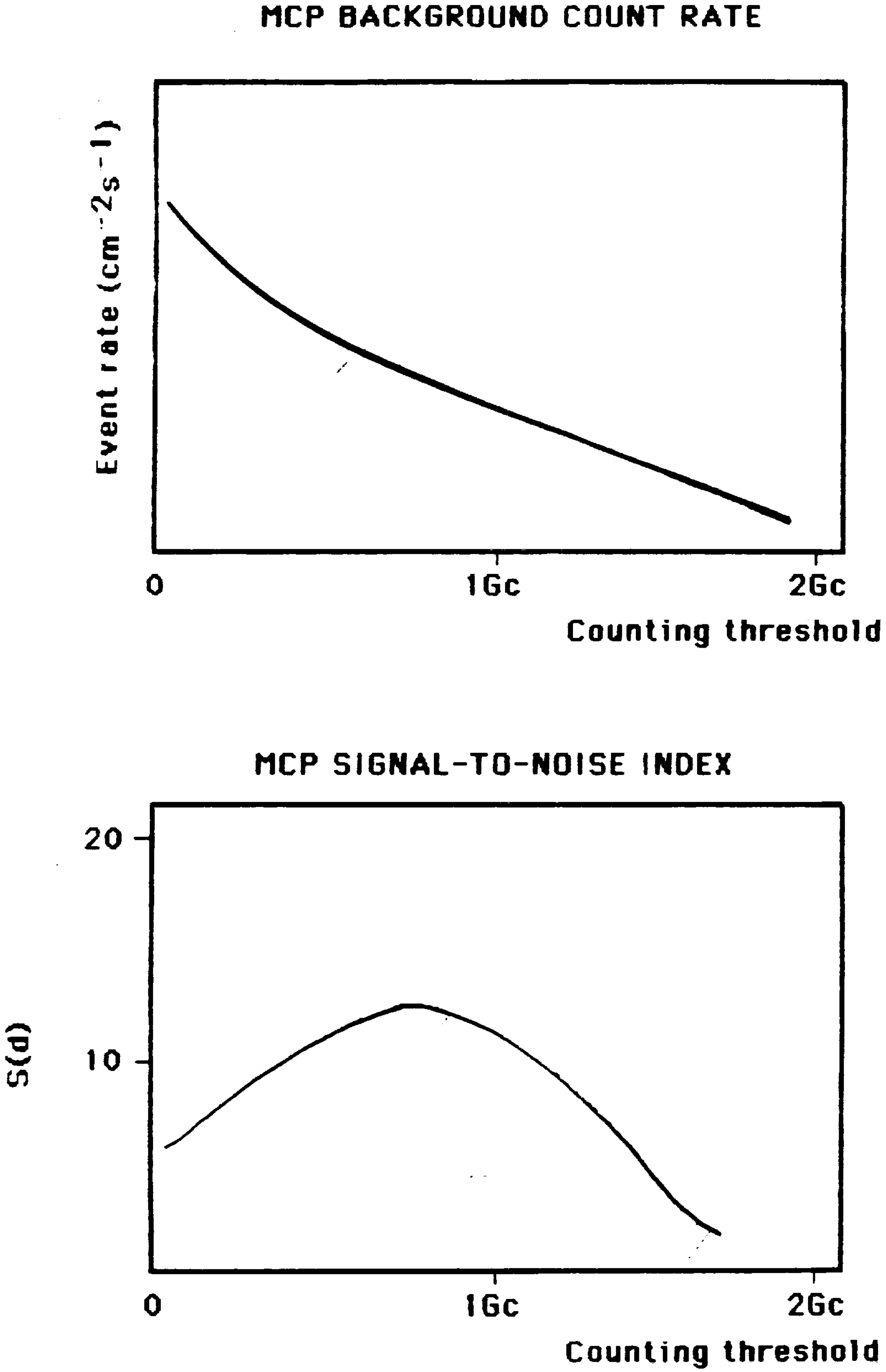

Figure 7. Dark noise measurements.

figure actually observed in a working (i.e., optimized) detector. It will typically be three to four times lower than $N_n(0)$. Both noise figures, $N_n(0)$ and $N_n(d)$, will be given here for a low-activity detector body (below).

First group of low noise MCPs

In this section summary results are presented of background measurements made at the University of Leicester on the first lot of low noise MCPs; these results were first presented in greater detail at the recent "X-ray Instrumentation in Astronomy" conference (San Diego, 1988) [23]. This group of MCPs was fabricated from a composition designed to be free of radioisotope contamination, in particular ^{40}K and ^{87}Rb. The MCPs had dimensions identical with standard Galileo production plates as shown in Table 1. (Although the average plate resistance for this particular group was 30 megohms, it should be noted that the characteristic resistance of prototype low noise MCPs was found to be capable of ranging over several decades, and could be specially tailored during processing.)

Table 1

Dimensions of low noise MCPs (first group)

L/D	40
Channel diameter (μm)	10
Channel pitch (μm)	12
Bias (degrees)	11
Resistance (megohms)	30 @ 1000 V
Nominal OD (mm)	33
Active dia. (mm)	25

Low noise detector requirements

Due to the relatively high noise level of currently available MCPs, the background contribution due to radioisotope contamination in detector components, such as ceramic mounting spacers or blocks, had never been seriously considered. Indeed, the MCP contribution always dominated the observed noise. However, during initial tests of low noise MCPs, it was discovered that radioisotope activity in ceramic detector components (MACOR, containing about 8.5 wt% of K_2O) was being observed [23]. Accumulated noise images showed a distinct annular structure of enhanced contrast that could not be accounted for by the MCP background. When the detector body was rebuilt using non-radioactive plastic components (Kel-f) instead of MACOR, this noise feature all but disappeared, with a 40% drop in the noise count. Consequently, in the design and construction of future demountable or sealed tube detectors in which the use of low noise MCPs is contemplated, components having little or no

Review of noise measurements

The first group of low noise MCPs received no preconditioning treatments (bakeout or burn-in). Over a two month period, noise measurements were made on a tandem (two MCPs stacked together) in a quiet detector body (below) using a graded-density wire readout. The modal gain G_c and the pulse height distribution (FWHM) of the low noise tandem (V_f=V_r=1000V, V_g=400V) were determined to be 1.2 x 10^7 and 140% at the MCP center, using a 14.5 mm^2 collimated beam of C-K (0.28 keV) X-rays. As shown in Figure 8, the average background rate measured within the central 17mm of MCP active area and extrapolated to zero charge, was approximately:

$$N_n(0) = 0.07\ cm^{-2}s^{-1}$$

For the full 25mm MCP active area, the figure was slightly higher, approximately 0.09 $cm^{-2}s^{-1}$, since it included additional noise due to one or two 'hot spots' (field-emitting debris on the MCP input face).

This noise level is an order of magnitude lower than an equivalent tandem made of Galileo's standard production Long Life™ MCPs, and three times lower than a tandem from Philips (Nn(0) = 0.25 $cm^{-2}s^{-1}$) of nearly identical geometry (12.5 micron pores instead of 10 microns). The noise count due to internal radioactivity scales with front plate thickness, hence it is important that this dimension be specified. For the same set of measurements, the signal-to-noise index S(d) is shown in Figure 9, yielding a noise figure:

$$N_n(.8G_c) = 0.02\ cm^{-2}s^{-1}$$

This value is representative of what would be observed in a detector having optimized signal-to-noise parameters.

Although these numbers represented a substantial advance over anything previously measured, they were still four to five times higher than expected on the basis of the known radioisotope content of the MCP glass composition. Summing all the known residual contributions, such as alkali oxide impurities (below) and the cosmic ray-induced background (.006 $cm^{-2}s^{-1}$ @ d=0), at the time the measurements were reported (August 1988) only 22% of the observed noise counts could be accounted for. As discussed in Ref. 29, local MCP outgassing, ion feedback, field emission, and readout noise were all eliminated from consideration when the noise count was found to be relatively insensitive to controlled changes in MCP voltage, temperature, and chamber pressure. Due to the relatively high thermionic work function of reduced lead silicate glass,

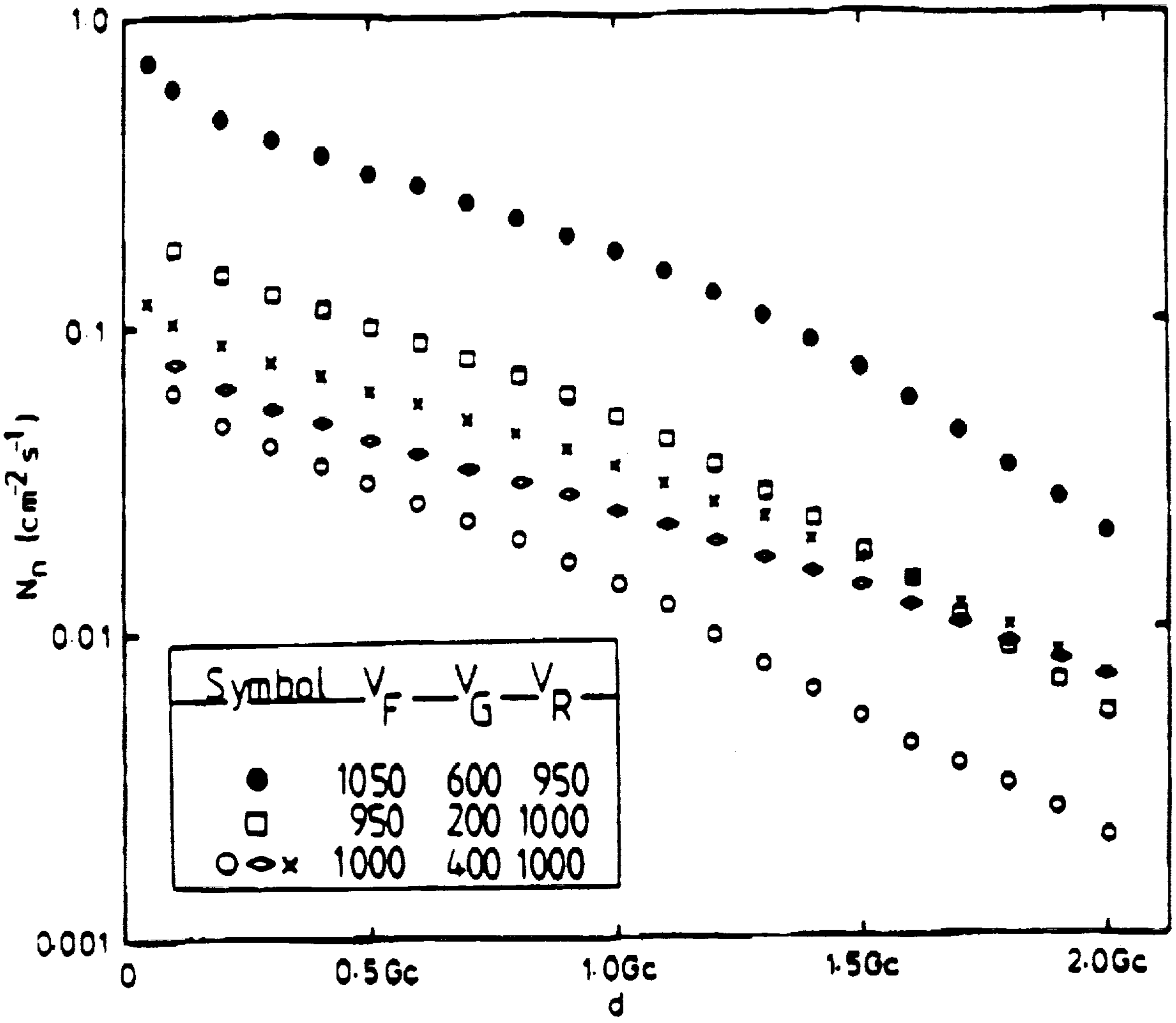

Noise pulse height distributions. Filled circles: Galileo Long Life^{TM} MCPs (L/D = 40:1, channel dia.= 10 microns). Squares: Philips MCPs (40:1, 12.5 microns). Crosses: Galileo low noise MCPs, first lot (40:1, 10 microns); MACOR detector body, 17mm image diameter. Diamonds: Galileo low noise MCPs, first lot; low activity detector body, full face illumination. Open circles: Galileo low noise MCPs, first lot; low activity detector body, 17mm image diameter.

Figure 8. [from Ref. 23]

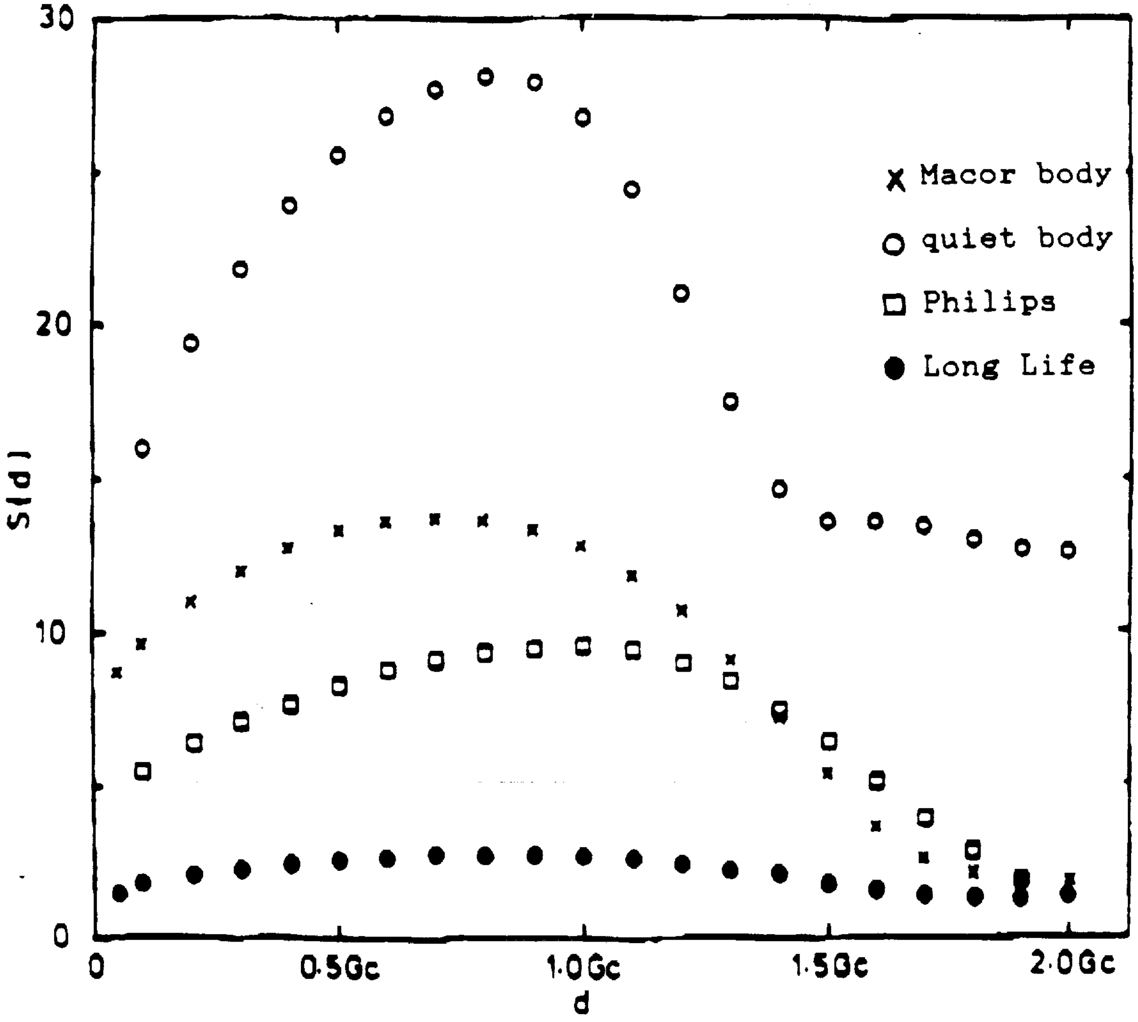

Figure 9. Signal-to-noise indices corresponding to curves in Fig. 8. [from Ref. 23]

thermionic emission was not considered to be a factor [20,21]. Even though the first group of low noise MCPs was fabricated with Long Life™ (Rb-containing) rims, and ^{87}Rb activity might conceivably cause at least some of the observed background, this contribution was shown to be negligible, with an attenuation factor of 10^{-9} within the central MCP region where the background was measured.

Remaining background source

An examination was subsequently undertaken of remaining noise sources which might be thought to have only a second-order effect. First, the purity of the raw materials used in the low noise MCP glass melt was studied. Radioisotope contamination of lead oxide, the major constituent of MCP glass, has occasionally been suspected of being a possible background source. Although ordinary lead often contains low levels of radioactive contaminants, properly refined lead is expected to be relatively free of radioisotope activity. Since no specifications on alpha- or beta-emitting isotopes or actinide contaminants in the lead oxide were available from the manufacturer, a mass spectrographic analysis of the lead oxide raw material was performed. The samples revealed undetectable levels of any emitting contaminants except potassium, present at the negligible level of 10 ppb. However, this did not include an isotopic analysis of the lead. Therefore, to assess whether alpha or beta emission was occurring, a counting test was done on a sample of known mass. The combined alpha and beta count rate determined from a 16 hour integration was found to be 1.6×10^{-4} $g^{-1}s^{-1}$, corresponding to a negligible MCP background count rate of 2×10^{-5} $cm^{-2}s^{-1}$.

The other main constituent of the low noise MCP glass possibly containing contaminants is Cs_2O. The manufacturer's specification for rubidium in both standard and high purity grade $CsCO_3$ (the raw material) is, respectively, 3000 and 300 ppm. For potassium, the levels are considerably less, 500 and 100 ppm. The first group of plates were made from standard grade $CsCO_3$. A residual content of rubidium and potassium was calculated for the final glass.

An assay was performed on an MCP active area, again using mass spectrographic analysis. This showed a rubidium level in the glass matrix much higher than the level calculated from the raw material specification, approximately 10-20% of the amount observed in a similar analysis on Long Life™ MCPs. Moreover, the presence of potassium was observed at a similarly elevated level. However, this analytical method is only accurate to within an order of magnitude. Still, for comparable amounts of Rb and K, the Rb will contribute far more to MCP noise, due to the high isotopic abundance of ^{87}Rb, ~28%. Given the accuracy of the assay, these numbers were consistent with the observed background, which was an order of magnitude less than that measured for a Long Life™ tandem [18]. Consequently, low-level alkali contamination was indicated.

Second group of low noise MCPs

A second lot of prototype low noise MCPs was produced, with the goal of preventing trace alkali contamination. These plates were made using low noise glass, in both the rim as well as the active area. Their dimensions are shown in Table 2 (designed to be compatible with the Advanced X-ray Astrophysics Facility High Resolution Camera [31]). Two new glass melts were separately fabricated using high purity $CsCO_3$ raw material in one melt, and a selected lot of standard grade $CsCO_3$ in the other. First, the raw material was analyzed for trace contamination.

The standard $CsCO_3$ was analyzed for rubidium content with energy dispersive X-ray fluorescence (EDXRF) using a standardless technique. Regular additions of $RbCO_3$ were made to the unknown, and the concentration in the undoped sample was determined by linear regression. This analysis was repeated seven times to average out effects of packing variations. The rubidium content of the undoped sample was measured, and corresponded to approximately 35 ppm Rb in an MCP made from this material - equivalent to an MCP background rate of about .001 $cm^{-2}s^{-1}$. The manufacturer's analysis of the high purity $CsCO_3$ lot showed only trace potassium and a level of Rb comparable to what was measured in the standard lot of selected material. Comparative EDXRF analyses of glass made from these materials showed equivalent Rb peak heights, consistent with the raw material analyses. (However, quantitative EDXRF analyses of glassy samples was not possible due to interference effects.) The glass prepared from the high purity $CsCO_3$ was used for the second group of MCPs. Mass spectrographic analysis of this glass showed a sixfold reduction in Rb content and a 40x reduction in potassium content, as compared with the first lot of low noise material.

Table 2

Dimensions of low noise MCPs (second group)

L/D	80
Channel diameter (μm)	10
Channel pitch (μm)	12
Bias (degrees)	8
Resistance (megohms)	100 @ 1000 V
Nominal OD (mm)	38
Active dia. (mm)	30

Initial noise measurements

Two different sets of MCPs from the second group were tested at both Leicester and Harvard, and the initial noise figures were found to be essentially the same. For consistency, the Leicester measurements will be reported here. As with the first group of low noise MCPs, no bakeout or burn-in treatments were carried out on the second group, and a graded-density wire readout was used. These initial noise measurements were carried out after only three days under vacuum, on a tandem with identical 80:1 front and rear plates housed in a low-activity detector body. However, it has been observed [20] that the MCP dark count rate normally approaches a plateau after fifty to sixty hours under vacuum, when high voltage is continuously applied. Hence, the contribution of local outgassing to the noise figure was expected to have diminished to insignificant levels. The modal gain and FWHM were 1.0×10^7 and 130% ($V_f=V_r=1200V$, $V_g=400V$) using C-K X-rays. The measured background rate for the full MCP active area was (Figure 10):

$$N_n(0) = 0.10 \ cm^{-2}s^{-1}$$

This figure is almost identical with the figure given earlier for a tandem composed of 40:1 plates. The signal-to-noise index shown in Figure 11 yields an optimized noise figure of:

$$N_n(.9G_c) = 0.03 \ cm^{-2}s^{-1}$$

Assuming that the noise source is uniformly distributed throughout the thickness of the MCP, this impliesthat the second group of low noise MCPs was fabricated from a glass which was twice as quiet as the glass used in the first group. Had the measurements instead been carried out on a tandem using a 40:1 front plate, the noise figure would be expected to be roughly one-half the 80:1 value. The second group of MCPs thus represented an MCP background twenty times lower than standard Galileo production plates, and up to six times lower than the quietest plates from Philips.

Nevertheless, this was a smaller reduction in background noise than expected from the observed reduction of both the Rb and K content of the MCP glass, and was still several times higher than the cosmic ray-induced background. Using the same experimental procedures as with the first group of low noise MCPs, outgassing, field emission, and other noise sources besides radioactivity were eliminated from consideration. Additional radioisotope assays of the matrix glass in finished MCPs from the second set were underway, when finally the puzzle was solved.

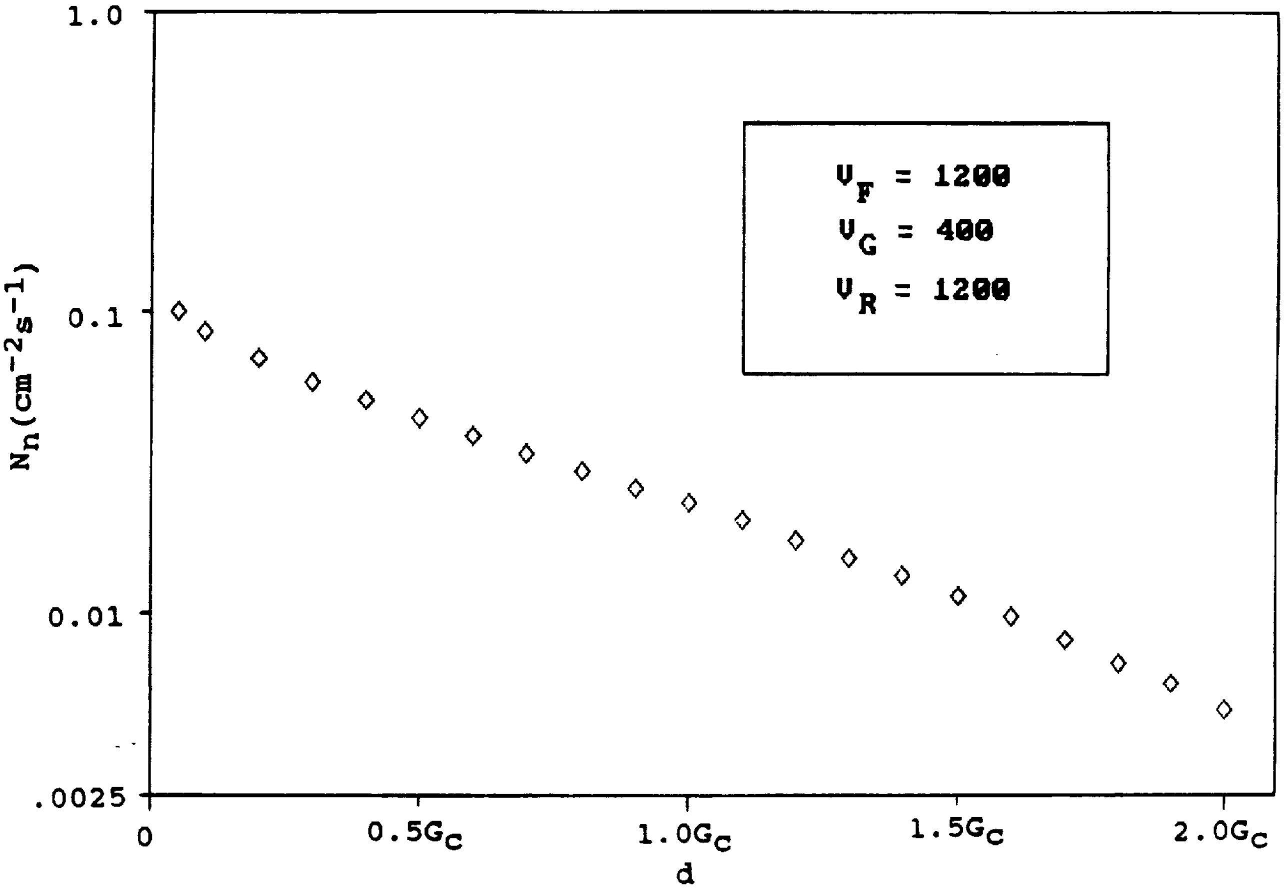

Figure 10. Noise pulse height distribution, second group low noise MCPs. [from Ref. 22]

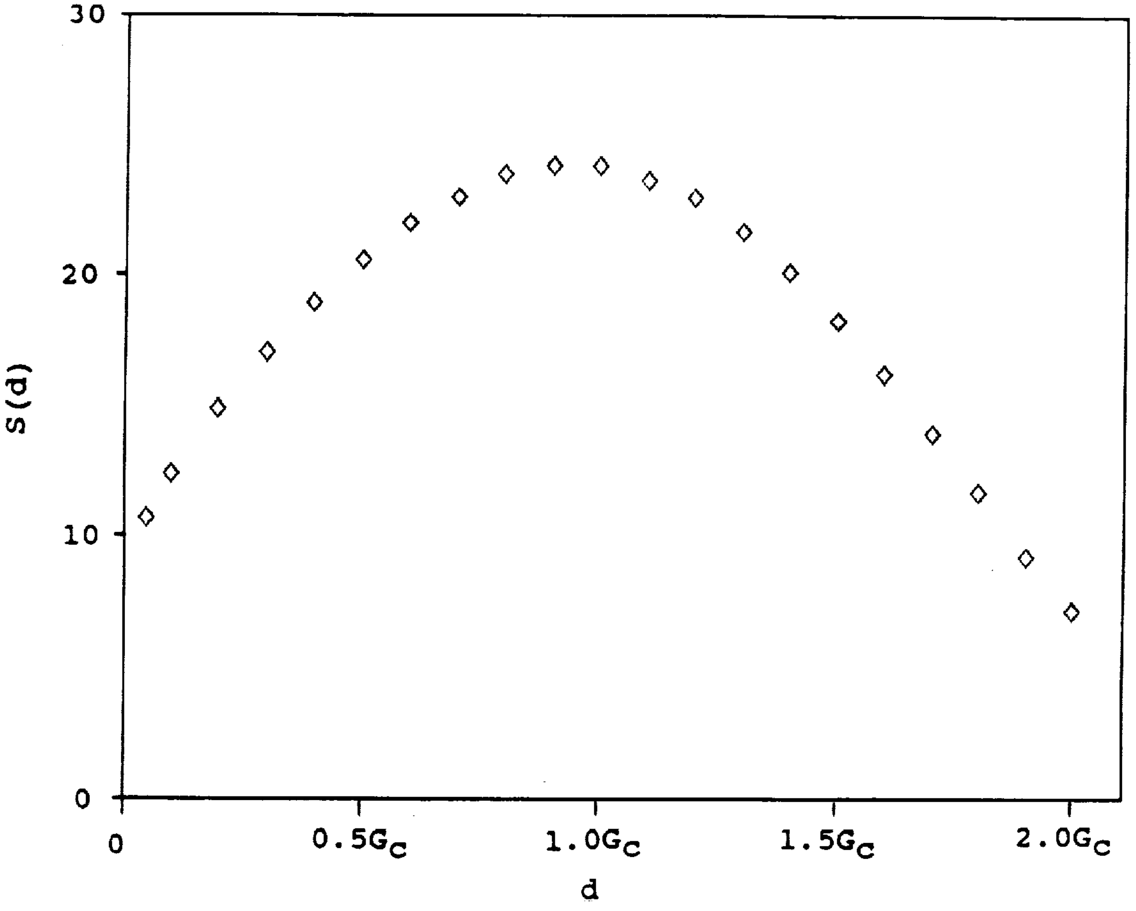

Figure 11. Signal-to-noise index for data shown in Fig. 10. [from Ref. 22]

Experiments had been carried out at Leicester to see if cosmic ray-induced events were being supplemented by noise events induced from other sources external to the MCP. A 300 kg lead shield composed of 5 cm thick bricks was constructed around the detector housing. This shield provided a considerable degree of attenuation (30:1) to MeV gamma rays from the environment, yet was relatively transparent to high energy cosmic ray muons. Although the shield did not completely cover the detector, when extrapolated to 4π steradians, the MCP internally-generated background noise was found to be .02 $cm^{-2}s^{-1}$, only twice the cosmic ray background limit. Thus the second group of Galileo MCPs was virtually noise-free (although the residual dark count of .01 $cm^{-2}s^{-1}$ suggested that an extremely low level of trace radioisotope contamination was still present).

Interestingly, within the past few months of this writing (June 1989) Philips has also succeeded in fabricating low-noise MCPs; these were included in the Leicester experiment. Although only two data points are shown (Figure 12) due to a publication deadline (SPIE-Paris Conference, April 1989), it appears that the level of trace radioisotope in their glass is somewhat less. A third group of Galileo low noise MCPs are now being made, and samples are being taken at each processing step. Assays will be conducted on each sample, to determine the ultimate source of the remaining radioisotope contamination. At such low levels (~10 ppm), rigorous manufacturing control is very difficult to achieve; even so, the attempt will be made, and we are confident that totally radioisotope-free MCPs will soon be available.

Note:

-- It must be noted that latter portions of the low noise MCP work were internally funded by Galileo, as stated in the quarterly reports. However, since the stimulus for this work as well as the basic glass formulation derived from contract funding, we feel it is appropriate to include all results to date in reducing MCP background.

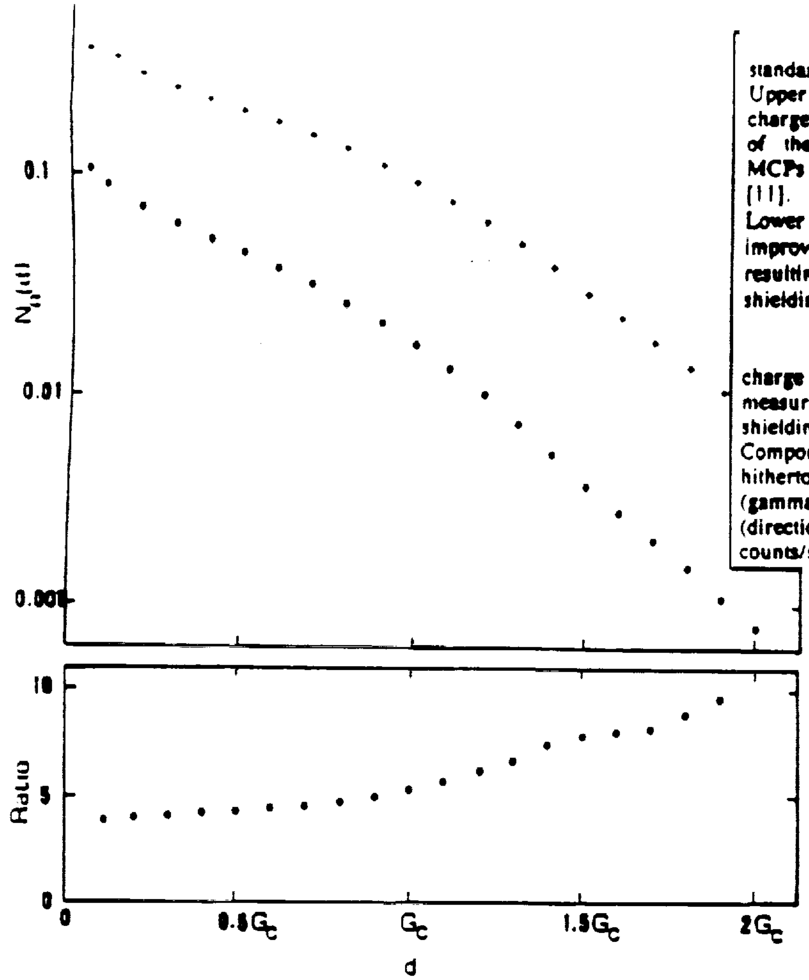

Comparison of noise pulse height distributions from standard and low noise chevron microchannel plate detectors. Upper figure - Noise count rate as a function of lower level charge discriminator setting in units of G_c, the modal X-ray gain of the relevant detector. Crosses- Philips Components L/D = 80:1 MCPs manufactured from lead glass containing bulk potassium [11]. Circles- Galileo low noise L/D = 80:1 MCPs [14]. Lower figure - Ratio of noise count rates, showing four-fold improvement in dark noise at practical counting thresholds resulting from use of low noise MCPs (without additional shielding against external background sources).

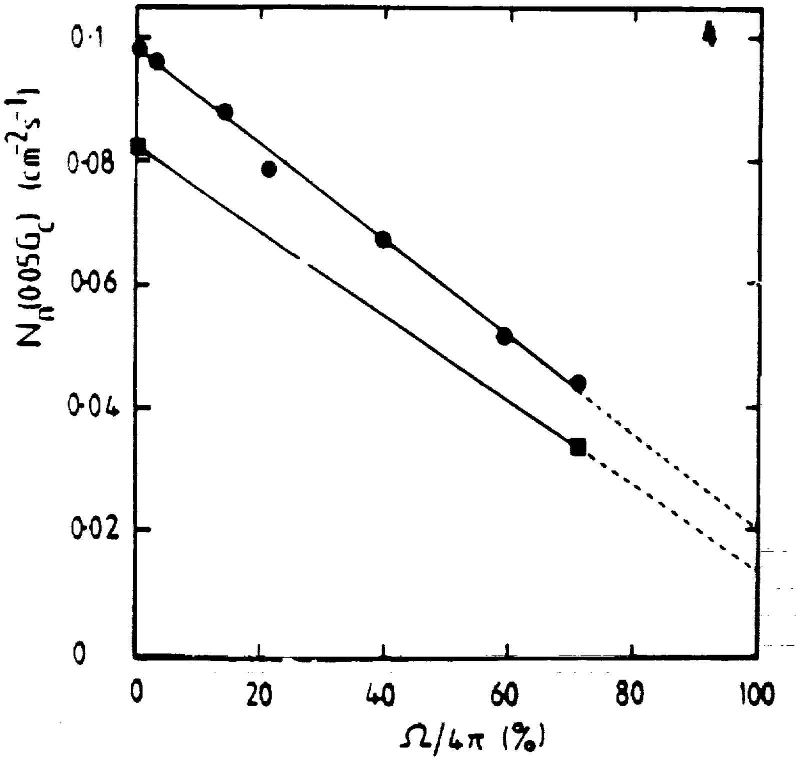

Low noise MCP background count rate (above a charge threshold one-twentieth that of the detector signal gain) measured as a function of solid angle enclosed by 5 cm lead shielding. Ω Circles- Galileo MCPs. Squares- Philips Components MCPs. The linear decrease suggests that most of the hitherto irreducible MCP background is due to an isotropic (gamma ray) flux arising in the laboratory. Recall that the (directional) muon flux is expected to contribute about 0.01 counts/square cm/s, dependent on MCP orientation.

Figure 12. [from Ref. 60]

2.2 HIGH FLUX ENHANCEMENT

This section describes how the MCP count rate capability was extended well beyond the upper limit discussed in the Statement of the Problem section (1.2).

2.2.1 LOW RESISTANCE MCPs

(Due to the proprietary nature of Galileo's production processes, certain details must be omitted here.)

Since their introduction, MCPs have been fabricated using glass. The most stable and widely used MCP glass system has been a lead silicate glass containing roughly 50 wt% lead oxide, 5-10% alkali oxides, with the remainder silicon dioxide. After the MCP array of millions of hollow microscopic channels is fabricated, the inner channel walls must be made semiconducting. For lead silicate, this is done by exposing the channels to hot hydrogen (400-500 °C), which chemically reduces the lead oxide to a form of metallic lead with dramatically lowered resistivity. The hot hydrogen treatment is a thermally activated process where lead oxide is reduced to lead, with water being the chief reaction product. The activated surface, extending to a depth of 2000-3000 Å, becomes differentiated into essentially two sublayers (Fig. 13 and 14) through competing processes of reduction, diffusion, and evaporation of Pb and other constituents [24,26]. The superficial 100-200 Å emitting layer, where the secondary emission takes place, is composed mainly of vitreous silica. The underlying layer, from about 200-2000 Å, is the conductive layer, and possesses a far higher concentration of lead. The conduction mechanism is presumably a hopping mechanism between electronic states associated with Pb atoms [25].

As a result of the hydrogen reduction process, standard 25 mm MCPs possess an overall (face to face) resistance on the order of 10^8 ohms. By varying this process, Galileo has been able to produce working Long Life™ MCPs with considerably lower resistance values, about 5 megohms. Moreover, as can be seen in the lower left-hand corner of Figure 15, very low resistance MCPs with resistance values below 100 kilohms can also be fabricated -although they have usually been considered "outliers" and seen as aberrations, since they thermally self-destruct within seconds when standard bias voltages were applied, in standard mounting configurations. However, it is clear that if such low resistance MCPs could somehow be operated without the occurrence of thermal runaway, the high bias current approach to MCP dynamic range enhancement could be exploited. Indeed, this will be our strategy in this program.

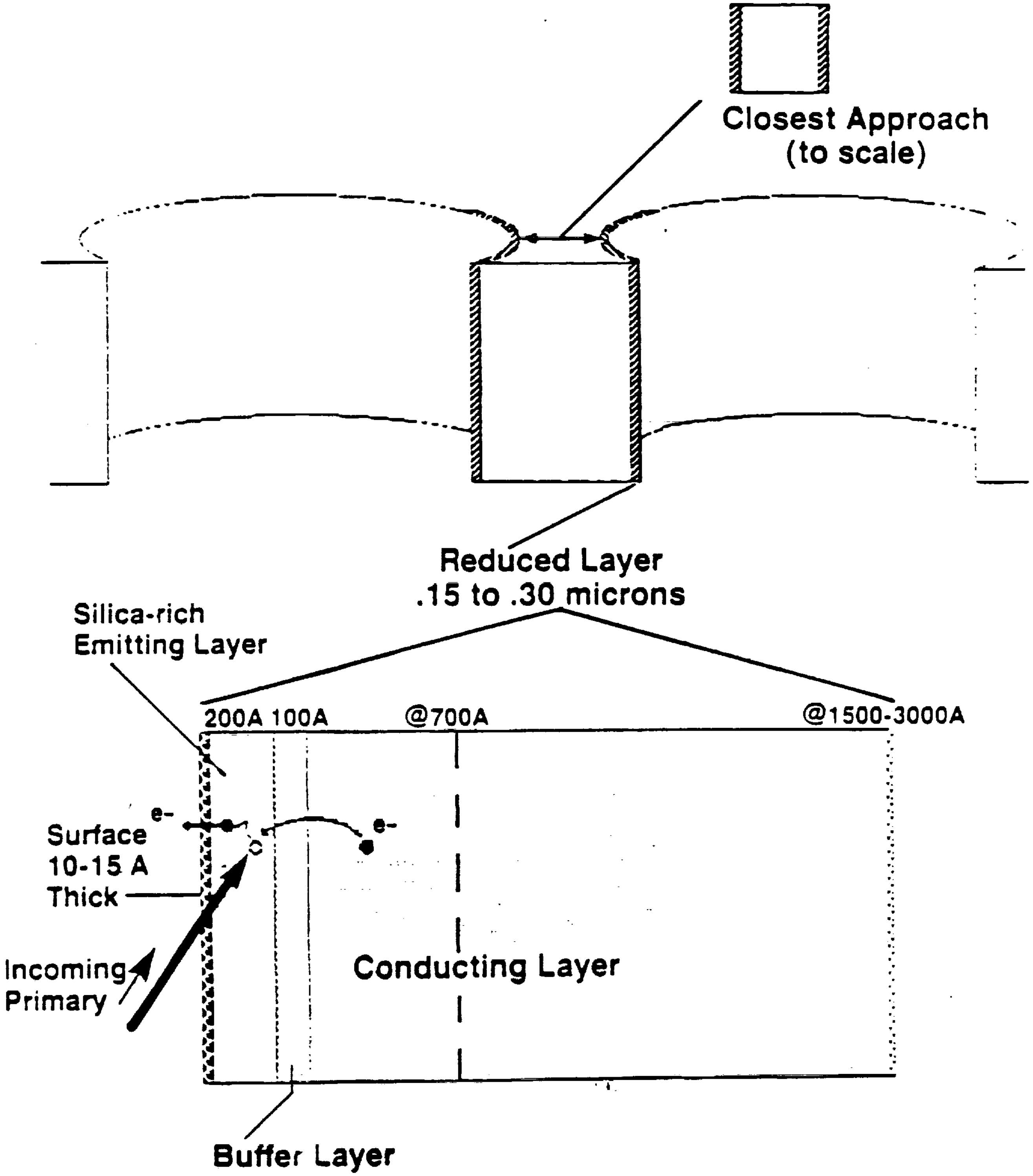

Figure 13. MCP active surface, differentiated into secondary emitting and semiconducting layers.

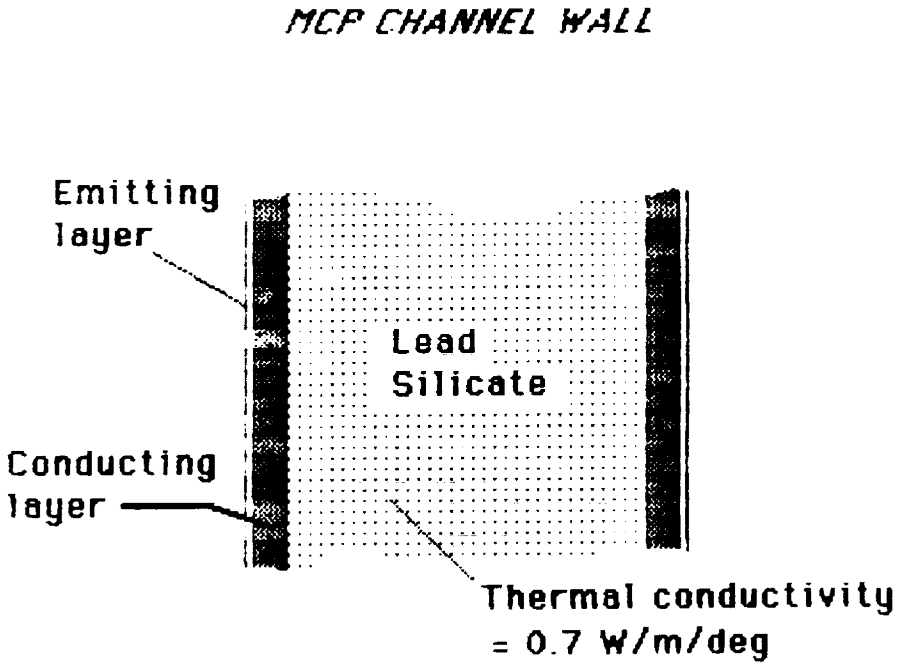

Figure 14. MCP interchannel web, predominantly bulk lead silicate glass.

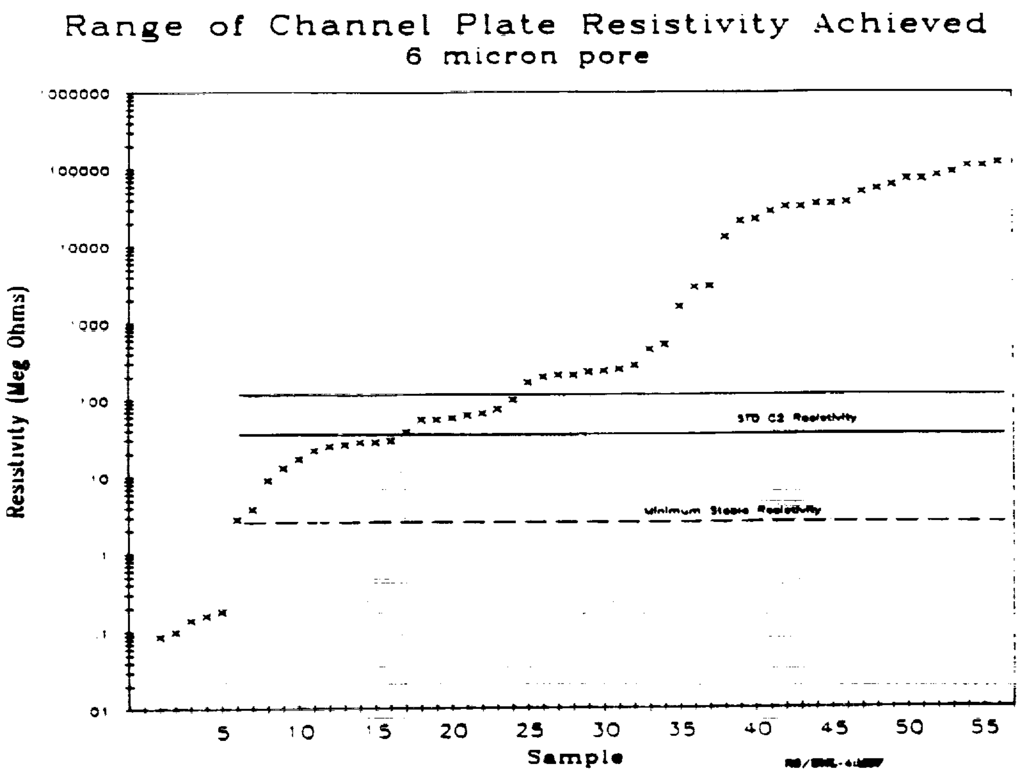

Figure 15. Long Life^{TM} MCP resistance range, 6 micron channel diameter. [from Ref. 8]

Pb-DEPTH PROFILES

Before tackling the thermal control problem of very high bias MCPs, we wanted to see if qualitative differences existed within the active surfaces of standard (10^8 ohms), low resistance (10^7 ohms), and very low resistance MCPs (10^5 ohms). ESCA lead depth profiles were made on Long Life™ MCPs of varying resistances, which received a range of processing schedules. The results indicated that the surface layer structure of very low resistance MCPs was essentially the same as that of high resistance MCPs - except that the lead concentration in the conducting layer was found to be considerably higher. This seems reasonable, in light of results [26] showing that a slight reduction (~20%) in the mean interatomic spacing of lead ions in the conducting layer (from 5.5 to 4.5 Å) increases conductivity by almost three orders. Moreover, the superficial secondary emitting layer (100-200 Å) appeared to be silica-rich in all cases, so that the very low resistance MCPs would be expected to have a channel surface with comparable secondary electron yield.

RESISTANCE CHANGE AND WARPING

A further concern was the electrical and mechanical stability of very low resistance MCPs. Standard resistance MCPs will normally undergo an increase in resistance (5-10%) over a period of several days, when kept in air at room temperature. This is presumably due to reoxidation of some of the reduced lead in the conducting layer. Very low resistance MCPs, with elevated amounts of reduced lead, could conceivably be more susceptible to this process. However when tested, they behaved no differently than standard MCPs.

When standard MCPs are subjected to a humid environment, the glass surfaces undergo hydration, with consequent volumetric expansion. Although the fraction of MCP active area glass which participates in this process is relatively small, the stresses generated in the interaction with the solid glass rim are large enough to cause warpage of the MCP. Although a correlation had earlier been noted at Galileo between lower MCP resistance and warping, the very low resistance MCPs were found to behave no differently than standard MCPs in this regard.

LOW NOISE GLASS

The low noise glass (Sect. 2.1.2) was processed according to the same schedules used to obtain very low resistance Long Life™ MCPs. The resistance values obtained were found to be essentially the same (~100 kilohms). This important step demonstrated that MCPs with both very low noise and very high bias currents could be successfully fabricated - the precondition for extremely wide dynamic range MCPs.

MCP GAIN

Although the ESCA lead depth profile verified the presence of a silica-rich secondary emitting layer in very low resistance MCPs, standard MCP gain performance could only be demonstrated through an operational test. We performed an analog gain experiment.

A very low resistance 134 kilohm MCP (40:1, 12 micron) was attached to a large copper heat sink, and held in vacuum (10^{-7} torr) for two days to allow outgassing. Bias voltages of 700 and 850 V were then applied sequentially. Analog gain levels of 550 and 2000 were respectively measured with an electrometer, at an input electron current (300 eV) as high as 100 nA cm^{-2}, roughly a hundred times higher than the maximum input current for standard resistance MCPs. This experiment demonstrated normal MCP gain levels, removing any concerns that the elevated concentration of reduced lead would somehow be detrimental. A crude lifetest was also conducted. Since the MCP generated about 5 watts of heat, the uncooled heatsink would heat up to over 80 °C within 15-20 minutes requiring that the MCP voltage be switched off and the heatsink allowed to cool. After three 20 minute "on" cycles with an input current of 100 nA cm^{-2} at 850 V, an abstracted charge of 0.2 to 0.4 C cm^{-2} was calculated. At this point, the gain had dropped to about 1400 (@850 V), or 70% its initial value.

LOW TEMPERATURE APPLICATIONS

These results may have implications for use of MCPs at very low temperatures. Standard resistance channel multipliers, when cooled to 77 °K and below, will undergo an increase of resistance of two to three orders of magnitude, severely degrading dynamic range. However, if the starting resistance (at room temperature) is on the order of 10^5 ohms, the cooled resistance will rise into the standard operating region of 10^7-10^8 ohms - possibly allowing normal MCP operation with standard mounting configurations and readouts. To demonstrate this, an MCP having a room temperature resistance of 228 kilohms was cooled to 77 °K. The resistance increased to 28 megohms. (However, it should be pointed out that the Stefan-Boltzmann law at such low temperatures requires the MCP temperature to rise several degrees higher than ambient.) Further experiments are underway independently of this program to characterize low temperature MCP behavior.

2.2.2 THERMAL CONTROL

Although MCPs having very low resistances and normal gain behavior had been fabricated, they would only be able to operate for a few seconds prior to thermal runaway in standard mounting configurations. Our task was to find a way to prevent this.

In Phase I a novel "sandwich" MCP was proposed which would allow very high output count rates, but which would avoid runaway Joule heating. As proposed, the sandwich or laminar MCP construction would be achieved by bonding together two MCPs of differing thickness and wall conductivity. The front plate would be roughly ten times as thick as thick as the rear plate, with a respective conductivity difference of about 1:10; the output section could resupply the large numbers of secondary electrons required in the multiplication process, on time scales short enough to allow pulse-counting channel recharge times of microseconds instead of milliseconds (the latter being typical of current MCPs).

In Phase I, it was calculated that only 1-2 watts of Joule heating would be generated by the bias current flowing in a sandwich MCP, as opposed to around 10 watts from a conventional MCP of comparable count rate capability. At the time, it was thought that radiative cooling from both faces of the sandwich MCP would dissipate the heat load, through control of radiative heat transfer to the surrounding tube enclosure (Figure 16).

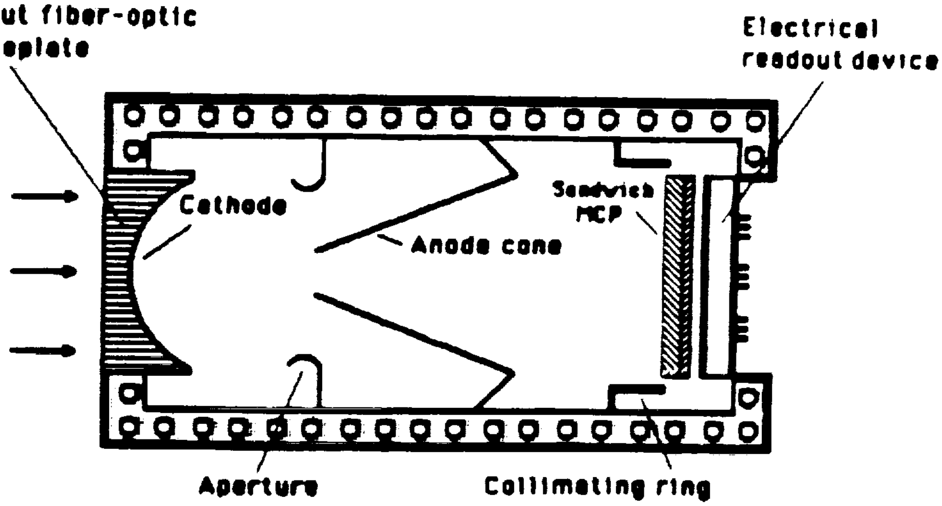

Electrostatic image-inverting tube with thermoelectric cooling jacket

Figure 16. Original high frequency MCP detector design, from Phase II proposal.
[for NASA Contract NAS1-18482]

Consequently, one of the earliest tasks in the Phase II program was to perform a thermal balance analysis of the proposed sandwich MCP. These calculations showed that radiative heat transport alone would be unable to prevent thermal runaway for any sandwich MCP configuration capable of gains larger than 10^5 (pulse-counting) and channel recharge times of 100 microseconds or less. Radiative transport, as shown by the Stefan-Boltzmann law (Sect. 1.2.1), could at most dissipate ~0.1 W/cm^2 from the sandwich MCP.

Since the program goal was to achieve pulse-counting recharge times as low as tens of microseconds, a different approach was needed. Clearly, given the MCP configuration required for high pulse-counting gains, a more efficient heat removal mechanism than radiation was called for. Since MCPs operate in vacuum, precluding convection as a heat removal mechanism, conduction into a solid was the only alternative.

Due to the disklike geometry of the MCP and low thermal conductivity of the glass matrix, the fraction of heat lost through the sides to electrode connections and mounting hardware is insignificant. Moreover, as shown in Fig. 2, the heat lost from the MCP rim would in any case have only a minor effect on the temperature at the center. The only solution, given the low thermal conductivity of the matrix glass in current MCPs, is to conduct the MCP heat directly out of the active area by placing it in complete contact with a thermal interface, in turn connected to a heat sink (Figure 17). Obviously, if it were placed across the input face, input radiation would be blocked (unless a thermally conductive grid with a high open area ratio were used preventing complete thermal contact). Consequently, the thermal interface would have to be mounted to the MCP output face, serving a threefold role as heat sink, charge collecting anode, and high voltage bias electrode.

Aside from the role as a heat sink, this configuration - with an anode collector directly attached to the end of a channel multiplier and serving as a high voltage bias electrode - is not without precedent (for single channel multipliers). Although it is more common to use a physically separate, electrically isolated collector with a single channel electron multiplier (CEM), for several years end-capped CEMs have been used for pulse-counting applications (Figure 18). Here, the signal connection is common with the high voltage, and must be capacitively coupled to the pulse-counting electronics (otherwise, it would be riding on the d.c. bias current). The motivation for this configuration has usually been to minimize the chances of channel wall contamination, by sealing off the end of the channel. However, the contact anode configuration was virtually never used with MCPs (although two references were found which did mention its use [27],[28]).

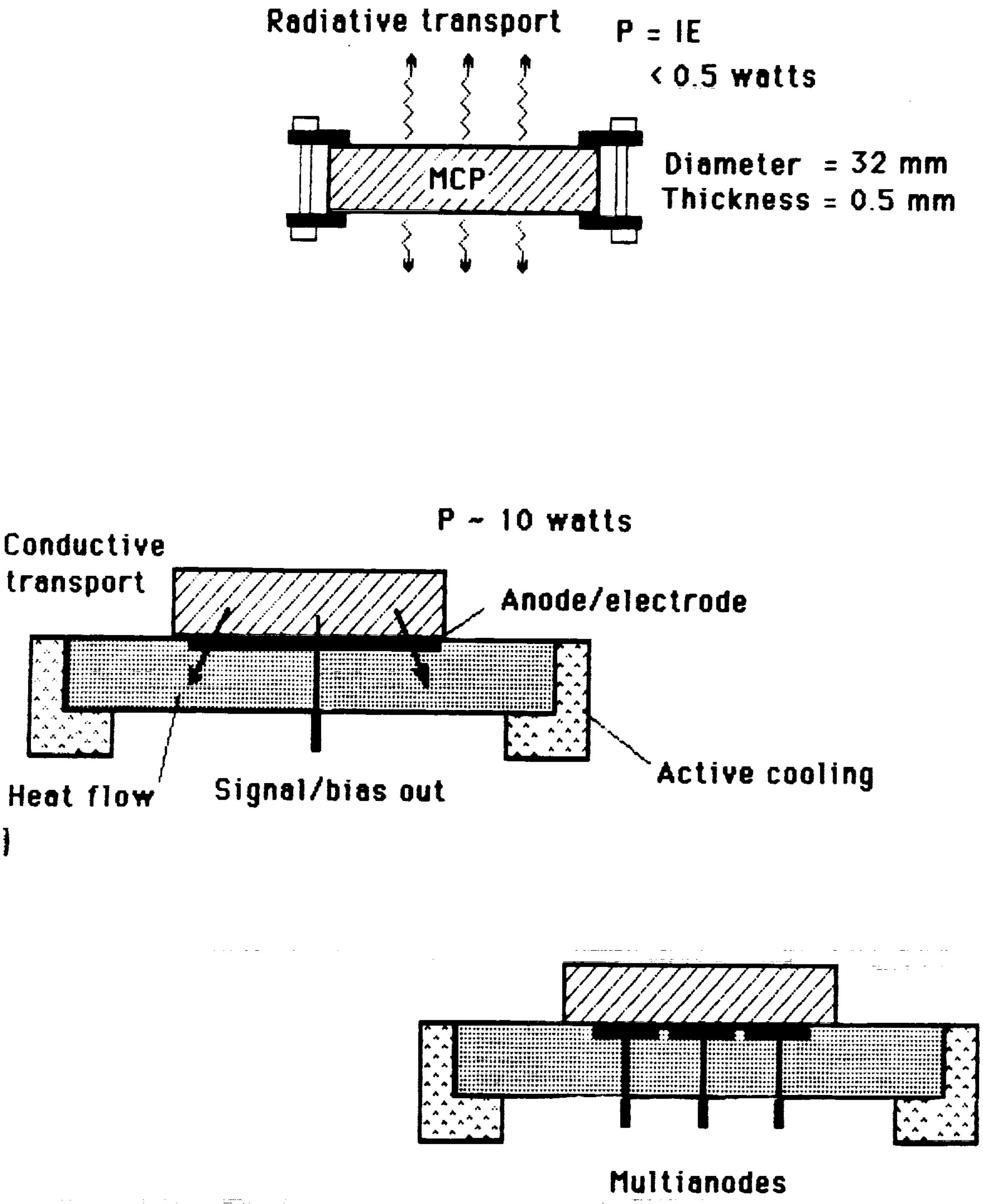

Figure 17. Radiative vs. conductive MCP heat removal.

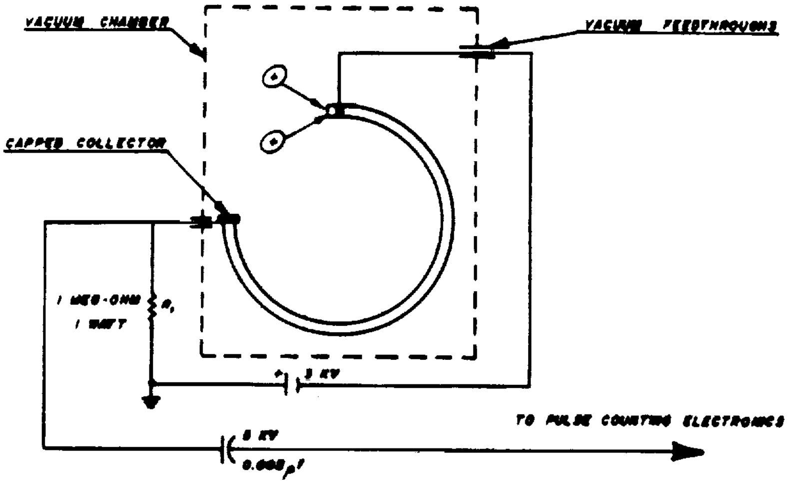

Figure 18. Capped anode pulse-counting single channel multiplier. [from Ref. 63]

THERMAL MODELING

To determine the plausibility of the unorthodox MCP heat sinking approach and to fully understand the MCP thermal behavior, we realized that some modeling work was needed. No adequate thermal models had ever been constructed for this configuration.

Numerical Thermal Model

The initial model used iterative techniques to obtain the temperature profile through an MCP mounted on a heat sink. This model convinced us of the plausibility of conductively cooling an MCP through the output face. Here, several of the significant MCP heat flow terms were temperature dependent, requiring numerical solution of the heat flow equation. Here, the heat flow differential equation is replaced by a set of finite difference equations. Such a system of linear algebraic equations can be rather easily solved by iterative techniques, since the matrix representing it is nearly diagonal.

Figure 19 shows the axial temperature profiles resulting from these numerical calculations. A single MCP channel (10 micron diameter, 40:1 L/D) was modeled with a negative temperature coefficient of resistance, roughly equal to that measured for standard MCP glass. Only conductive cooling was considered, since it would easily dominate radiative cooling at these temperatures. Curves are presented for heat dissipation ranging from 1 to 10 watts at the center of the MCP active area, where the temperature would be expected to be highest.

Figure 20 shows axial temperature profiles for a tandem MCP assembly, composed of channels with the same geometry as above. The power dissipation of the bottom MCP, bonded to a heat sink, was assumed to be 10 watts ($R_{mcp} = 10^5$ ohms), while that of the top MCP was varied between 1 to 3 watts. For the top plate, at an input power greater than 3 watts, the calculations failed to converge, indicating a condition of thermal runaway. Therefore, the temperature profile in a sandwich MCP would be expected to be very sensitive to the heat dissipated by the top MCP.

The "depth vs. dose" profile according to which an MCP is heated has a marked influence on the final temperature of the assembly. If this profile is shaped such that the most of the Joule heat generated is close to the heat sink, then large heat inputs will result in only a modest temperature rise. One illustration of this is Figure 21, comparing the temperature profile of a channel having a zero temperature coefficient of resistance with one having a negative coefficient of about -.01, typical for a Long Life™ MCP. (The change in resistance with temperature is commonly expressed as $R(T) = R_o(1+\alpha_o.dT)$, where R_o and α_o are respectively the resistance and temperature coefficient of resistance at some initial temperature.)

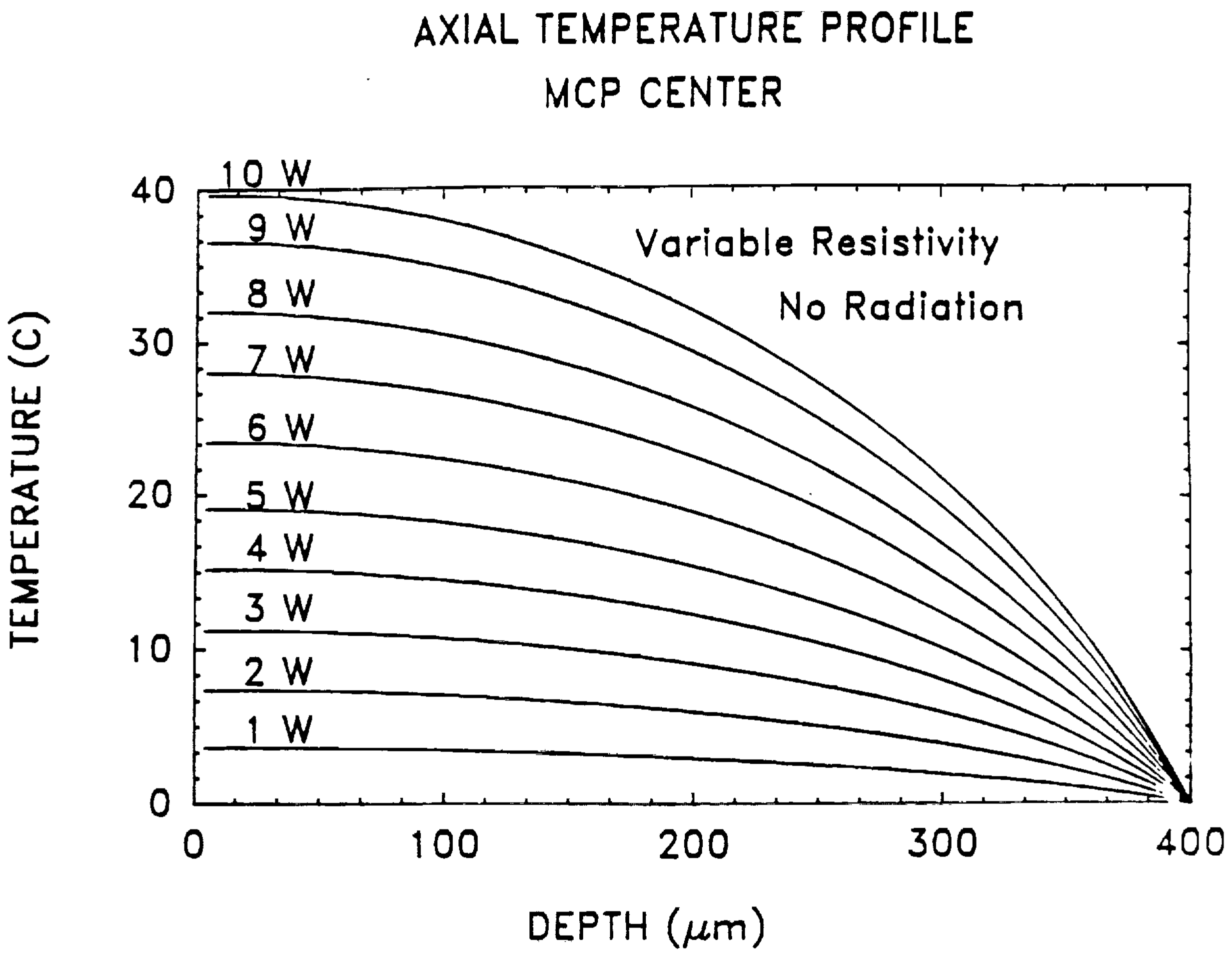

Figure 19. Axial temperature profiles for an MCP bonded to a heat sink, for a range of MCP power dissipation levels.

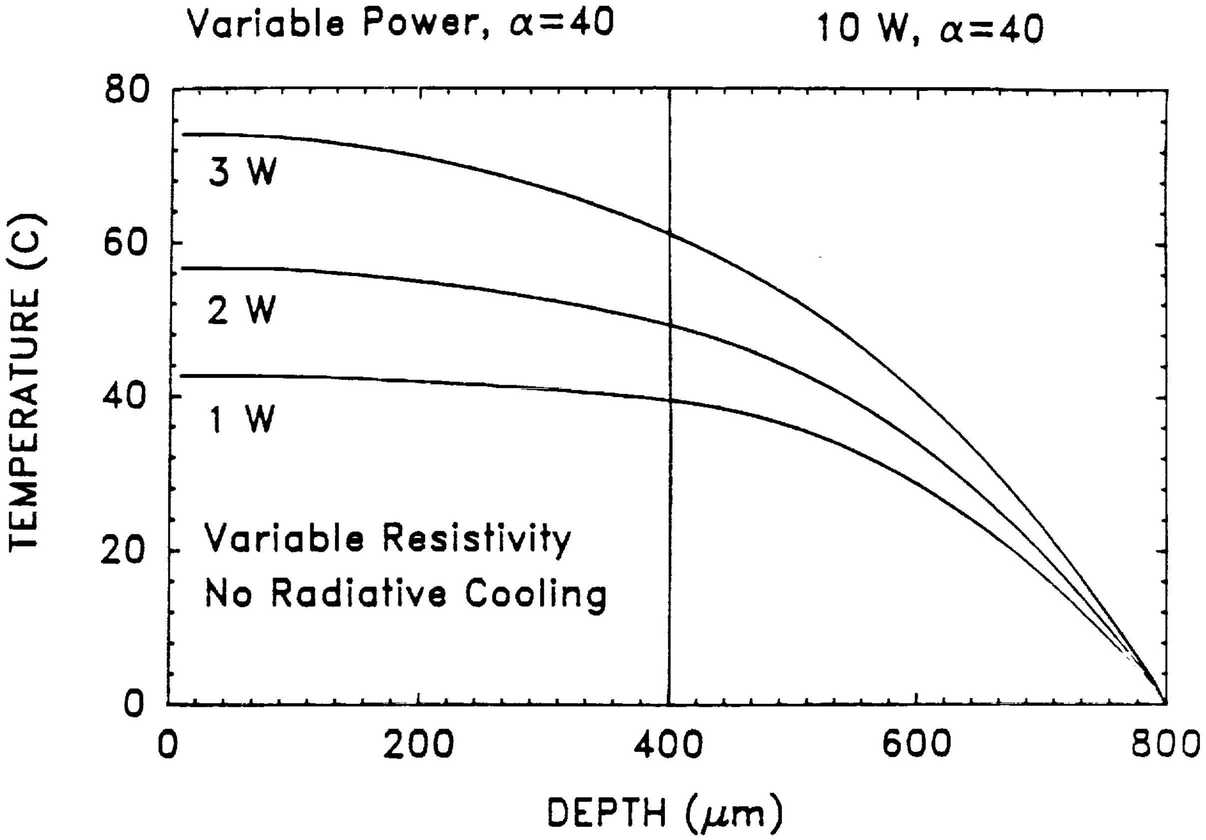

Figure 20. Axial temperature profiles for a tandem MCP (two 40:1 plates) mounted to heat sink. Rear MCP power level is 10 W, front MCP power level as indicated.

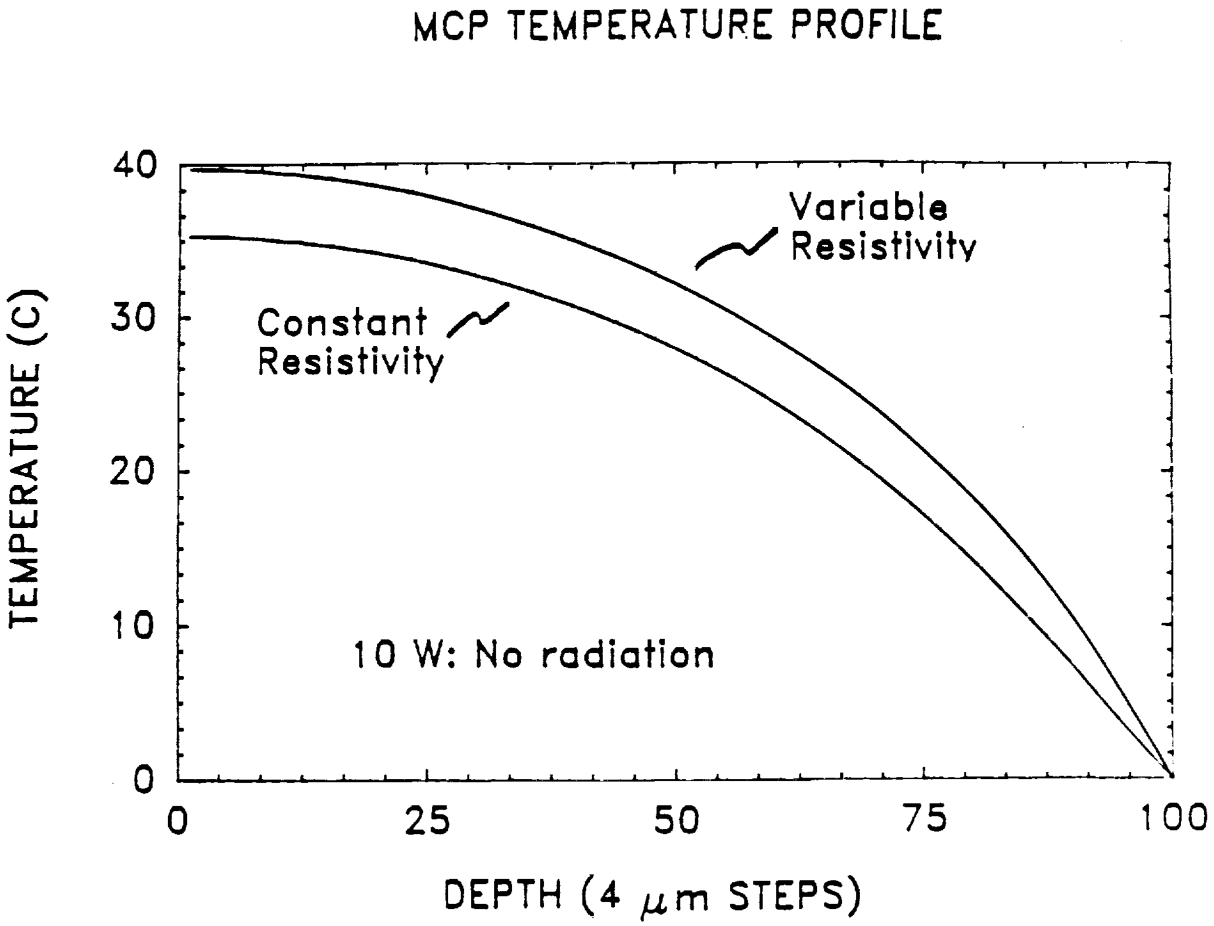

Figure 21. Comparison of channel having negative (-.01) and zero temperature coefficient of resistance.

Although the total heat input increases substantially (~30%) for the entire channel, the temperature increase at the top of the channel is only a few degrees. As mentioned above, this is because most of the additional Joule heat is generated rather deep in the channel, close to the heat sink (where the channel wall temperature is lowest).

Heat Dissipation from MCP Web

In a subsequent thermal model, developed to further aid our understanding of the MCP heat flow problem, a theoretical study of heat dissipation processes occurring within the interchannel web of MCP matrix glass gave an analytical expression for the web temperature profile. The maximum temperature rise at the MCP input face was computed for different combinations of physical and operational parameters. These results were then compared with the observed temperature rise to determine the accuracy of the model (Sect. 2.2.6 below). In all cases the MCP was assumed to be of conventional geometry, with a 25mm diameter active area.

An analytical expression was developed for the thermal profile of the interior of an MCP attached to a heat sink, for the case of fixed heat flux into the MCP web. The enthalpy source was assumed to be Joule heating caused by the MCP bias current. The temperature coefficient of resistance was assumed to be zero, to avoid complicating the model. Conduction was assumed to dominate the heat transfer process, and radiative dissipation was assumed minimal, with the maximum operating temperature only being in the 300-400 °K range.

The MCP thermal profile was determined by solving the heat conduction equation. The MCP web geometry is quite complex, having circular holes positioned in a hexagonal array. An acceptable approximation was to represent the web two-dimensionally with appropriate boundary conditions, as illustrated in Figure 22. The y-dimension extends from the bonded output surface of the MCP to the input surface. In the x-dimension the domain extends from the "midplane" between two adjacent channels to the channel wall. This geometric simplification resulted in a conservatively high estimate for temperature: the interstitial portion of the web was not included as part of the y-direction conduction path, and the calculated thermal conductance of the web was lower than its expected actual value. The calculated temperature rise was therefore higher than what would be expected. The temperature is directly proportional to MCP power dissipation and thickness, and inversely proportional to the glass thermal conductivity. Moreover, the web aspect ratio was also found to affect temperature.

The temperature field using typical values for geometric and performance parameters ranged between the ambient temperature and 21 °C above ambient. A lack of significant temperature

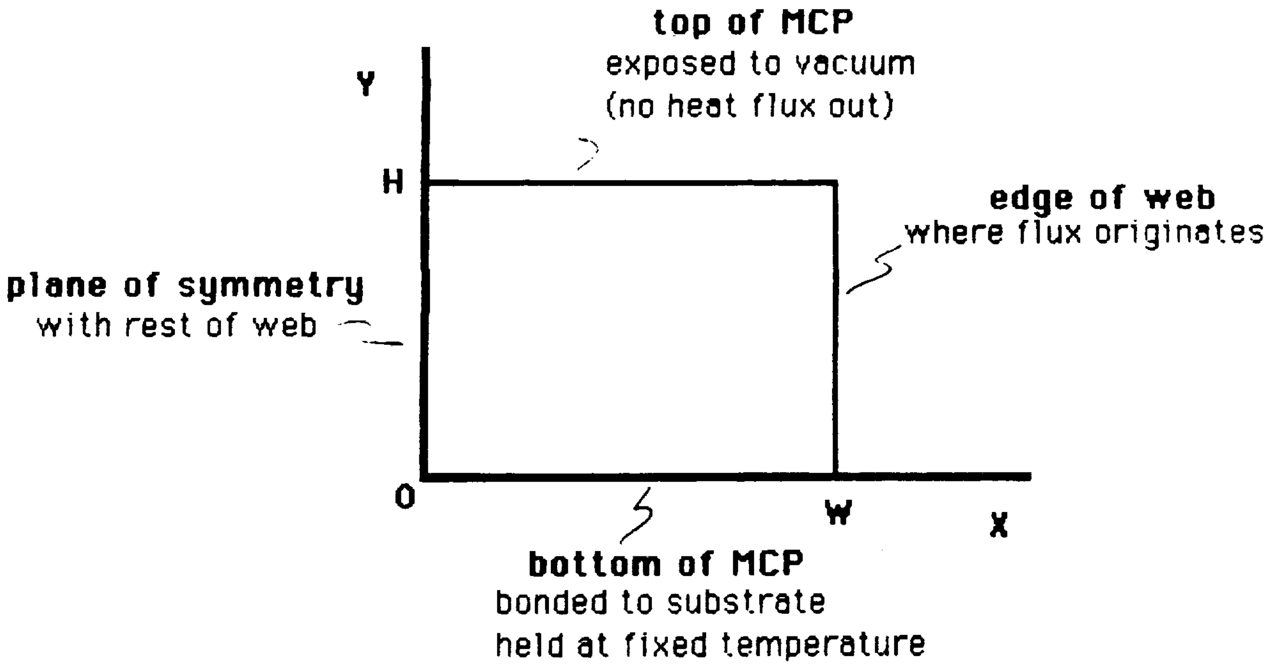

Figure 22. Two-dimensional MCP web model.

dependence on lateral position was shown. This indicated that the interior of the MCP web (between channels) is not appreciably cooler than the channel walls. Figure 23 illustrates this temperature profile. The maximum temperature rise occurs at the input surface.

Table 3 shows the influence of power dissipation on maximum temperature for a typical configuration. The output surface of the MCP, bonded to the heat sink, is assumed to be held at 20 °C. Note the direct power scaling of the temperature. Even with a power dissipation of 10 watts the estimated maximum temperature is a moderate 41 °C.

Table 3

MCP input face temperature vs. power dissipation
MCP output face held at 20 °C.
(Temp. coeff. of resistance = 0)

Power (watts)	Surface temp. (°C)
0.1	20.2
1.0	22.1
10.0	41.1
100.0	230.6

Heat Dissipation from MCP Substrate

In another study of the heat equation, we derived an analytical expression for the temperature profile within an alumina ceramic substrate, serving as the MCP heat sink. The temperature rise within the substrate was computed for different combinations of MCP physical and operational parameters. An analytical expression was developed for the thermal profile of the interior of an actively cooled alumina substrate bonded to an operating MCP. The power dissipated within the MCP was assumed to be conducted into and through the substrate, to the actively chilled perimeter. The total dissipated power was assumed to be evenly distributed across the MCP output surface. As before, conduction was assumed to dominate the heat transfer process. The substrate thermal profile was found by solving the Fourier heat conduction equation.

Mathematically the substrate was represented as a cylinder with no angular dependence, and with appropriate boundary conditions (Figure 24). The domain for the conduction equation in the radial direction extended from the central axis of the substrate to the actively chilled substrate perimeter. In the z-dimension the domain extended from the substrate rear surface to the top

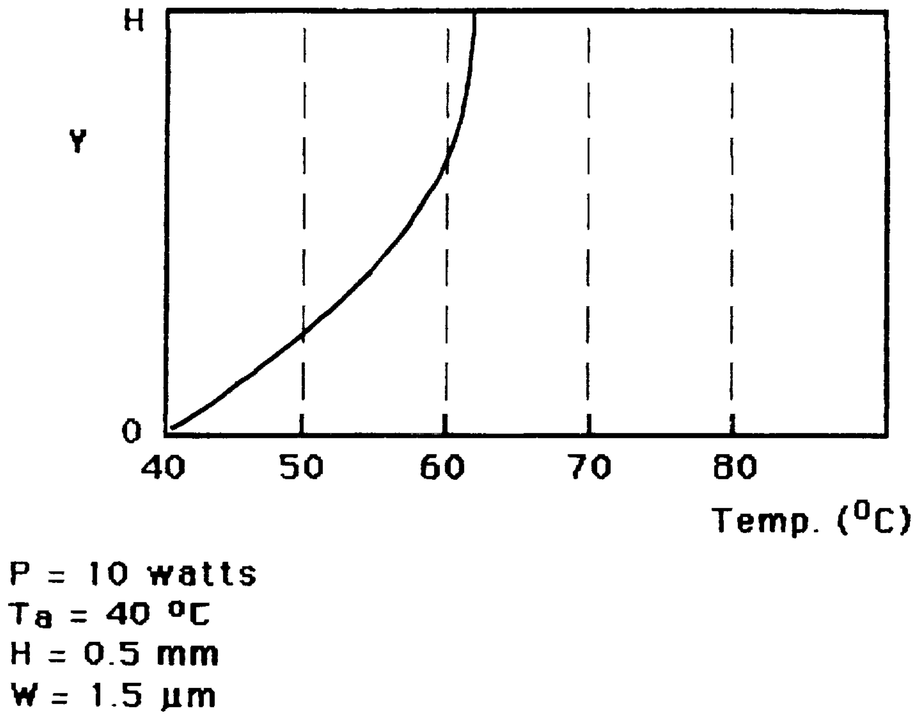

Figure 23. MCP web temperature profile.

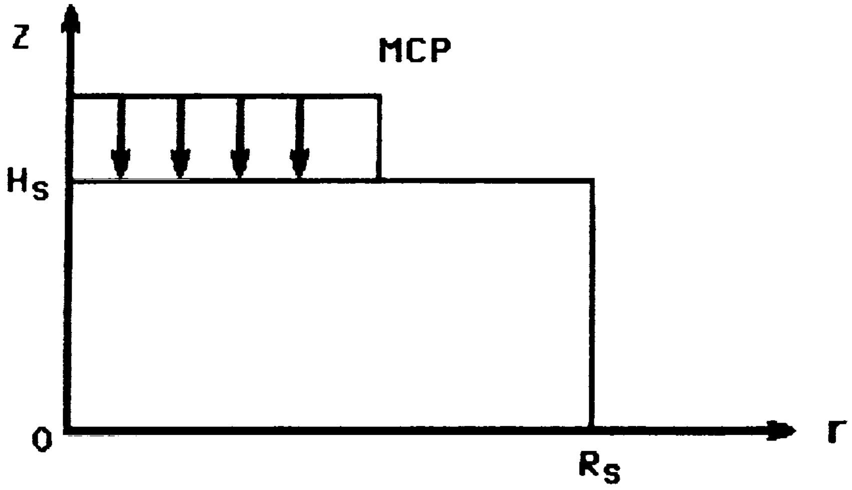

Figure 24. Cylindrical substrate model.

surface, where the MCP is bonded. The substrate temperature depended directly upon dissipated power, and inversely upon substrate thermal conductivity and MCP radius.

The temperature field was calculated using typical values for geometric and performance parameters. A lack of major temperature dependence on z was found. Figure 25 illustrates temperature profiles for the front and back surfaces of the substrate in a typical configuration with the substrate edge held at 20 °C. The maximum temperature rise occurs in the center of the substrate surface on which the MCP is bonded. In a typical configuration this maximum temperature is estimated to be 37 °C.

A parametric analysis was performed using the model. The maximum temperature within the substrate was calculated for several combinations of substrate thermal conductivity, substrate radius, and substrate thickness. The temperature range of the substrate surface in contact with the MCP was also calculated.

In the worst case examined, thermal conductivity was set at half the value reported for alumina, with the substrate radius at 10 cm, and the thickness 0.25 cm. In this somewhat extreme situation the maximum temperature was determined to be 200 °C, with the temperature range across the output face of the MCP around 39 °C. For a nominal design which could be used in this program (4.5 cm radius, 0.6 cm thick), the peak temperature was determined to be 37 °C with a range of 7 °C. Even more favorable temperature profiles were obtained by reducing the substrate radius, increasing substrate thickness, or increasing thermal conductivity.

Experimental Results

An experiment designed to check the analytical models was carried out later in the program. It gave reasonable agreement, and is reported in greater detail below (Sect. 2.2.6).

MCP HEAT SINKING

From the results of our thermal modeling, we felt confident in the plausibility of conductively cooling an MCP through the output face. The next task was to determine how to attach an MCP to a thermally conductive substrate, which was also required to be electrically insulating to allow electronic readout of the MCP.

Bonding

When it was determined that bonding an MCP to a heat sink would be required, we investigated the various approaches for bonding composite layers of glass (MCP), metal (electroding), and ceramic (substrate). To assist us at the start of this investigation, we enlisted the aid of a sealing and joining consultant.

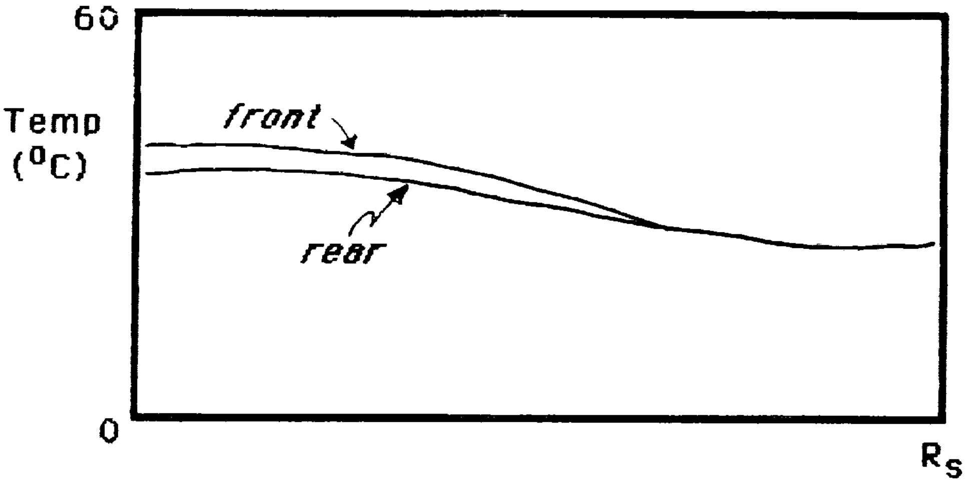

P = 10 watts
T_a = 20 °C
k = 0.167 W/cm-K

R_m = 1.6 cm
R_s = 3.25 cm
H_s = 0.75 cm

Figure 25. Substrate temperature profile, for front and rear faces of substrate.

The substrate material was the first topic discussed, and several possibilities were considered, including alumina, beryllia, and aluminum nitride. Although the latter two have high thermal conductivity, it was decided that alumina would be used for this program because of its ready availability, relative ease of fabrication, and almost perfect thermal expansion match with the MCP glass.

If the thermal expansion coefficients of both the MCP and the ceramic substrate are different, a stress field will develop as the assembly cools down from the bonding temperature. An MCP fabricated from either Long Life™ or low noise glass has a coefficient of about 77 (x 10^{-7}) $°C^{-1}$, while alumina ceramic ranges between 70 and 78 (depending on purity). Figure 26 illustrates the stress developed as the MCP/substrate assembly cools. Somewhat fortuitously, in actual operation as the MCP temperature rises above the heat sink temperature, this stress would be released. In any case, stress levels of around 1000 psi are not considered unusually high for an MCP, and a stress level twice this could probably be tolerated. Only if the MCP temperature increased 100 °C above the alumina heat sink temperature, or if the substrate material had a coefficient below 67 or above 87, would there be reason for concern. Moreover, a thick film bonding layer attaching the MCP to the substrate would act as a buffer layer, and would 'give' somewhat, further widening the safety margin.

Discussions concerned with bonding together two MCPs focused on the possibility that a very thin MCP, as proposed for the sandwich MCP output plate, would be highly prone to warping. Due to the thermal treatments used in manufacturing MCPs, a stress field can occur because of the interaction of the porous MCP active area and the solid rim. This will only worsen as the plate aspect ratio (thickness vs. diameter) diminishes, and is further exacerbated by hydration and swelling of the siliceous layer lining the channel walls. In order to insure a hermetic bond between two MCPs, almost perfect flatness is required for the various bonding methods discussed. This constituted a strong argument against using a very thin MCP (in addition to the other arguments concerning gain which will be discussed in Sect. 2.2.3).

For attaching an MCP to an alumina substrate, we investigated four different bonding approaches: 1) Mallory anodic bonding; 2) ultrasonic thermal diffusion bonding; 3) epoxy bonding; and 4) indium solder alloy bonding.

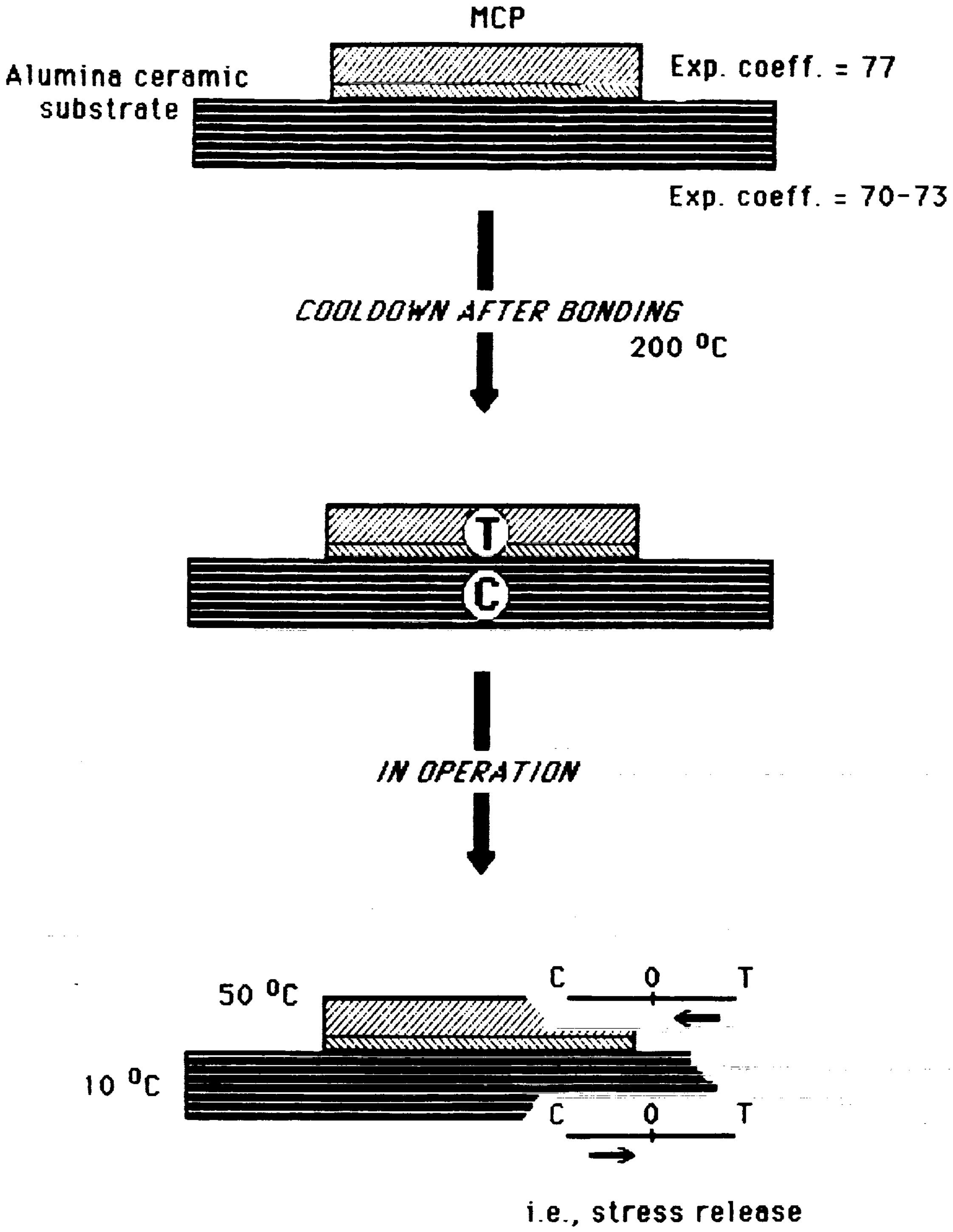

Figure 26. Stress configuration of an MCP bonded to an alumina substrate.

Mallory bonding

Mallory bonding is also known as field assisted metal-glass bonding. High voltage is applied across a glass-to-metal junction, at temperatures approaching 300 °C, the glass annealing temperature (Figure 27). Ionic migration in the glass coupled with electrostatic attraction results in a knitting together of the glass and metal [29].

The important parameters of this process are temperature, voltage, surface finish, and thermal expansion coefficient. The temperature required for Mallory bonding is 200-400 °C below the glass softening point. For Long Life™ glass, the corresponding range would be 240-440 °C. The voltage must be low enough to prevent dielectric breakdown. The surface finish is a key parameter, to insure precise contact between the two materials, since a roughness greater than 0.1 μm has been shown to result in poor bonding [30]. The thermal expansion of the two materials is important, otherwise stress will be frozen in upon cooldown.

A number of bonding trials were performed. Several 18 mm MCPs were bonded to glass slides coated with a thin film of nichrome alloy, using a hot plate. When bonding was attempted at various temperatures ranging from 300-440 °C, weak bonds were formed between MCPs and nichrome-coated glass slides. None of the resulting bonds were deemed adequate.

Ultrasonic diffusion bonding

Ultrasonic diffusion welding allows the bonding of similar materials at relatively low temperatures. This is accomplished by using ultrasonic vibrational energy to increase the temperature at the bonding surface. The method is commonly used for joining foils, plastics, and for producing high power-density metal parts for electric utility companies. Experiments were carried out to ultrasonically bond an MCP to an alumina substrate. The MCP and substrate were both gold-coated. Pressure and ultrasonic agitation were applied while the parts were heated to 200 °C. The resulting bonds were quite weak, and this bonding method was abandoned.

Epoxy bonding

The use of adhesives would seem to be a straightforward way to attach an MCP to a substrate. There are a number of conductive epoxies on the market; some of them have very low levels of volatile constituents, and therefore have low outgassing rates. Such epoxies have a wide range of working times and viscosities, allowing some latitude in epoxy application and sample alignment.

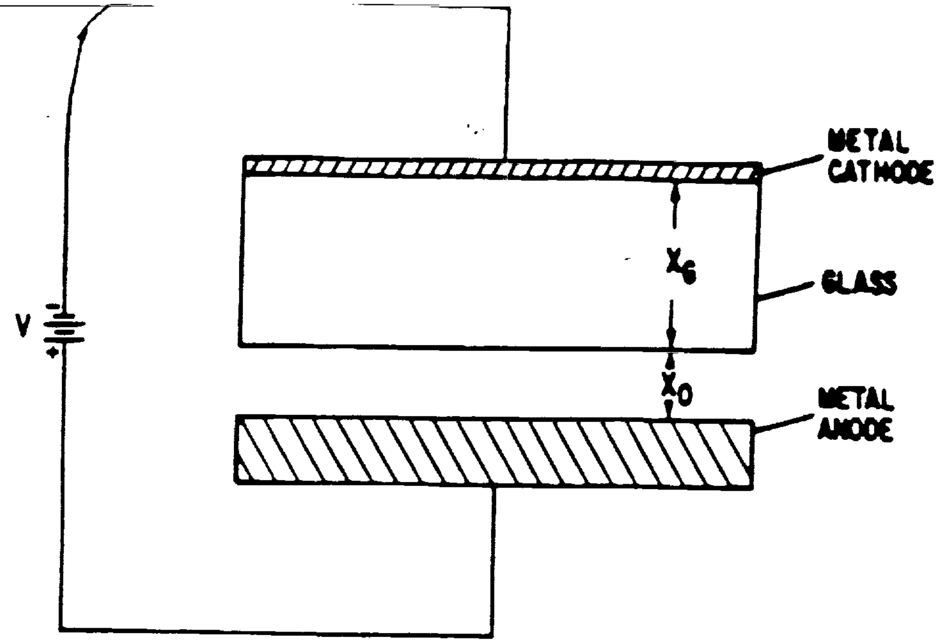

Nonconducting glass during anodic bonding.

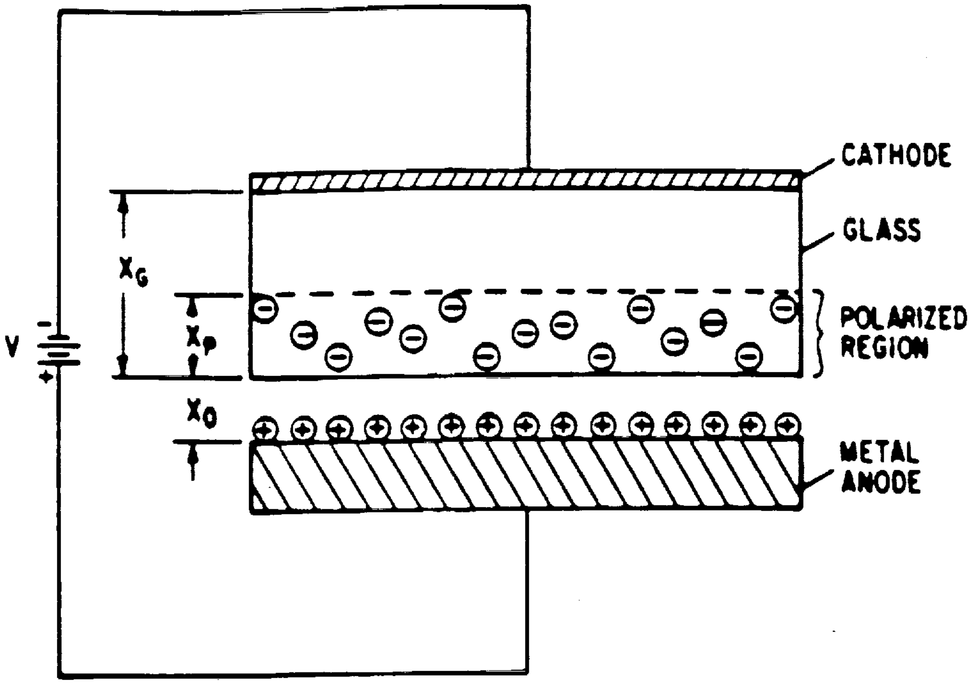

Conducting glass with a polarized region adjacent to the anode during anodic bonding.

Figure 27. Mallory glass to metal bonding process.
[from Ref. 29]

One of these epoxies was tried with excellent results, yielding a strong bond. However, there was a great deal of organic material on the surface of the plate when the epoxy was cured at room temperature. When the epoxy was cured at 150 °C, there were no visible contaminants on the MCP. Although not developed sufficiently for this program, this method has some promise for further development work.

Solder bonding

Low melting-point solder bonding was determined to be the most promising method for mating the MCP to a ceramic substrate. Of particular interest were indium-based solders. These solders have a low melting point, low outgassing rates, wettability with glass and ceramics, and aggressive alloying with certain metals. The wetting characteristics of the solder and the joint materials is a key factor in producing a good bond. Indium solders were bonded to a wide variety of materials in order to check both the bond strength and wettability. The experiments were conducted in air at a controlled temperature.

These experiments showed poor wetting of the solder to glass and ceramics, but excellent wetting of gold, copper, silver, and alumina. It was apparent that the MCP/substrate bond would have to include at least one of these three metals. Next, when the phase diagrams for binary systems of indium and metal were studied, it was apparent that the best alloying properties would be obtained with gold, which had the most favorable eutectic point. (The other metals would result in some crystallization.) Since the bond would undergo a large number of thermal cycles with an operating MCP, a strong bond was required. Currently, moly/manganese (Mo-Mn) is the material which has the greatest bond strength when fired onto alumina, and has been widely used for thick film ceramics, chip carriers, as well as vacuum headers. Since the Mo-Mn layer itself is not very wettable, additional layers would have to be bonded and plated to it.

Bonding method used

Finally, we arrived at the approach that yielded the best results for this program, given the available resources. As will be discussed in Sect. 2.2.4, we decided to use a 2 x 2 array of metal anode pads. These would serve as the MCP output charge collectors, bias electrodes, and thermal interface. They would need to be metallized onto the alumina substrate directly over the anode lead pins.

To attach the MCP to the substrate using the anode pads, a 3000 Å nichrome electrode pattern is first vacuum deposited (resistive heat evaporation) onto the MCP output surface, followed by a 6000 Å gold layer, evaporated through the same mask (Figure 28). Next, the alumina substrate is metallized (Figure 29). A Mo-Mn

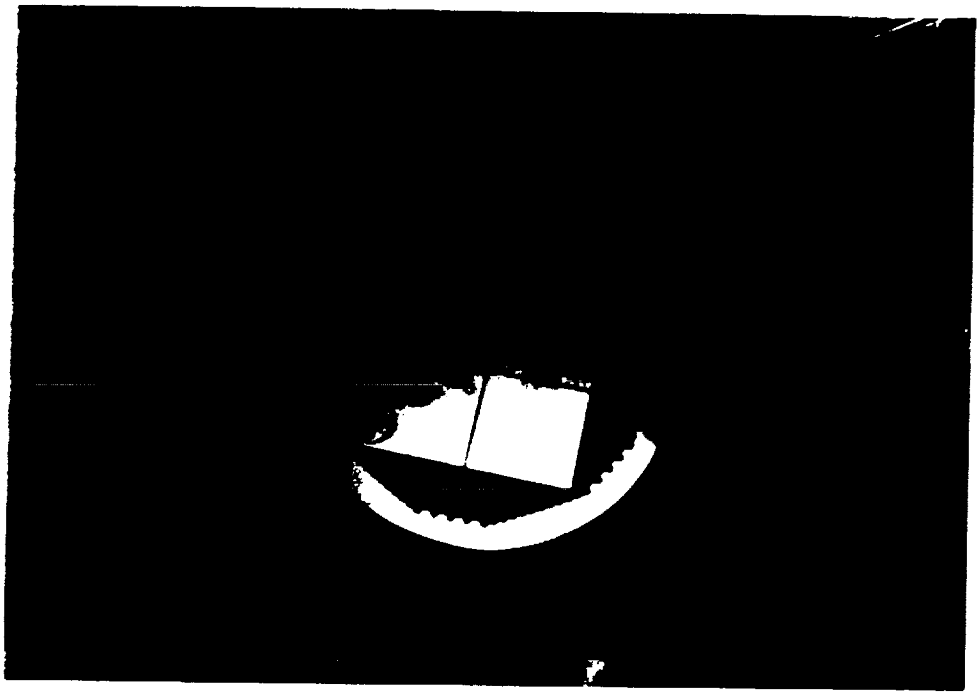

Figure 28. 2 x 2 MCP electrode pattern used with the solder bonding method.

SYM	DESCRIPTION	CHANGE NO	DATE	APP'D
	REVISIONS			
	PRELIMINARY			

Figure 29. Metallized alumina substrate specifications.

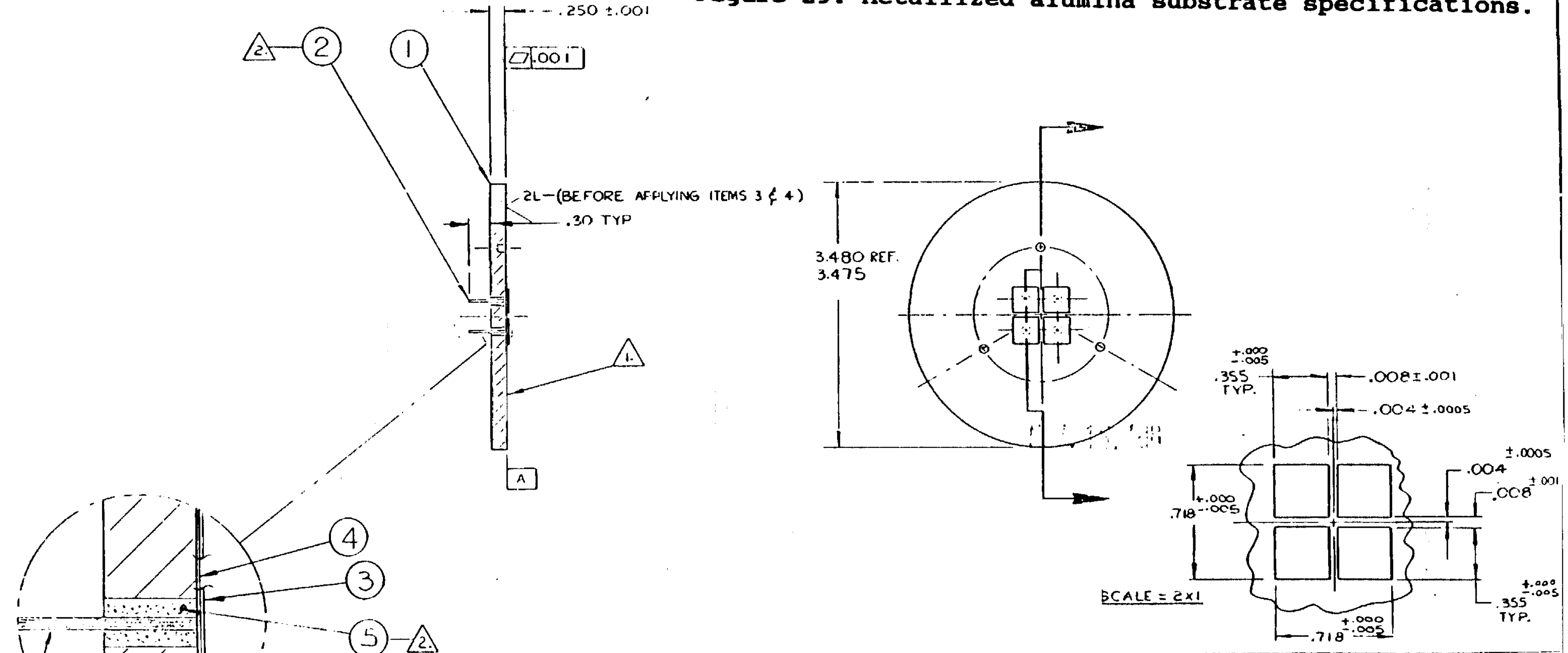

ITEM	QTY	DWG NO.	DESCRIPTION	MATERIAL	SPECIFICATION
5	A.R		GLASS, SEALER	7052	
4	A.R.		COATING, MOLY MANGANESE	MOLY MANGANESE	.001/.0015 THICK
3	A.R.	3412-0002	GOLD OVERCOAT	GOLD	3000 - 5000 Å THICK
2	4		PIN	KOVAR OR EQ	.028 DIA. x LG. TO SUIT
1	1	3399-0040	SUBSTRATE	ALUMINA	

NOTES:

1. MUST BE VACUUM TIGHT TO 10^{-8} TORR, ACROSS ENTIRE SURFACE.

2. PIN SEAL METHOD IS OPTIONAL ,TO SUIT VENDOR. PINS TO BE MACHINED & LAPPED FLUSH TO SURFACE "A" HAVING 2√ FINISH.

UNLESS OTHERWISE SPECIFIED

REMOVE BURRS & BREAK SHARP EDGES

125√ FINISH ALL OVER

UNLESS OTHERWISE SPECIFIED
DIMENSIONS ARE IN INCHES
TOLERANCES

INCHES		MILLIMETERS	
.X	± .030	X.	± 1.
.XX	± .015	.X	± .5
.XXX	± .005	.XX	± .10
ANGLES	± 1°	ANGLES	± 1°

MATERIAL:
SEE PARTS LIST ABOVE

PROCESS:

NEXT ASSY. NO.

	BY	DATE
DRAWN	DANO	10-11-88
CHECKED		
APP'D		
APP'D		

APPROVED

APPROVED

Galileo Electro-Optics Corp.
STURBRIDGE, MASSACHUSETTS

TITLE
SUBSTRATE SUB-ASSEMBLY
SHEET (1)

SIZE	CODE IDENT NO.	
C	28719	3399-0041

SCALE FULL | PROJECT 30974 | SHEET 1 OF 2 thick film pattern duplicating the MCP electrode pattern is fired at 1450 °C onto the alumina. Nickel oxide is silk-screened onto the Mo-Mn, and placed in a reducing atmosphere to obtain a nickel coating. Indium alloy tape is then carefully applied over the nickel pads on the substrate. The MCP is carefully positioned over the substrate, so that the electrode pattern is registered with the anode pads, and light pressure is applied using mounting hardware.

The assembly is then heated to 200 °C in a hydrogen furnace for several hours, and reflow soldering of the indium (m.p. 118 °C) occurs (Figure 30). Very close pad spacings have been tried with this approach; the surface tension of the indium is sufficient to prevent it from spreading to adjacent pads spaced only 200 microns apart. This process has been found to result in a very strong, hermetic bond between MCP and the substrate metallization, with essentially no contact resistance. (Obviously, it is important that the MCP or the substrate not be heated above the solder melting point.) No significant penetration of the indium solder into the MCP channels was noted, which might otherwise lead to gain reduction through "end spoiling", reducing the effective channel length.

There is one potential concern with this technique, however. The MCP output face metallization pattern must be precisely registered to a discrete anode pattern appearing on the anode substrate, in order to maintain anode electrical isolation. Although indium solder bonding can still be used for higher pixel densities, (for example, the flip-chip solder bump bonding method), the approach used in this program is probably only useful for the current 2 x 2 prototype device. Further development work would be required for higher pixel density arrays.

Substrate Fabrication

Quotes were requested from three different ceramics houses for providing the alumina substrates. Only one ceramics house provided a quote, due to the limited size of the order. This vendor claimed it could only process the substrates as far as substrate wafer fabrication, and the drilling of via holes and blind holes. Following this, the substrates would have to be sent to another vendor for metallization of the actual anode pads and pinout leads, and for the addition of mounting studs.

Galileo had previously done business with the ceramics house that responded, and they assured us that they could meet our requirements without difficulty. The main requirement was that the substrate have a thermal expansion coefficient between 72 and 77, to prevent large stresses from developing. The substrate

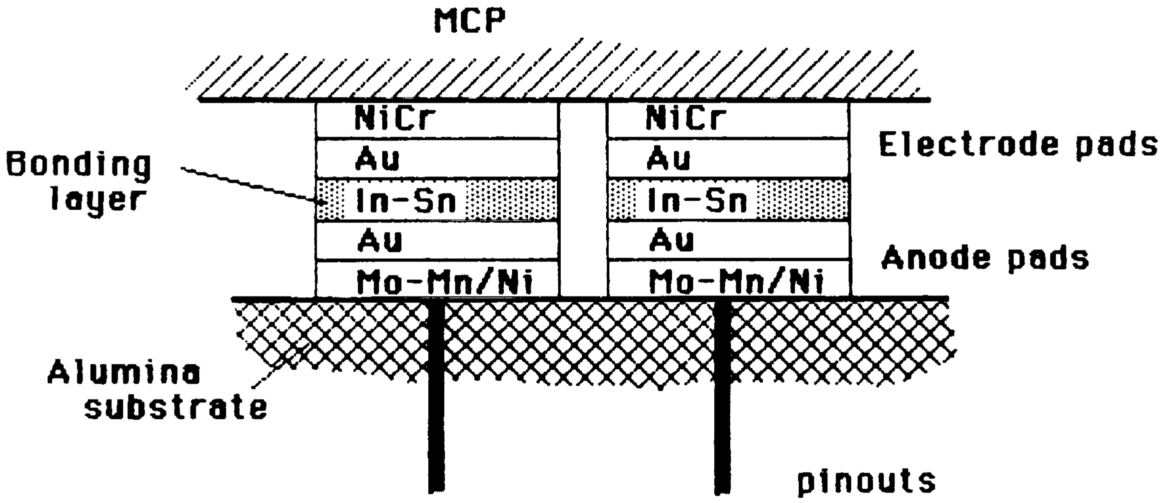

Figure 30. Indium alloy solder bonding process, used in this program.

fabrication took somewhat longer than planned, and then the substrates were sent to the metallization house. When metallization was attempted with the substrates, considerable difficulty was encountered in getting the metal to wet the alumina. Although the supplied material was 96% alumina as originally specified, there appeared to be an inadequate degree of "glassy phase" in the fired ceramic, which is necessary for achieving good wetting and bonding with common refractory metallization mixtures. The metallization mixtures typically used on 96% alumina did not work very well, failing to adhere properly and failing to provide a leak-tight seal after brazing. Microphoto-graphs then showed that the ceramic was too dense, with the proportion of glass being too small for attainment of a strong metal-glass bond. Next, the substrate vendor was asked to provide a 94% purity alumina sample for tests. This sample underwent metallization with the standard mixtures used for 94% alumina. All test results were positive, and these samples behaved as well as standard 94% alumina material supplied by other vendors.

Because of time constraints, we were unable to obtain finished substrates made from 94% alumina. The ceramic house claimed they would have to retool in order to fabricate them, and the lead times were prohibitive. MACOR was suggested as an alternative, but a simple thermal calculation performed earlier had showed that MACOR would not be able to remove the heat generated from a very low resistance MCP.

Consequently, considerable unplanned effort was expended in metallizing the 96% alumina substrates. Fortunately, good results were eventually achieved, with the Mo-Mn/Ni approach outlined above. Although some spots on two of the anode pads showed poor adhesion, so that the metal actually peeled off, the other metal areas remained well-bonded (Figure 31). Later, a thin-film gold layer was evaporated onto the Ni pads at Galileo, filling in the remaining weak spots. The other problem encounted during metallizing was the difficulty in achieving a hermetic ceramic to metal seal for the pin leads. However, this was solved through the use of a vacuum seal compound on the rear (air) side of the substrate, at the points where the pins exited the vias.

In retrospect, the metallization problem could not have been predicted. At the outset, both vendors were confident that the materials were well-matched, although they had not actually been tried together. Although 96% alumina from a different ceramic vendor may have behaved differently under metallization, the fact remains that no other vendors responded. The learning curve is now behind us; if future work occurs with higher pixel density substrates, 94% alumina can be used with complete confidence.

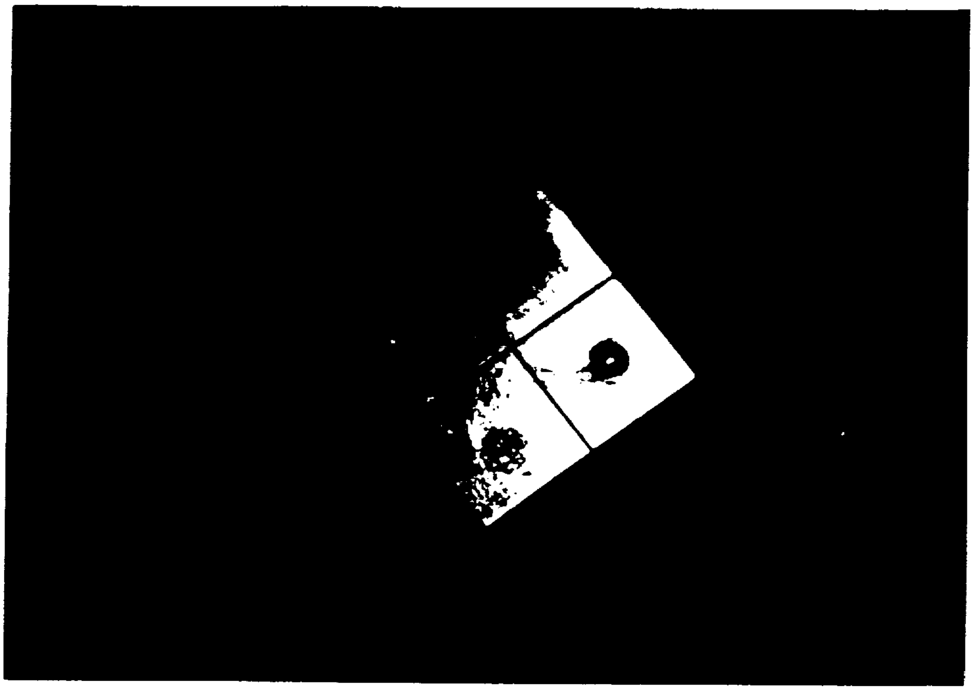

Figure 31. Metallized anode pads showing areas of poor metal adhesion. A gold coating was added to fill in any open areas.

2.2.3 MCP CONFIGURATION

High bias current MCPs in direct contact with a heat-sinking contact anode must operate in the pulse counting mode since the bias current must be decoupled from the signal processing electronics. For pulse counting MCP operation, requiring peaked PHDs at gain levels above 10^5 (to properly activate the electronics), MCPs with straight channels will almost always give rise to regenerative ion feedback, an unstable condition where residual gas in the channel is ionized by the electron cascade. These positive ions accelerate up the channel towards the input, where they collide with the channel wall, causing spurious electron cascades. To circumvent this, the straight channel geometry must be modified so that the ion drift path is shortened, and the kinetic energy gain prior to impact is too small to result in a significant secondary electron yield. Two methods for achieving this are commonly employed: 1) curving the channels, and 2) stacking multiple MCPs with angled channels, so that ion trajectories are intercepted at the interplate boundary.

The MCP stacking configuration can be a tandem (2 MCPs), or a Z-stack (3 plates), and stacks of up to five MCPs have even been constructed at Galileo. A tandem composed of two 40:1 MCPs will have high gain, ~10^7, since the input plate charge cloud spreads into several channels in the output plate. If the MCPs are stacked together with no gap, then the electrons from the input MCP spread into three channels of the output (assuming equal channel diameter). If there is a gap (typically 50-150 microns), many more channels will be involved, giving a higher gain but a degraded PHD (100-200% FWHM), since the output channels will be more weakly saturated. (However, the PHD can be improved by applying a bias voltage across the gap, diminishing charge cloud spreading.) Curved channel MCPs, in contrast, have a lower gain than a tandem, for a given channel diameter and L/D, since only a single channel will be used for each input event. For the same reason, when operated in saturation, the curved channel PHD will be tighter (30-50% FWHM).

SANDWICH MCP

In the Phase II proposal it was thought that a sandwich (i.e., tandem) MCP would be required, having a very thin and highly conductive output section in order to attain channel recharge times approaching 10 microseconds, while avoiding runaway Joule heating through radiative dissipation of 1 watt or less. This thin MCP section was to be no thicker than 100 microns, with an L/D of around 10. However, during the first month of the Phase II program, calculations showed that this configuration would be unable to avoid thermal runaway, if the only way to dissipate MCP heat was through radiation. Conductive cooling of the MCP was then proposed (Figure 17).

Somewhat later, gain calculations were carried out to study the feasibility of the sandwich MCP configuration if it was attached to a heat sink. It was found that pulse-counting gain levels of 10^5 could not be generated in a tandem with such a thin output section, at recharge times as low as tens of microseconds. A maximum achievable input MCP gain of ~4000 was calculated, constrained by the fast recharge requirement. The gain G_c of coupled MCPs in tandem configuration is given by the empirical relation [32],

$$G_c = G_f^{1-\beta} \cdot G_r \cdot N_c^{\beta}$$

where G_f and G_r are the respective front and rear MCP gains, and N_c is the number of channels in the rear MCP illuminated by a single front MCP channel (3 for a sandwich MCP). For 12 micron channels, β is 0.6. To attain $G_c > 10^5$, given the maximum allowable front plate gain G_f, this relation implies that $G_r > 2000$, a level impossible to achieve with current MCPs having an L/D < 10. Consequently, the results of a simple gain analysis showed that a heat-sunk sandwich MCP with a thin output section would be unable to achieve the short channel recharge times needed.

It was then calculated that an output MCP having an L/D greater than 30 would be required, using a computer program able to predict channel recharge times for a range of input and output MCP L/D ratios and resistance values, at gain levels above 10^5. (The program included the effect of a nonuniform thermal profile along the MCP channel axis, leading to a nonuniform potential distribution). It was found that an L/D of 40 could be used for both input and output MCPs, with an input plate resistance of 10^6 ohms, and an output MCP resistance of 10^5. This choice of L/D ratio was not of course entirely fortuitous, due to the ready availability of finished MCPs of this geometry, making special grinding and polishing treatments unnecessary. Moreover, thicker MCPs imply greater mechanical strength, and hydration warping would be less likely.

Nevertheless, there were concerns regarding the PHD of a tandem with 40:1 plates operating below its maximum gain capability, leading to a possible conflict between the requirement for fast channel recharge (low gain) and a tight, pulse counting PHD. The tightest tandem PHDs are achieved when the output plate is operated under conditions of hard saturation (i.e., high gain). This conflicting requirement, combined with concerns about the bonding of separate MCPs to allow uniform heat flow (Sect. 2.2.2), as well as the requirement for two separate power supplies connected to a center tap located at the interplate boundary, led us to consider using a single curved channel MCP. In addition, the following heat sink experiment, which tested the heat dissipation capability of a 40:1 MCP, gave further evidence that use of a curved channel plate might be a more sensible alternative.

A 40:1 25mm MCP with a resistance of 110 kilohms (@ 21 °C) was attached to a thermally conductive heat sink, a large nickle-coated copper block, which was not actively cooled (Figure 32). A thick film of indium was used to bond the electroded MCP to the block. As the MCP voltage was stepped up to 1070 V, the MCP remained thermally stable, reaching thermal equilibrium within a second or two at each step, with the MCP heat quickly being removed into the substrate (Table 4). No instability was observed in MCP strip current (an accurate reflection of MCP temperature stability-). The maximum power dissipation with thermal stability was 14.6 watts (13.7 mA @ 1070 V). Above this level, thermal runaway occurred. On the basis of the drop in MCP resistance, the MCP temperature rise was determined to be 20-25 °C. (There is reason to believe that even higher power dissipation levels are possible with 40:1 MCPs: the indium film we used in this crude experiment was somewhat thicker than necessary, and active cooling was not employed.)

For a single 80:1 curved channel MCP, twice as thick as the MCP used in this experiment, the 'center of gravity' of Joule heating would be expected to shift further away from the heat sink. Nevertheless, it would still be closer to the heat sink that the midplane, due to the thermal profile (higher local resistivity, $P = V^2/R$). Obviously another experiment was called for, using an 80:1 MCP. A 1 mm thick, 80:1 25 mm diameter curved channel plate (25 micron channels) was bonded to a 0.7 cm thick alumina substrate with a 1 cm^2 gold-plated metal surface pad. The output face of the MCP was electroded with a 1 cm^2 gold electrode. An indium film was used to join the MCP and substrate. When the voltage was stepped up to 1600 V, the MCP remained thermally stable, at a bias current density of 1230 $\mu A/cm^2$, corresponding to a power level of 2 W/cm^2. (Over the 4.9 cm^2 area of a 25 mm MCP, this would be equivalent to 9.8 watts.) The integrated power dissipation into the substrate was calculated, and the substrate temperature increase during the experiment was determined, knowing its heat capacity. The effective MCP temperature rise above the substrate was determined to be 44 °C, on the basis of the decrease in resistance.

A computer gain simulation was then carried out, which included the effect of a nonuniform thermal profile along the MCP channel axis. The channel length was divided into ten sections, with each section having an independent gain given by an analytical formula [33]. The MCP was assumed to be bonded to a heat sinking substrate, with the MCP output face pinned to the substrate temperature. A resistance profile was derived from the thermal profile, giving the potential distribution along the channel. The section gains were then convolved to give the total channel gain, as a function of the effective MCP temperature rise above the substrate (Figure 33). It is important to note that, as the MCP temperature rises, the resistance profile (hence potential profile) becomes

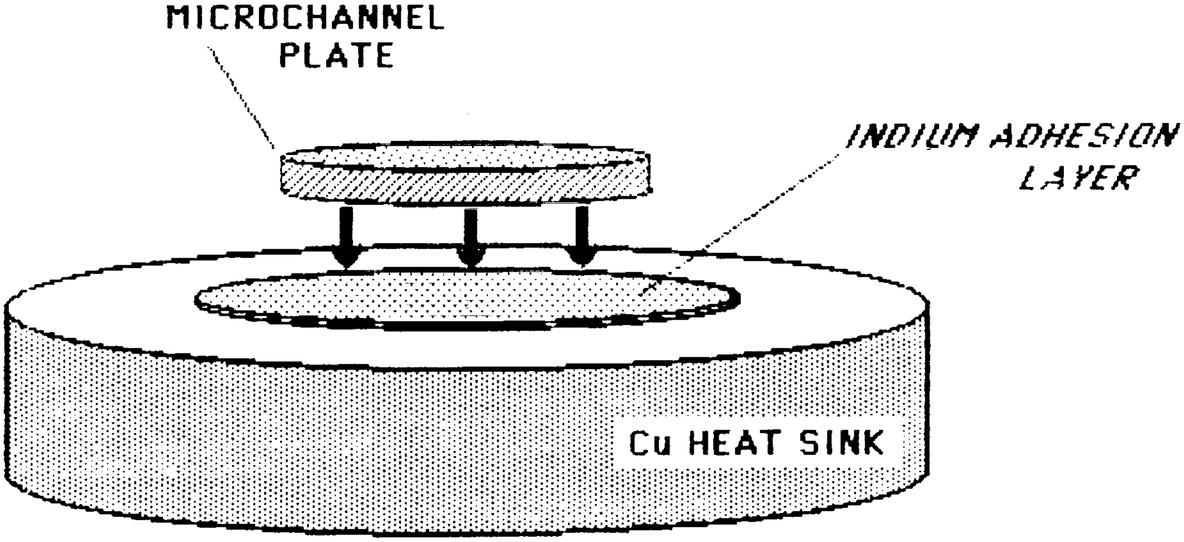

Figure 32. Initial MCP heat sink experiment. A 40:1, 25mm MCP (110 kilohms) attained a power level of 14.6 W without thermal runaway.

Table 4

MCP on heat sink, indium thick film bond
25 mm diameter, 40:1 L/D, 10 micron pore

Active area 4.9 cm^2

V_{mcp}	I_s	P (= $I_s V_{mcp}$)	R_{mcp} (= V_{mcp}/I_s)
0 volts	0 microamps	0 watts	- kilohms
100	941	.09	106.3
200	1898	.38	105.4
300	2880	.86	104.2
400	3898	1.56	102.6
500	4950	2.47	101.0
600	6060	3.64	99.0
700	7220	5.05	96.9
800	8510	6.81	94.0
900	9750	8.77	92.3
1000	11500	11.50	86.9
1070	13700	14.66	78.1
1070+	unstable	-	-

Initial MCP resistance:

R_{mcp} (V=0) = 109.6 kilohms

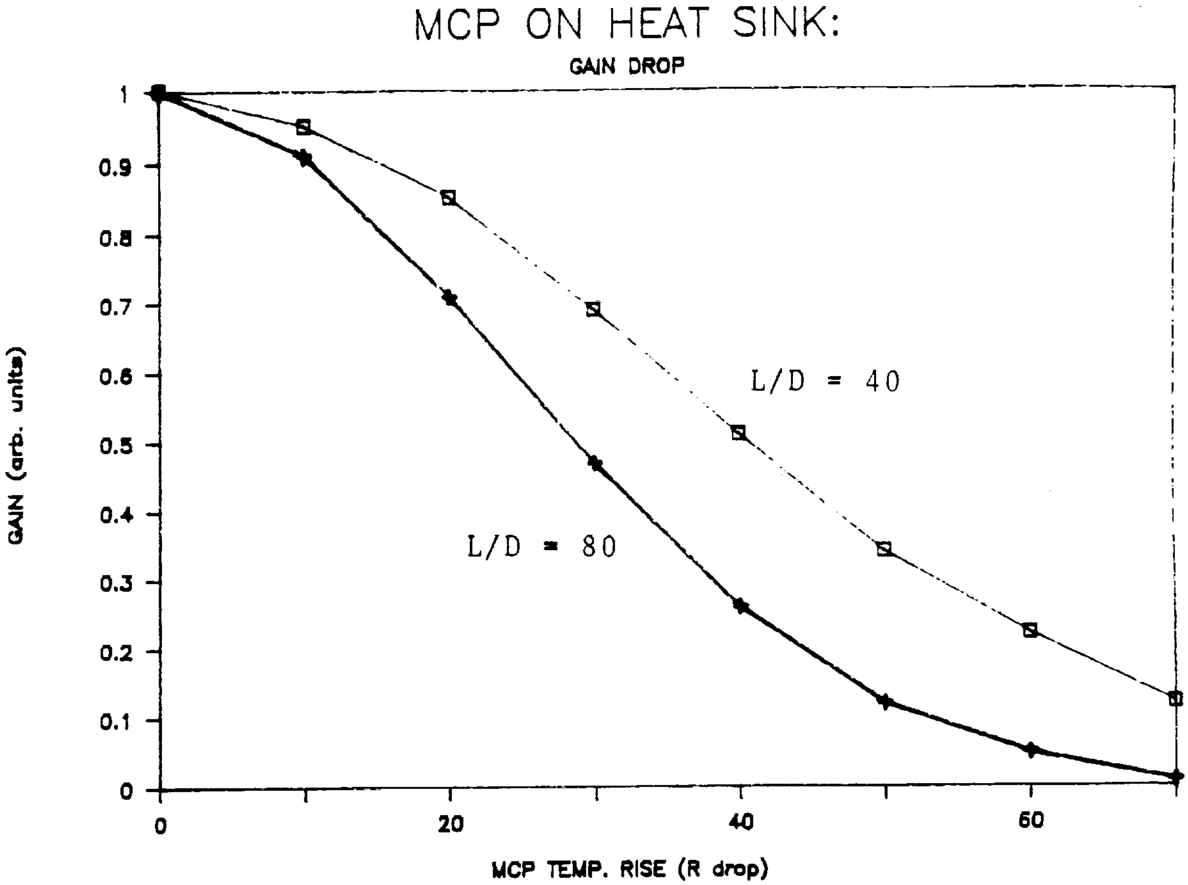

Figure 33. MCP gain reduction, as average MCP temperature rises above heat sink temperature.

increasingly nonuniform, resulting in a reduction in gain, with longer L/D channels being more sensitive. Clearly, the MCP temperature rise should be minimized, to optimize the gain for a given bias voltage (hence power dissipation).

Given the promising results for heat sinking an 80:1 MCP, the decision was made to abandon the sandwich MCP approach, and to use an 80:1 curved channel MCP instead. Aside from the concerns mentioned above for a sandwich MCP (bonding, power supplies, center tap) there are further advantages:

-Charge cloud sharing between channels of the rear MCP in a tandem degrades spatial resolution; on average, a charge cloud exiting a single channel in the front plate, if the plates are in contact, will enter no less than three channels in the rear plate (assuming equal channel diameters). As mentioned above, this degrades the PHD, due to the larger statistical spread in pulse amplitudes from a single event activating many channels in parallel.

-There will be less parasitic capacitance and inductance coupled into a contact anode circuit, since MCP electrode spacing is doubled, and one power supply circuit is eliminated. This will help keep time constants (and pulse widths) as narrow as possible.

-Mechanically, a single MCP is superior to a sandwich MCP (of equivalent thickness) in terms of flatness and strength. This is useful during bonding of the MCP to a ceramic substrate. It also circumvents possible hot spot formation, which might occur in the sandwich MCP if the MCPs warp and separate, causing loss of thermal contact.

-The count rate performance of a single curved channel MCP is superior to a tandem, all else being equal. For the tandem, the charge exiting a single input MCP channel is shared with several channels in the output MCP. Conversely, each channel of the output MCP sees several channels of the input MCP, and is activated at a higher effective rate. Also, the gain of a tandem tends to be higher than for single MCPs of the same overall L/D, slowing the recharge process. There may also be a third factor, not usually considered. As mentioned in Sect. 1.2.1, recent work indicates that the count rate capability of MCPs depends upon the area illuminated, where local channel dead time increases with the MCP input area illuminated. It has been suggested that capacitive coupling between active channels is responsible, since this raises the time constant. A multilayer MCP stack might possibly worsen the situation by adding interplate channel coupling to lateral intraplate coupling.

-Finally, curved channel MCPs confer a benefit for applications involving UV photon detection. UV reflections down straight channels are known to degrade MCP gain and PHD [27]. Channel curvature mitigates this problem.

Final configuration used

With the above in mind, we arrived at a desired configuration. It would preferably be a 25 mm 80:1 curved-channel plate with 12 micron pores (Table 5), having a room temperature resistance (23 °C) across the active electroded area (2 x 2 electrode array, .76 cm^2 per electrode) equivalent to 500 kilohms across an MCP of 4.9 cm^2 active area. It was further expected that the plate would heat up somewhat in operation, lowering the resistance 15-20% to an equivalent full area MCP resistance of about 400 kilohms, with an effective temperature increase of about 25-30 °C. If pulse-counting gain of 1 x 10^5 at 1400 V was achieved, as numerical gain models predicted [23] (Figure 34), this implied a channel recharge time of roughly 14 microseconds (Table 7). However, if our experiments showed that an MCP contact anode requires hard saturation operation, and thus higher MCP voltages, the channel recharge time will necessarily increase. From Table 7, for example, at a gain of 5 x 10^5 at 1800 V (R_{mcp} = 400 kilohms), the recharge time has increased to 56 microseconds.

These numbers can be derived from a simple recharge calculation. Given that a channel releases charge Q from a single electron (or ion) event, and that the channel is effectively 'dead' until replenished with channel wall current I_{ch}, the recharge time is

$$\tau = Q/I_{ch} = eGN/I_s$$

where e is electron charge, G is the gain, N is the number of channels in the MCP, and I_s is the bias or 'strip' current. Although one could easily complicate this simple model, possibly making it more accurate, it has proved quite useful in practice giving better results than the predictions of RC models [34,35].

Low noise curved channel plates

Due to production priorities, we were unable to fabricate curved channel plates made with the low noise glass formulation in time for program completion. This has no effect on high input flux dynamic range testing, and straight channel low noise MCPs have been thoroughly tested and documented (Sect. 2.1). There is no reason to believe that the channel curving process would yield results significantly different from standard Long Life™ glass, due to the virtually identical physical properties of both glass systems. Nevertheless, low noise curved channel plates having very low resistances will be made at the earliest opportunity.

Table 5

Dimensions of curved channel MCPs, as used in Phase II program.

L/D	80
Channel diameter (um)	12
Channel pitch (um)	15
Bias (degrees)	5-8
Open area fraction (%)	70
Nominal OD (mm)	33
Active dia. (mm)	25

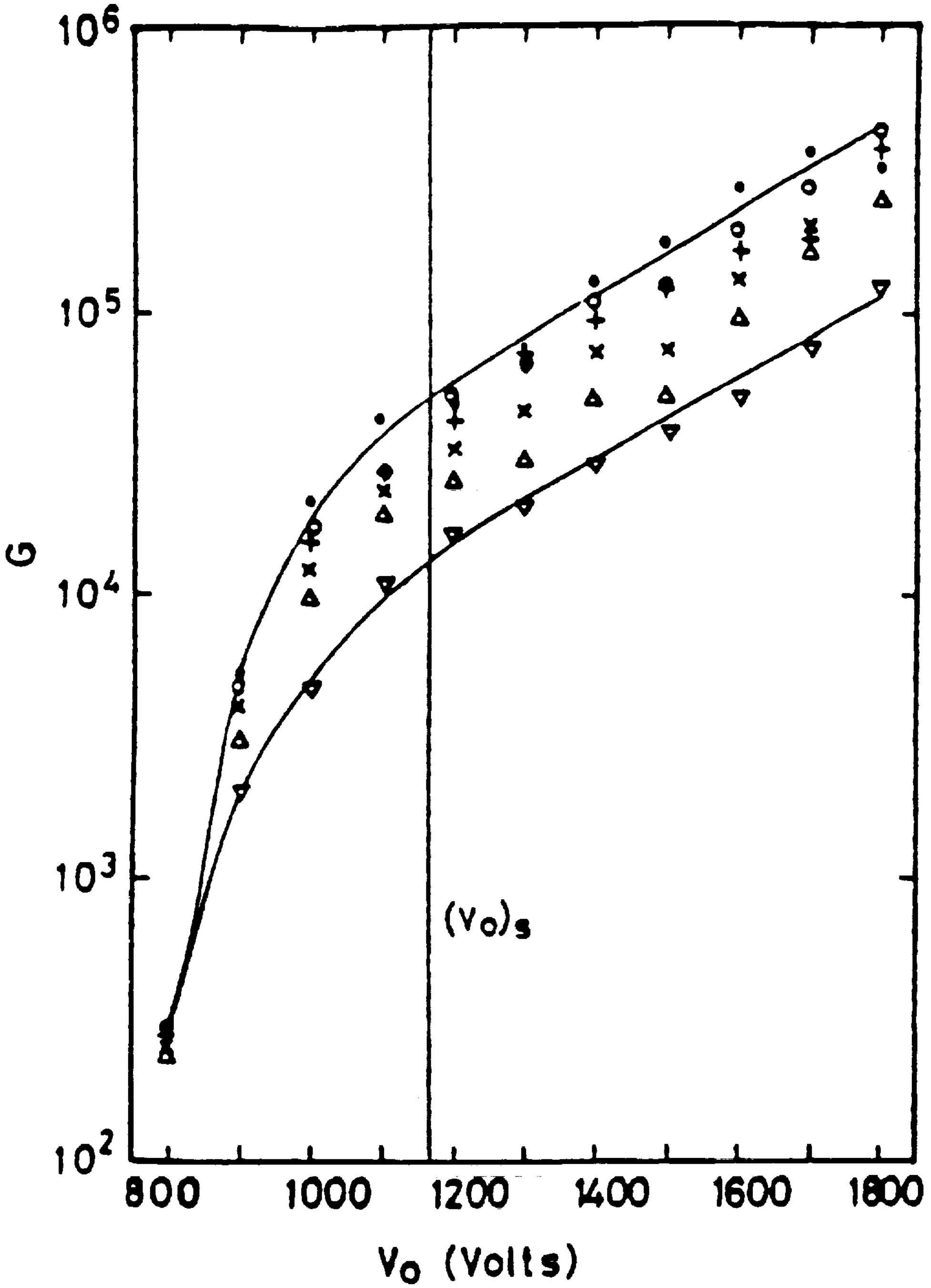

Figure 34. Calculated gain-voltage curve of single 80:1 MCPs, having various channel diameters. ● 12.5 microns, o 10 microns, + 8 microns, x 6 microns, Δ 4 microns, ∇ 2 microns [from Ref. 23]

Table 6

Calculated channel recharge time

25mm MCP resistance = 600 kilohms

Gain	Voltage	Channel recharge time
1×10^5	1200 V	26 microseconds
	1400	22
	1600	20
	1800	18
3×10^5	1200	76
	1400	66
	1600	58
	1800	50
5×10^5	1200	128
	1400	110
	1600	96
	1800	84
7×10^5	1200	178
	1400	152
	1600	134
	1800	118
1×10^6	1200	254
	1400	218
	1600	190
	1800	168
3×10^6	1200	762
	1400	654
	1600	572
	1800	508

Table 7

Calculated channel recharge time

25 mm MCP resistance = 400 kilohms

Gain	Voltage	Channel recharge time
1×10^5	1200 V	17 microseconds
	1400	14
	1600	13
	1800	12
3×10^5	1200	51
	1400	44
	1600	38
	1800	34
5×10^5	1200	85
	1400	73
	1600	64
	1800	56
7×10^5	1200	119
	1400	101
	1600	89
	1800	79
1×10^6	1200	170
	1400	145
	1600	127
	1800	113
3×10^6	1200	509
	1400	436
	1600	382
	1800	339

2.2.4 MCP ELECTRONIC READOUT

As mentioned in Sect. 1.2, the dynamic range of MCP detectors is limited at the high end not only by MCP gain falloff, but just as importantly, by the PPR and sensitivity of the electronic readout. Hence, it is crucially important that the proper readout be selected. Since a number of different electronic readouts are currently used for registering MCP output charge pulses, we will very briefly review each type. We will also show why only the discrete anode type of readout was considered appropriate for this program, where our goal was to achieve MCP count rates in excess of 10^9 $cm^{-2}s^{-1}$, and where the readout was to be mounted in direct physical contact with the MCP, serving as a bias electrode as well as a thermally conductive path. All readouts discussed are capable of two dimensional imaging.

ALTERNATIVES

Resistive Anode Encoder (RAE)

RAEs operate by using a four-cornered anode which encodes event locations, by electronically ratioing the relative charge amplitudes appearing at the anode corners [1,36]. Alternatively, a difference in pulse development times can be processed by a time-to-amplitude converter, since risetimes are proportionally stretched depending on the distance from the event location. However, both spatial resolution as well as throughput are degraded by thermal noise generated from the resistive film (~5000 electrons RMS). Consequently, image resolutions of 500 x 500 and overall response speeds no greater than 10 microseconds are possible. This speed limitation clearly precludes use of this type of readout for high count rate applications; moreover, heat dissipation from a bonded MCP would be likely to generate appreciable thermal noise.

Delay line anodes

These use a delay line coupled with timing circuits to establish the spatial location of an event. The MCP charge pulse is collected on either a helical winding or a zigzag strip, and divides into two parts traveling in opposite directions. Since the charge pulse travels at a known propagation velocity, the difference in arrival times at opposite ends of the line gives the required positional information. These readouts were originally developed for large format, high spatial resolution applications. However, they were not designed to be used at high count rates.

Multiwire Readouts

Multiwire readouts, originally used with imaging radiation detectors other than MCPs, are made from two planar sets of closely-spaced parallel wires which are orthogonal to one another, allowing x-y event locations to be determined. Although resistors interconnect adjacent wires, only a subset of the wires (typically one in eight) are connected to preamplifiers. Hence a grid of 100 x 100 wires requires only 26 amplifiers. Still, electron cloud spreading is required, precluding direct MCP/anode coupling, and thus use as an MCP heat sink. Even if this were not a consideration, it is difficult to see how an anode structure having more than one plane (implying a significant open area fraction), could provide a uniform thermal path for all areas of an MCP.

Wedge and Strip readout

The wedge and strip is a set of interdigitating metal electrodes (usually three), with areas that vary depending on the position coordinates [37]. One electrode is shaped like a parallel set of wedges, which furnish a charge collecting area that depends linearly on the y coordinate. Another electrode is shaped like a set of parallel strips, with the strip widths becoming gradually wider in the x direction. The third electrode fills the gap between the other two and normalizes the charge. When a charge cloud falls on the pattern, as long as it covers more than one repetition period the centroid position can be computed in the electronics with a simple algorithm. The requirement that at least one period must be covered by the charge cloud rules out the use of this readout with a bonded MCP, and in practice around 1cm MCP to anode spacing is used. (Although one could conceive pattern periods as small as a single MCP channel, the interelectrode capacitance would be orders of magnitude too high for a realizable system.) Also, to reduce voltage noise bandwidth, the wedge and strip throughput is limited by long amplifier risetimes as well as algorithm processing, so the speed is limited to 10^5-10^6 $cm^{-2}s^{-1}$; it is most often used in astronomical MCP detectors, where count rates are typically low.

Multi-anode Microchannel Plate Array (MAMA)

The MAMA is a coincidence array, where the coincidence of signals from a number of different electrodes defines an event [38]. By connecting half of the anodes to a small number of amplifiers which give the local (or fine) position, and the other half to a set of amplifiers giving the coarse position, an event is localized with a twofold ambiguity in position. Then, by comparing the pulse amplitudes on the two anodes, this ambiguity is removed. In this way N x M locations can be encoded with only N + M amplifiers for linear arrays [39]. Area arrays have also been built, using fourfold coincidence (N x M x O x P). This type of readout has been successfully used in a number of different spectroscopy and imaging applications.

To properly register an event, either two or three adjacent electrodes must simultaneously be activated by a charge pulse having an amplitude above a preset discriminator level. Events activating only a single electrode more than three electrodes, are disallowed by the MCP-anode gap spacing and voltage, as well as by the coincidence logic (i.e., this limitation is caused by the array layout, which can only assign a unique address to events of this size). This places strict demands on the PHD of the MCP, so that a well-saturated C-plate is usually used.

The MAMA detector positional resolution and subpixel photometric accuracy have recently been improved, and are now superior to that of any other pulse-counting imaging readout [40]. By moving from a coarse-fine array to a fine-fine array, and using a different coincidence logic, cross-coupling between pixels has largely been eliminated. The remaining flat-field variations are now dominated by photon-limited Poisson statistics. The accuracy of centroid measurements is now as high as 0.04 pixel, with the smallest pixel sizes currently around 25 microns.

Unfortunately, the MAMA cannot be used with a bonded high speed MCP. First, since the coincidence detection circuit is triggered by every event, the PPR of this circuit determines the maximum count rate for the entire array, and is currently limited to a few MHz [41]. Second, the MAMA requires that at least two electrodes are simultaneously activated, which is not possible for a single channel discharging onto a bonded MAMA. Moreover, an imaging MAMA has an anode plane with an open area ratio of about 50%. It is difficult to see how uniform thermal dissipation across all MCP channels could be achieved with a bonded MCP. For these reasons, the MAMA was not considered for this program.

CODACON

Another example of a readout utilizing coincidence techniques is the CODACON, consisting of a set of parallel collector strips [42]. These strips or anodes capacitively couple through a dielectric substrate to pairs of binary code tracks. Use of differential amplifiers connected to the binary code pairs then gives a binary readout, so that digital encoding of event location occurs directly at the anode plane. This simplifies the processing electronics, allowing higher speed operation. For example, a 1024-element linear array having 25 micron resolution requires only 10 amplifiers (n amplifiers are required for 2^n locations), with a maximum count rate up to 10 MHz over the entire anode area. This upper limit is set by the time constant induced by the anode capacitance. Although adequate for use with standard MCPs, this readout would be much too slow for this program. Furthermore, only one operational CODACON has been demonstrated.

Phosphor screen readouts

Phosphor readouts are commonly used in image intensifier tubes, and convert an electron charge pulse into an optical signal. They can then be coupled to TV cameras, CCDs, or photodiode arrays. The latter two devices are limited in area, but use of a tapered fiber optic coupler allows large format phosphor screens to be used. Since electron impact energies on the order of several kilovolts are required, an accelerating bias voltage is used, which must be applied across a gap between MCP and phosphor. This precludes heat sinking of the MCP at the output face.

CCDs

The CCD, or charge-coupled device, is an imaging array of solid-state capacitors which stores and transfers packets of charge across a semiconducting substrate. Each capacitor acts as a pixel, whereby a charge packet is created within the pixel by incident radiation (typically photons). The top surface of each pixel is a polysilicon gate structure comprised of three gates, forming a potential well when gate bias voltages are appropriately set. Input radiation penetrating into a deeper-lying region of p-type silicon generates electron-hole pairs in proportion to the intensity; this charge then accumulates in the potential well. After it is integrated, the charge packet is serially shifted across the array using a three-phase clock signal, and eventually appears in a serial register. This register empties into an on-chip amplifier, and the x-y intensity is then recorded. This sequence is repeated in turn for each pixel until the entire image frame is recorded.

This type of CCD, where radiation first penetrates the surface polysilicon gate structure, is not the only type of construction possible. Backside-illuminated CCDs are available for imaging UV and electron radiation, since these types of radiation cannot easily penetrate the gate structure to the underlying p-silicon. Instead, the CCD backside is used, with special processing allowing the rear silicon layer to be thinner than an electron diffusion length [43,57].

At first glance, bonding an MCP to a backside-illuminated CCD would seem to be a plausible solution to the simultaneous cooling and readout of low resistance MCPs. Unfortunately, there are several factors which make this implausible for high-speed MCP operation. Because of the serial readout of pixels, the CCD is inherently slow. A further limitation on CCDs for wide-dynamic range applications is that there is substantial time-independent noise at room temperatures. Thermal electrons will be added to the signal during readout, at a level corresponding to roughly 20 cts/pixel. Charge transfer inefficiencies, requiring "fat zero" corrections, will add further noise. CCD cooling to -100 °C is commonplace in astronomical applications, where long integration times are mandatory due to very low signal count rates. However, the high level of thermal dissipation from bonded low-resistance MCPs would effectively prevent temperatures this low from being achieved. Moreover, CCDs are small devices, limited to only a few cm^2 in area. Although somewhat larger devices are now under development, they will probably be quite expensive due to low yields. Finally, backside-illuminated CCD detection efficiency for the relatively low energy electrons (~30-50 eV) which comprise the MCP output charge cloud is only about 10-15% [57]. Moreover, the high energy tail of the MCP output electron energy distribution (extending as high as the MCP bias voltage), although small, could still create localized damage. For all the above reasons, CCDs were ruled out for this program.

Quadrant anode

This type of anode consists of a metal disc separated into quadrants, with each quadrant connected to a preamplifier. Charge clouds exiting the MCP output must spread out to an area of at least several mm^2 before striking the anode. Ratioing of opposite anodes gives the event coordinates. This type of readout has a very restricted image area, only a few mm on a side; moreover, images can be distorted due to charge division nonlinearities. Since MCP and the quadrant anode must be separated to allow charge cloud spreading, this type of readout was not considered.

DISCRETE CONTACT ANODE

The discrete anode type of readout (Figure 35) is the fastest of the MCP electronic readouts currently available, able to maintain Poisson statistics at very high count rates ($> 10^{10}$ $cm^{-2}s^{-1}$). It consists of an array of charge collecting pads, either linear (for spectroscopy) or areal (for imaging), where the signal collected by each pad is processed by a dedicated electronics channel. Thus, charge cloud spreading is not required. For these reasons, it was the logical choice for our application, a directly bonded MCP readout able to operate at very high speed.

The mode of operation is as follows. The load resistance in the anode circuit converts the charge pulse to a voltage (several mV) which must first be amplified before entering the pulse height discriminator, a fast integrated circuit voltage comparator. Each charge pulse that exceeds a preset discriminator threshold results in a logic pulse which is accumulated in a counter. The shutter

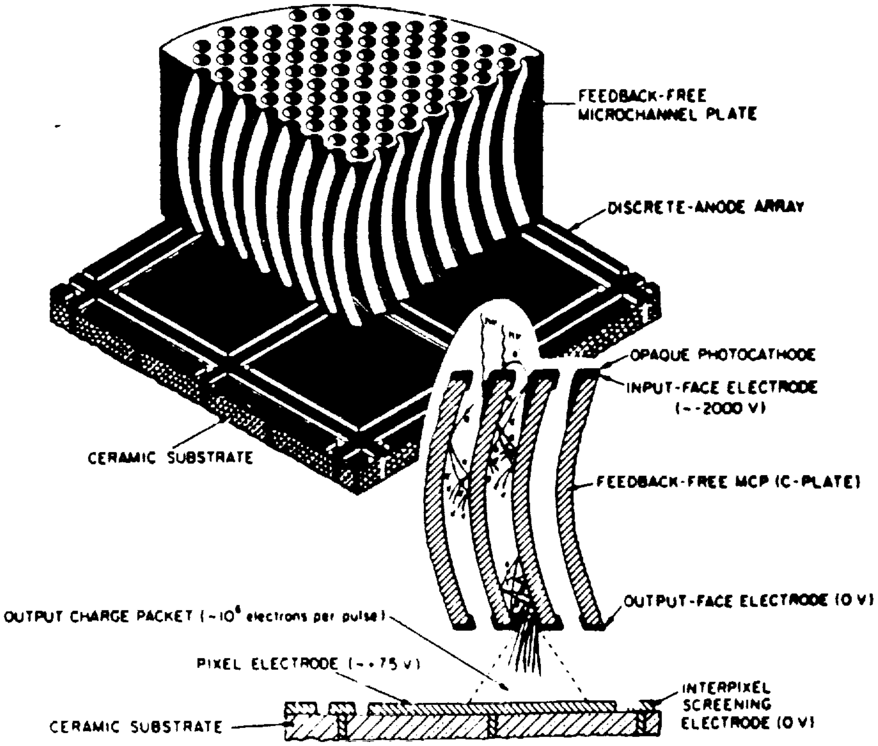

Multi-Anode Microchannel Array: Discrete-Anode Array

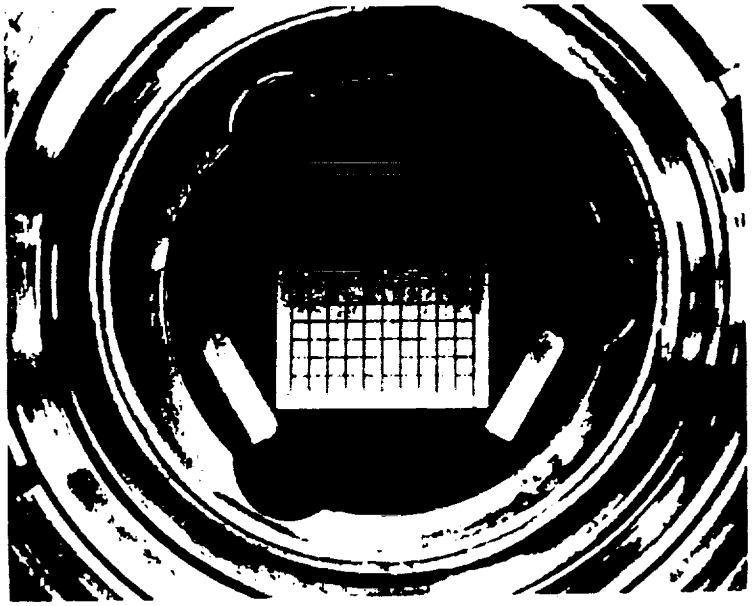

10 x 10 Discrete Anode Array

Figure 35. Discrete anode readout. [from Ref. 41]

period for the counter can be set from software, and a read command serially shifts the contents of the counter to the multiplexer/display. Wide bandwidth, inexpensive amplifiers can be used, but it is very important that good high frequency design techniques be used.

For higher pixel densities, interchannel crosstalk can become a serious problem. One of the most important factors is the stray capacitance across the anode load resistor (which determines the anode circuit time constant), as compared with the MCP pulse width. To maintain a relatively high amplitude voltage pulse across the load the parasitic capacitance must remain as small as possible (~1 pF). If the anode circuit time constant is much greater than the pulse width, the pulse amplitude will be maximized, but at the expense of the PPR. In the opposite case, where the time constant is less than the pulse width, the pulse amplitude becomes quite small, with the result that it may be obscured by noise.

Discrete anode electrical characteristics

Although discrete anode arrays have often been used with MCPs in proximity focus (separate from MCP output face), having such an array in direct contact with the MCP output is highly unorthodox. When we first proposed doing this, little or nothing was known about its plausibility except for some information on CEMs with capped anodes. The anode collector for a single channel electron multiplier (CEM) can be configured in two ways. The most common way is to hold the anode a small distance away (~1 mm) from the channel output end, so that there is electrical isolation between the bias current flowing along the channel and the output current. The anode is biased positively with respect to the channel output in order to rapidly collect the charge pulse, and to prevent space charge formation. This arrangement can be used either for analog or pulse counting operation. The other method, which is the approach used in this program, is to simply attach the anode to the end of the channel, so that it now serves as both bias electrode and collector. However, this can be used only for pulse counting, since the output current must always be somewhat less than the channel bias current, around 10-20% Normally a capacitor is used to decouple the a.c. (pulse) and d.c. (bias) components, and the charge pulse must develop a voltage drop across a suitable load resistor; otherwise it will simply flow back through the CEM bias supply. Depending upon the charge state and energy of the particles being detected, the voltage pulse can appear across a load held either at ground or at positive high voltage. In the latter case, capacitive decoupling is required, introducing additional impedance and inductance into the anode circuit, broadening the pulse fall time.

Contact anode pulse widths

One of our first concerns with directly attaching an anode to the MCP output face was to insure that there was no deleterious effect on MCP output pulse widths, particularly the risetime. To take full advantage of the high bias current MCPs, and to attain GHz response across individual anodes, the pulse risetimes developed across the anode load should be shorter than a nanosecond, with as little pulse broadening as possible resulting from the anode circuit (the theoretical risetime of a pulse from an 80:1, 12 micron MCP is around 300-500 ps [23]). The following analysis and experiment assured us that a contact anode would introduce no inherent limitation.

Electrons in a charge cloud emitted from the last few dynodes of a microchannel will be accelerated towards the contact anode by the potential difference between the dynode region and the anode. While in transit, this moving charge generates an induced current i_d in the external load circuit proportional to the electron velocity [45]. This velocity increases linearly with time-of-flight, and the current is given by $i_d = (q^2E/md)t$, where m and q refer to the electron mass and charge, E is the electric field strength, and d is the effective spacing from final dynode to anode with a corresponding time-of-flight t . The induced current therefore rises linearly, reaching a maximum just as the charge arrives at the anode. The signal voltage produced across the load resistor also rises to a maximum, but then begins decaying with the discharge time constant, which is solely determined by the anode circuit resistance and capacitance [46]. It must be pointed out that the voltage pulse at the preamplifier input is <u>not</u> caused by the charge collected at the anode, which subsequently flows through the load. Also, the induced current is independent of the magnitude of the load (as long as the in-transit electron velocity is not modified by the retarding voltage developed by current flowing through the load). Since the induced current is canceled when the charge cloud electrons strike the anode, the induced current flows only while the charge cloud is in transit. The moving charge exerts forces on the free charges in the anode circuit, causing the free charges to rearrange until the resultant electric field is zero. Thus the output pulse delivered by the MCP should not have its risetime affected by the contact anode, removing any concerns about pulse broadening (especially important with MCP channel diameters as small as 4 microns, with 100-200 ps risetimes).

An experiment verified this using a tandem composed of 40:1 MCPs, which has a broader pulse width than a single 80:1 MCP. We were able to demonstrate subnanosecond risetimes using a single 1 cm^2 bonded anode (Figure 36) with a 50 ohm load. Since there was some impedance mismatch to the conducting anode plane, some ringing was seen (although this did not effect the risetime).

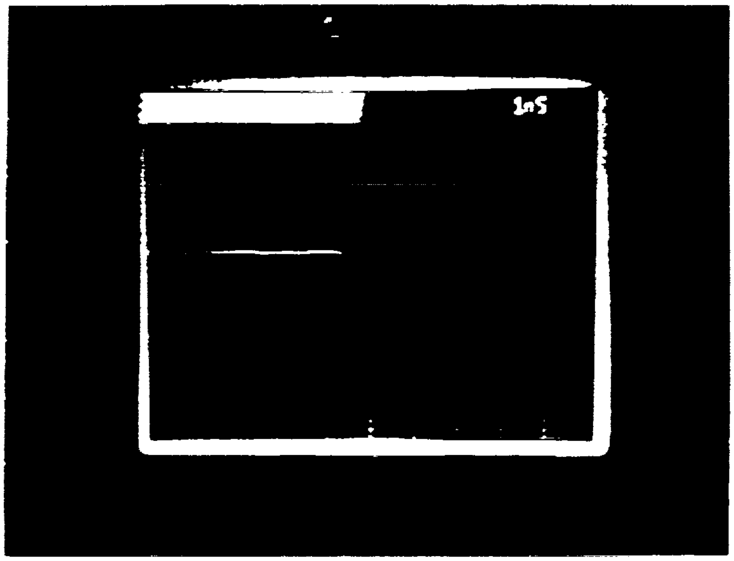

Figure 36. Measured pulse width from a tandem MCP with a contact anode.

For such short pulse widths, where a transition is being made into the microwave region, the measurement circuit topography becomes as important as the device itself in making accurate timing measurements (with the observation affecting the quantity measured). Here, pulse widths are strongly influenced by the discharge time of the anode line capacitance into the load resistance. (Whenever we increased the cable length during the measurement, pulse broadening invariably occurred.) For the final 2 x 2 device, we are therefore using short (~1 cm) anode leads feeding directly into the preamplifiers, which are mounted on a ground plane. These precautions will prevent any pulse broadening due to parasitic inductance and capacitance.

Poor anode bond: the effect on gain

A poor bond between MCP and anode will diminish the apparent MCP gain. Gain variations of up to 300% have been reported across the active area of a tandem, which is considerably larger than can be accounted for by gain variations of the individual plates taken together. These variations have been attributed to a lack of complete and uniform contact between the two MCPs, so that gaps of varying sizes exist between the plates. Space charge will accumulate in the regions, since no interplate electric field is present to remove the charge. (Presumably, only if the applied potential is significantly greater than the electron drift energy will space charge effects disappear.) This space charge will effectively lower the magnitude of a charge pulse exiting an MCP channel, causing the gain variation [47]. Models for the MCP output electron pulse show that the degree of gain reduction due to space charge formation across a small gap with no electric field present, will depend strongly on the size of the gap. Any nonuniformity in this gap translates into nonuniformities in the size of the charge pulse striking the anode. Thus it is essential that a contact anode makes uniform, hermetic contact across the entire MCP area to which it is bonded.

Bonded anode array

To test the concept of a discrete multianode imaging array directly bonded to an MCP, we began with a square array (Figure 37) having the smallest possible dimensionality (i.e., 2), so that our efforts could be focused on demonstrating proof-of-concept, rather than spending inordinate amounts of time and money duplicating and debugging electronics channels - only to find in the end that the concept itself was unworkable. The actual fabrication of this array was discussed earlier, in Sect. 2.2. We had initially proposed fabricating a 10 x 10 array, thus requiring 100 channels of high speed electronics. Arrays of this size have successfully been constructed for crude imaging [44] (however, ~100 pixels has been found to be the practical size limit, since smaller and more closely spaced would introduce unacceptable levels of crosstalk.)

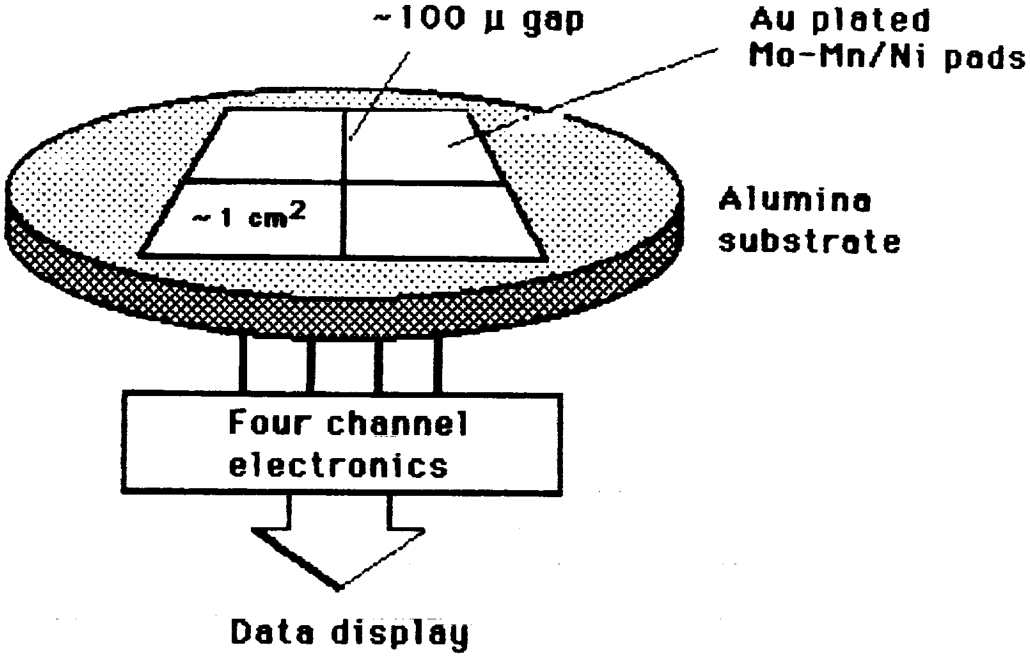

Figure 37. 2 x 2 anode array schematic.

Because of the highly unorthodox nature of the MCP/anode coupling, which had never been done and where proof-of-concept demonstration was critical as mentioned above, fabrication of a 10 x 10 readout system (metal anode array and electronics) would have been unduly taxing on the available resources, with no guarantee of success.

Crosstalk

The interchannel crosstalk between discrete anodes has often been the limiting factor in the spatial resolution of discrete anode arrays, even more important than having a large number of anode pins and amplifier circuits to contend with. As pixel density increases, interpixel separation decreases, leading to a rapid increase in anode coupling. A pad-pad capacitance C_p of less than 0.5 pF is desirable for prevention of pulse broadening, and a value no greater than 2 pF is desirable for both pads and pinouts combined [48]. Higher values will cause RC broadening, compromising the PPR delivered by the electronics. Since the MCP charge pulse is integrated on a total input capacitance of C_{in}, the anode coupling can be given as a percentage equal to C_p/C_{in}.

Although a 2 x 2 array represents the lowest dimensionality possible for a square array, it was still important to measure the crosstalk for our substrate, due to the relatively large size of the anodes. To do the measurements, fast 200 MHz pulses were injected directly into adjacent anode pads, and the voltage drop across 50 ohm terminating resistors was measured for each anode (Figure 38). At 200 MHz, the crosstalk was found to be roughly 20 dB, or 10%. Therefore, to discriminate against unwanted crosstalk, we determined that a discriminator level roughly 20% of the modal gain would need to be set for our pulse counting electronics (Figure 39).

10 x 10 array feasibility

Although we were unable to fabricate a 10 x 10 array of discrete contact anodes, one possible approach should be mentioned for bonding an MCP having a 10 x 10 output face electrode pattern with a 10 x 10 anode array, which is compatible with the bonding approach used in this program. This is the flip chip solder bump bonding technique, initially developed for early IBM computers. This method, which is commonly employed in hybrid infrared detector arrays [58], utilizes a solder alloy which is first evaporated through a mask onto discrete contact pad areas. When heated above the solder melting point in an inert atmosphere, surface tension forces the solder to form into bumps or droplets.

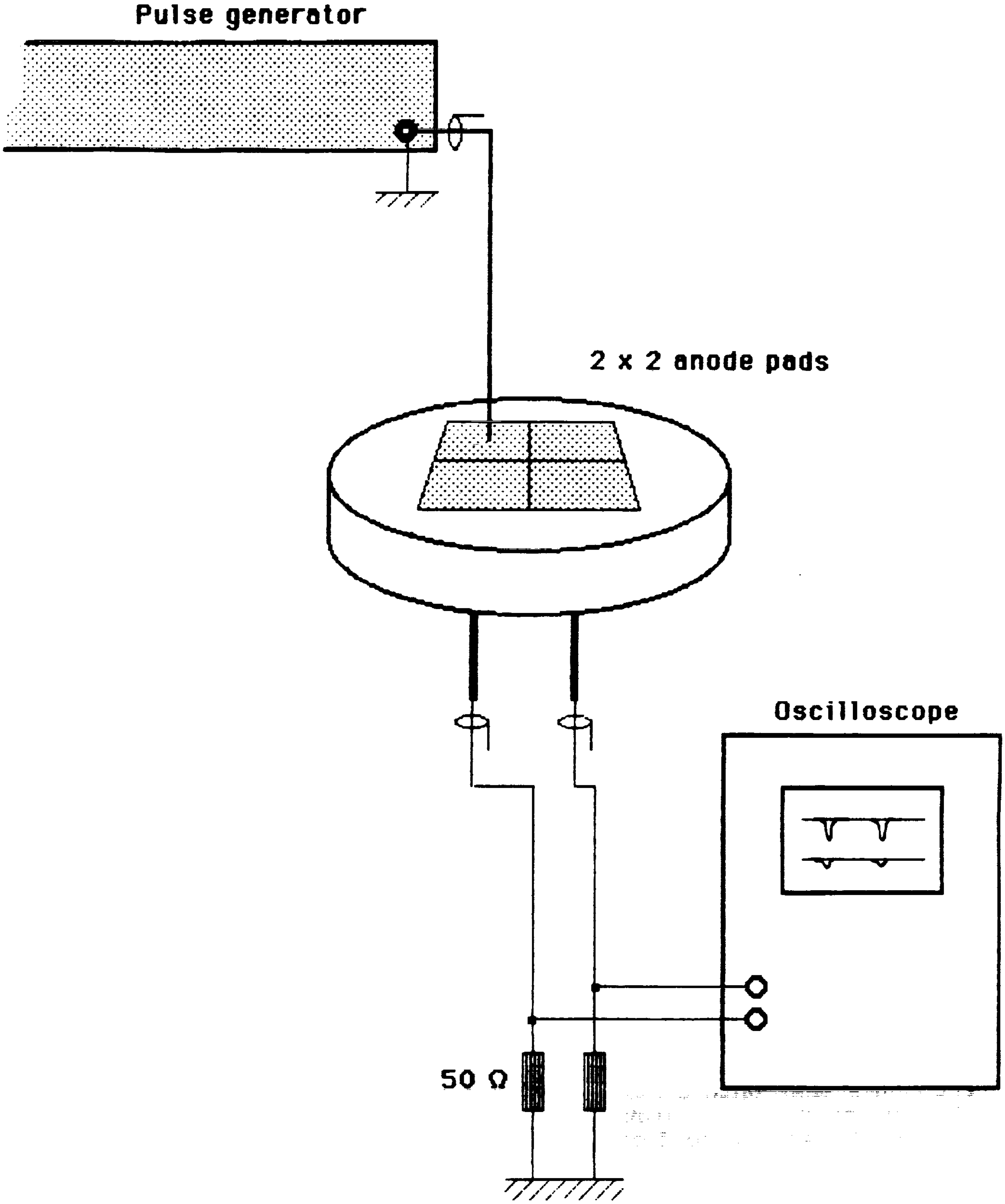

Figure 38. Crosstalk measurement schematic.

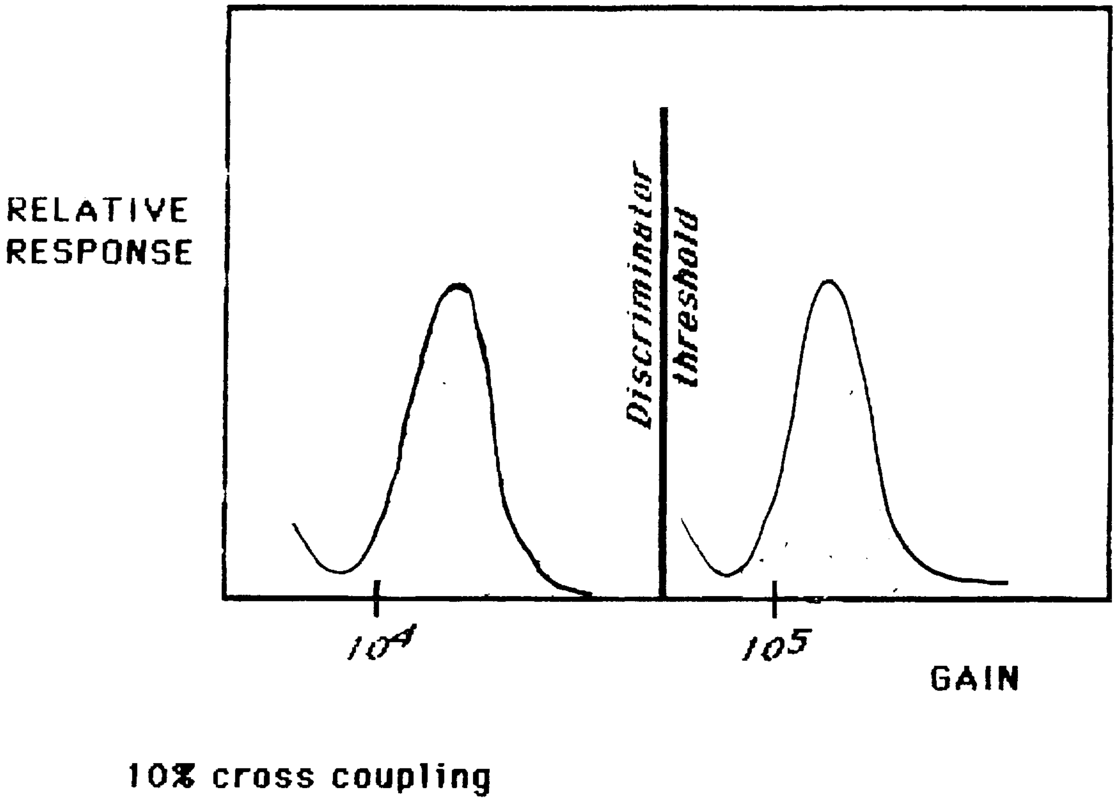

Figure 39. Discriminator setting to eliminate anode cross-coupling.

An identical pattern of contact pads on an opposing substrate is then aligned with the solder bumps so that upon remelting, opposing pads are connected, yet isolated from adjacent pads (Figure 40). The general shape of these bumps can be manipulated through control of the time and temperature profiles of the reflow soldering process. Thus, a thermally conductive path can be provided for all areas of the MCP output face provided with electroding. Unfortunately, resource limitations precluded further work on this approach.

FOUR CHANNEL HIGH-SPEED ELECTRONICS

During the initial stages of the program and by agreement with NASA, Galileo was to provide the front-end electronics up to and including the counters, with NASA providing the multiplexing and data display format. However, as the program evolved, it became clear that it would be less complicated and more expedient if Galileo provided the entire readout system.

This section will briefly explain the operation of a four channel high speed electronic readout system which was designed and built for this program (Figure 41). The main objective of the electronics was to provide an electrical interface between the bonded MCP and a computer system used to process the collected data. The key issue in the design was the wide bandwidth (DC to 1 GHz) that each channel of the readout would require. Therefore, RF and microwave layout techniques were deemed necessary.

Block diagram

Figure 42 is a simplified block diagram of the 4 channel electronics (with detailed schematics to be found in the Appendix). Each channel of the readout electronics consists of the following three parts: 1) pulse amplifier and discriminator (PAD); 2) high speed emitter-coupled logic (ECL) counter; and 3) computer interface containing multiplexing and control logic. When an incoming event is detected by the MCP the resulting signal pulse developed across a 50 ohm anode load is:

$$V = (eG/dt)50$$

where e is the electron charge, G is MCP gain, and dt is the pulse width. Table 8 is a brief summary of MCP output pulse current and voltage developed across 50 ohms, at various gains. The anode voltage pulse is first sent to amplifiers, where it is increased by 40 dB. After amplification, the pulse is sent to a integral discriminator which gives an ECL logic pulse whenever

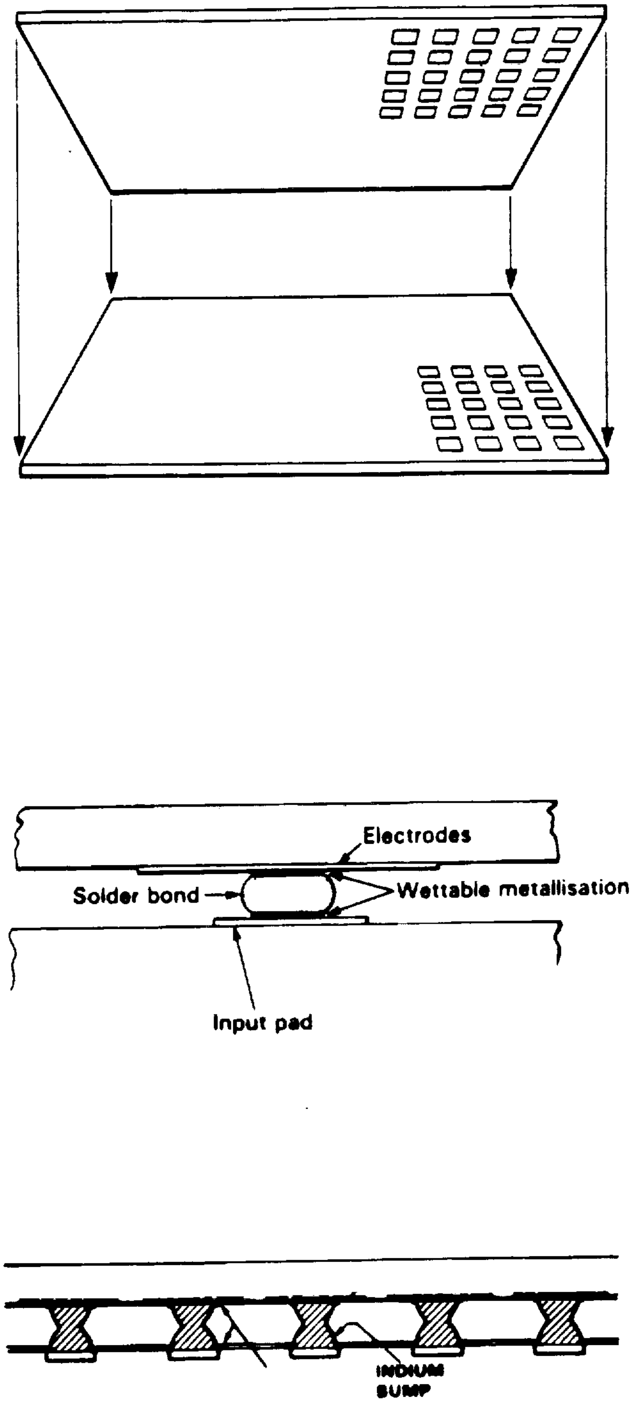

Figure 40. Indium flip-chip solder bump bonding method. [from Refs. 58, 59]

C-2

AMPLIFIER INPUT IMPEDANCE: 50 OHMS

DOUBLE PULSE RESOLUTION: 1.4 NANOSECONDS

REPETITIVE BANDWIDTH: 700 MHz

POWER REQUIREMENTS: +5 VOLTS @ 1.5 AMPS
-5.2 VOLTS @ 1.5 AMPS
+12 VOLTS @ 0.6 AMPS

DATA OUTPUT: 16 BITS WIDE
24 BITS MULTIPLEXED

CONTROL: 1 STROBE LINE
1 RUN LINE
1 DATA OVERFLOW

STORAGE CAPABILITY: 4-24 BIT INTERNAL DATA REGISTERS

AMPLIFIER GAIN: 40 dB @ 1 GHz

THRESHOLD CONTROL: INTERNAL ADJUSTMENT, INDEPENDENT FOR EACH CHANNEL

SENSITIVITY: ABOVE 1 X 10E5

INTERCHANNEL CROSSTALK: T.B.D.

DATA CONNECTOR: 37 PIN D CONNECTOR

POWER CONNECTOR: 9 PIN D CONNECTOR

Figure 41. High-speed four channel electronic readout specifications.

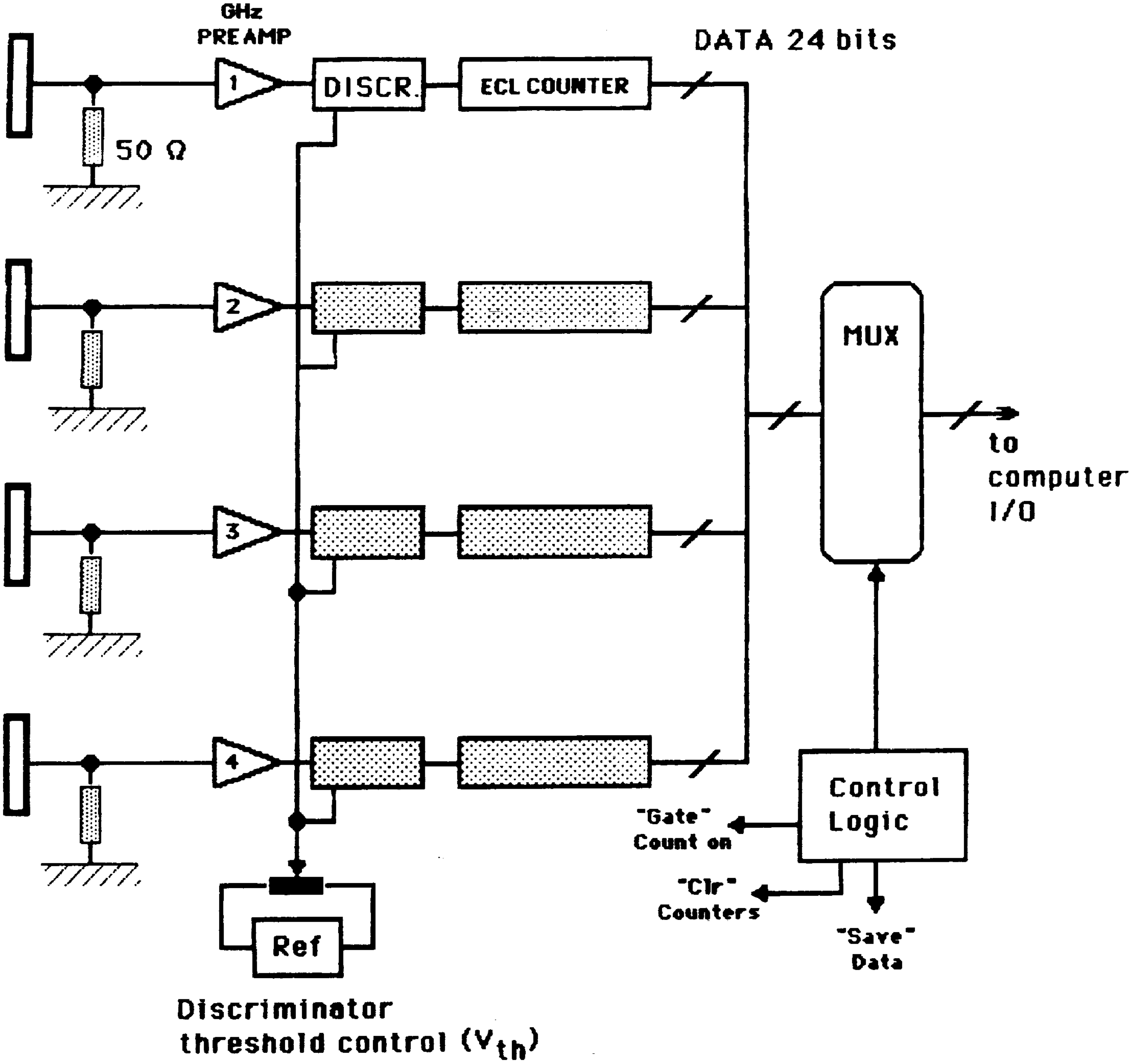

Figure 42. High-speed electronics block diagram.

the input pulse amplitude exceeds a preset threshold. All logic pulses are then counted and stored in temporary registers. When a complete integration cycle has elapsed, the control logic interrogates each channel and reads the count data into a defined memory array provided by the data acquisition software.

Timing

The timing signals for the system are shown in Figure 43, and are labeled accordingly. The run line, when held high, enables the counters; it is normally held this way for the desired integration time. The latch data line is activated by a shift from high to low in the run line. Initiation of this line stores the count data in each of the temporary registers. (Data is stored in the registers to allow the counter to be cleared for the next integration cycle.) The clear line (TTL and ECL) becomes active on a high to low transition of the latch data line. Activation of this line clears the current value of the counters to zero. This is done to prepare the counters for the next integration cycle. The strobe line is used to select one of the eight registers used for temporary data storage. Each pulse on the strobe line increments the internal decoder, to multiplex the proper data channel on the I/O data bus. There are eight channel select lines. Since a 16-bit wide data bus is used, data from the 24-bit counters must be read out in two parts, alternating between bits 1-16 and 17-24.

Components

Pulse amplifier/discriminator (PAD)

The amplifier system consists of two cascaded 20 dB stages. We chose not to design an amplifier using discrete transistors, since appropriate off-the-shelf ICs were available. Two Man-2 50 ohm amplifiers from Mini-Circuits Labs were obtained. One of the many advantages in using these amplifiers is that all AC coupling networks are completely self-contained in the amplifier packages. The interconnect lines between inputs and outputs were designed using microstrip 50 ohm transmission lines.

Using a GHz signal generator, gain vs. frequency measurements were made on the two stage amplifier. Figure 44 shows the resulting Bode plot. Figure 45 is the Bode plot from the manufacturer's data handbook for a single stage MAN-2 amplifier. Also included are VSWR vs. frequency and noise figure vs. frequency plots. We have measured pulse widths from standard MCPs to be shorter than a nanosecond, hence the objective of the amplifiers is to provide suitable pulse amplification, while preventing pulse broadening. This was successfully accomplished as shown in Figure 46, which provides actual oscilloscope photographs of nanosecond

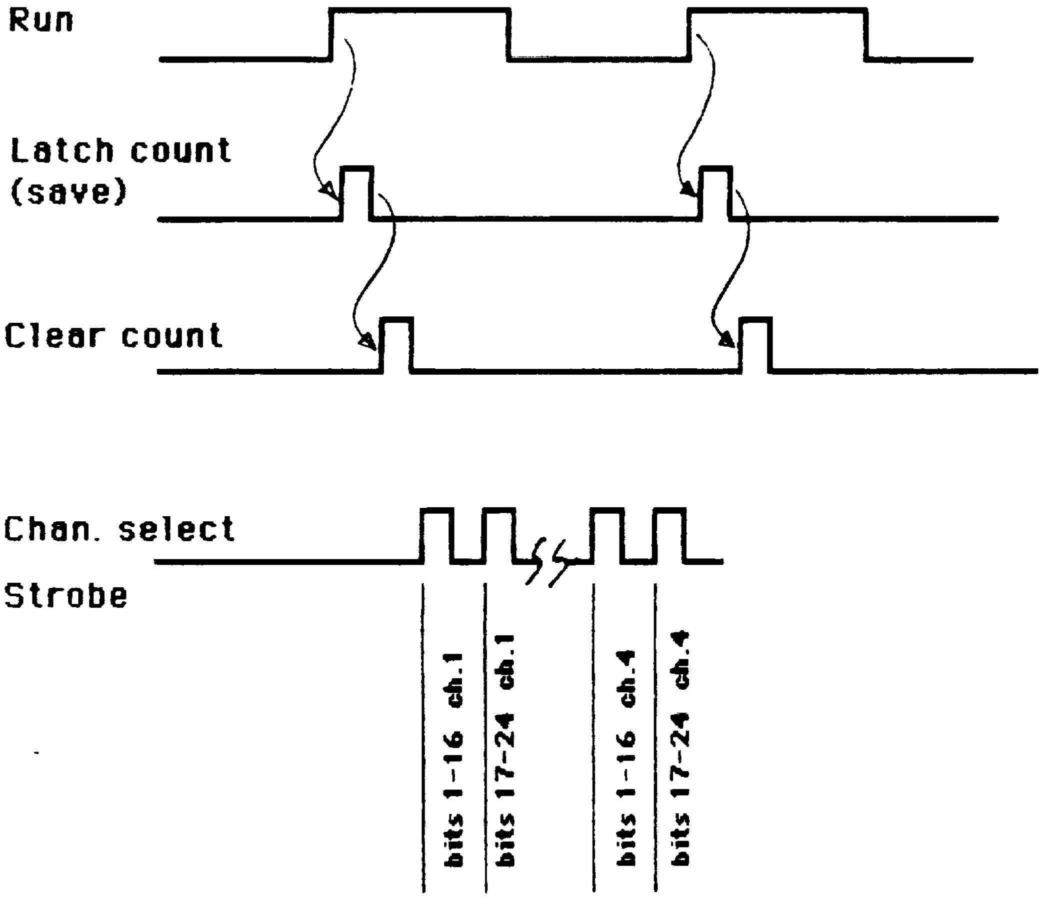

Figure 43. Timing signals for high-speed electronics.

Table 8

MCP output pulse - current and voltage across 50 ohms.

MCP GAIN	I	V
1×10^4	1.6 microamps	.08 mV
5×10^4	8	0.4
1×10^5	16	0.8
5×10^5	80	4
1×10^6	160	8
5×10^6	800	40
1×10^7	1600	80

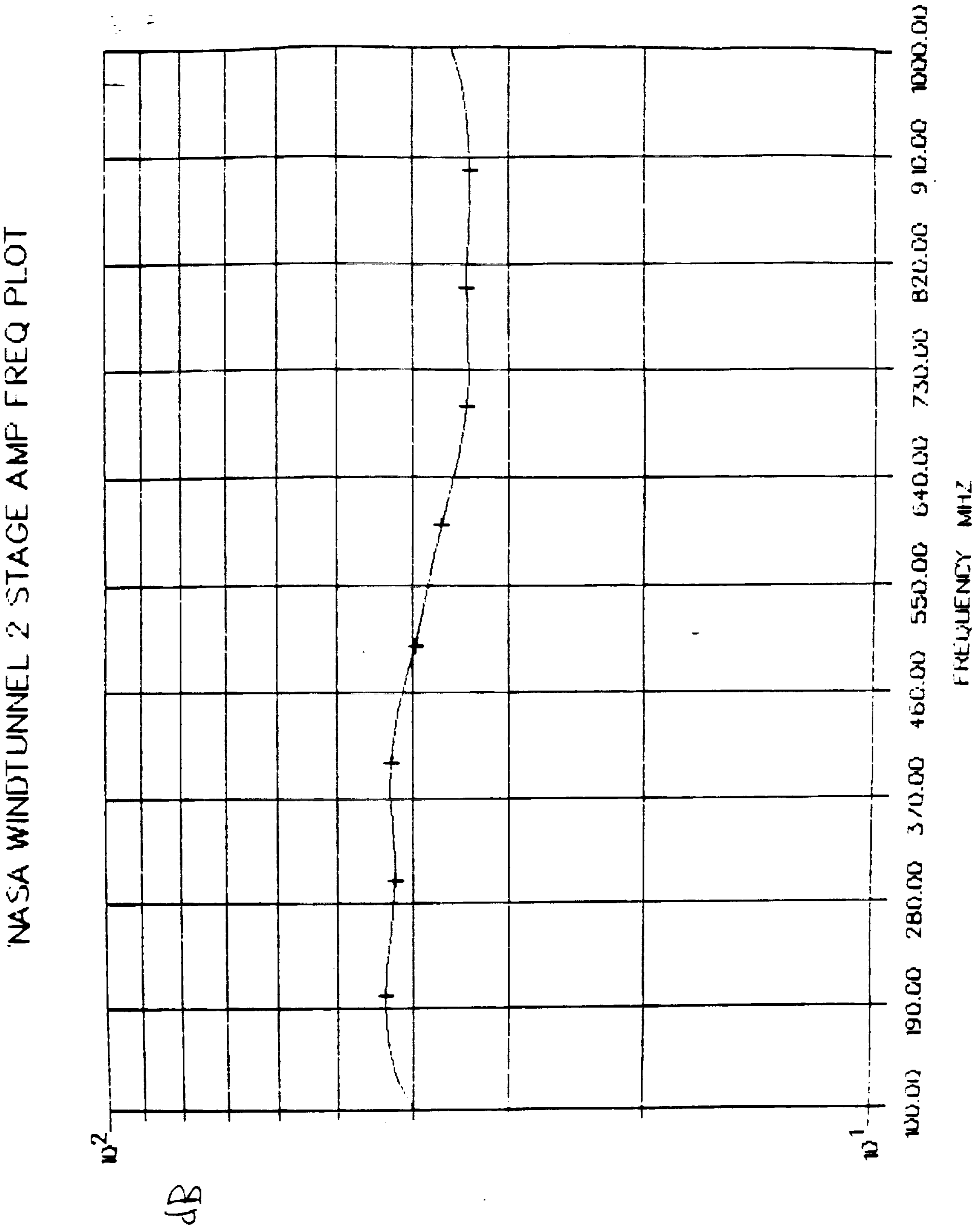

Figure 44. Frequency plot of preamplifier section.

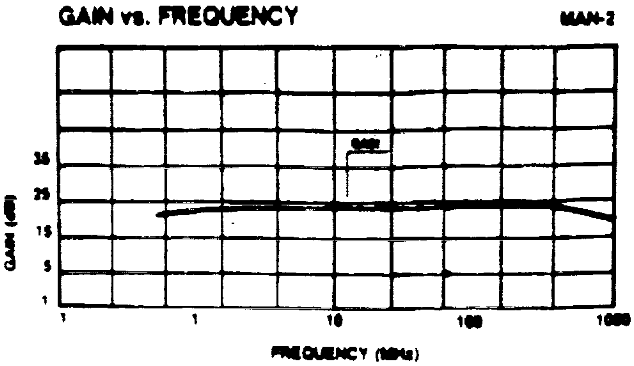

MAN-2

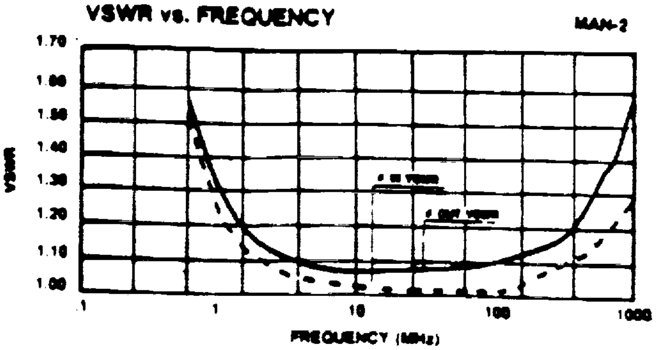

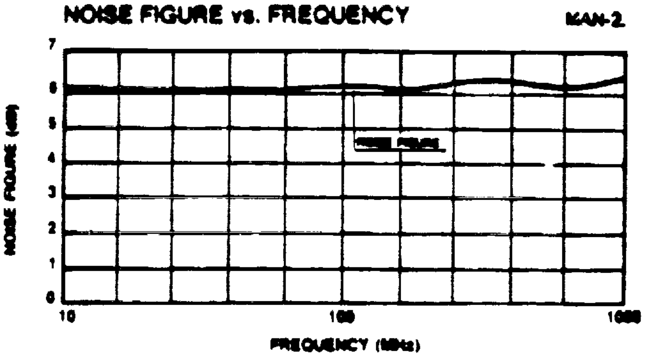

MAN-2

FREQ. (MHz)	GAIN (dB)	RETURN LOSS in	RETURN LOSS out
41	22 01	10 75	10 29
1 06	23 09	13 62	12 86
5.21	23.36	18.82	16 91
13 71	23 40	24.36	23 81
35.25	23.41	29 78	27 15
90.60	23.41	36.43	28 22
125.06	23 41	40.92	28 35
249.53	23.38	37 86	27 14
321.46	23.37	36.58	26 83
443.73	23.31	31.92	24 81
497 88	23.31	30.14	22 94
612.52	23.13	25.38	19 88
753.57	22.57	22 34	16 97
845.51	22.22	21 23	16 23
1167 14	20.60	22.29	14 55

Figure 45. Amplifier Bode plot from manufacturer's data sheet.

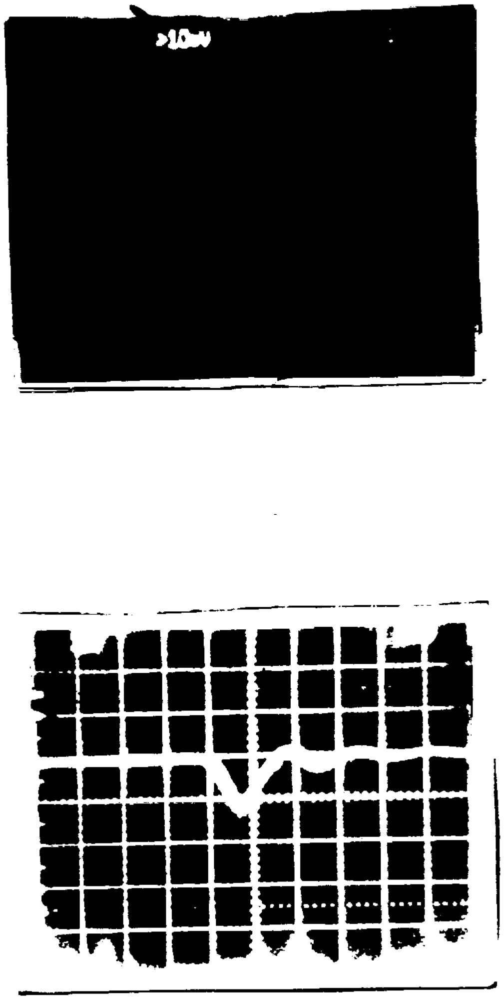

Figure 46. Nanosecond waveforms at input and output of amplifier section.

signals at both the amplifier input and output.

Integral discriminator

The discriminator is used to detect pulses from the amplifier that exceed a preset level, which is usually set to discriminate unwanted background pulses. It therefore plays a key role in the pulse counting electronics chain. The heart of the discriminator is a VC7695 (VTC Incorporated), an ultra-fast differential ECL output comparator. The propagation delay for this part is 1.3 ns, as given in the data sheet. When proper layout techniques are employed, the manufacturer has reported GHz operation for continuous waves (with use of a PC board with ground plane mandatory). Our own tests have shown repetitive rates exceeding 700 MHz. Threshold settings can be implemented either manually, by an on-board potentiometer, or automatically programmed by a Metrabyte Das-2 IBM expansion plug-in board. SMA connectors were used in conjunction with 50 ohm RG174U coaxial cables, to connect the discriminator output to the counters.

Emitter-coupled logic (ECL) counters

ECL logic from the Fairchild 100K family of ECL devices was used to perform the event counting for very high count rates. A VC7695 comparator was also used as a receiver with a dedicated threshold control to compensate for any attenuation arising from the high-speed connection between the discriminator and counter. A 6-bit high-speed front end counter was constructed solely from ECL devices (11C70 and F100136). The circuit schematic (Appendix) shows that the first two bits consist of two 11C70 master/slave D-type flip-flops capable of toggle rates greater than 650 MHz. The preceding 4 bits are processed by a F100136 high speed synchronous ECL counter. The output from the most significant bit of this counter is then routed through a ECL/TTL translator. Since the output from bit 6 is divided by 64, the bandwidth from TTL devices is more than sufficient. It should also be noted that bits 1-6 must be translated into TTL-compatible signals in order for there to be proper data transfer into the computer. Bits 1-24 from the counter are latched by three 74LS374 tri-state latches (registers).

Computer interface

The data transfer bus is limited to 16 bits. This is easily done by multiplexing the output enable lines to the respective registers. Since the IBM PC-XT that was used can only handle 8 bits, actual data transfer is also limited to that number. We have used a three port 24 bit input/output card supplied by Metrabyte (PIO-24). Ports A and B are dedicated for use as inputs while port C supplies the various control signals. Since the expansion data bus is weighted for 8 bits, the following data offsets must be separately treated in the display software.

a = bits 1 - 8
b = bits 9 - 16
c = bits 17 - 24

The actual count is then given by the formula

$$65{,}536\, c + 256\, b + a$$

As mentioned in the timing section above, there are twelve major control signals. The clear and latch signals are generated on the control interface board by one-shot signals. These signals become active on the falling edge of the run signal. The run signal is generated by the IBM. When this signal is at logic high the counters are accumulating events from the detector. To read the data into the computer, the strobe line is toggled after run line timeout.

Count rate data for each channel is generated by dividing the integrated counts by the shutter time; it is then displayed on the monitor as well as saved on disk. This data is used for plotting count rate performance curves.

Pulse pair resolution

The dynamic range of an MCP-based device is determined not only by the MCP count rate capability, but just as importantly, by the pulse pair resolution (PPR) of the readout electronics (Figure 47). Usually, tens or hundreds of nanoseconds are required for pulse counting amplifiers to return to zero-point baselines. Without a pile-up rejector, events occurring during this recovery period will sum with earlier events, and will therefore not be counted. Employing a pile-up rejector will improve this situation; however, this adds additional dead time to the counting chain, which degrades overall dynamic range.

Obviously, one way to avoid this problem is to simply design the electronics using very high speed components - the approach used in this program. For the channel recharge times expected with very low resistance MCPs, it is important that the PPR of the electronics approach the limiting value of the MCP pulse width, since pixel rates well over 100 MHz (for 1 mm^2 pixels and 10 micron pores) will become possible. (Smaller MCP pore sizes will require even shorter PPRs.) We have determined the PPR of our electronics system to be approximately 1.4 ns, based on the measured upper frequency limit of 714 MHz for the comparator, the slowest component in the electronics chain.

The system PPR will have a corrupting effect on the relation of the output count rate to the input count rate. Assuming the input flux follows a Poisson distribution, a relation between the output count rate R_{out} and the input rate R_{in} is given by

$$R_{out} = R_{in}/(1+r.R_{in})$$

where r is the PPR of the electronics system. Note that as R_{in} approaches the reciprocal of the PPR, significant numbers of input pulses begin to be lost (Figure 48). In this region, just before the onset of electronics saturation, a correction can be made in software by rearranging this expression to obtain R_{in} as a function of R_{out}, thus obtaining the actual input rate. This correction is carried out in our data routines.

2.2.5 DEVICE ENCLOSURE

A conceptual sketch of the initial device enclosure envisioned at the time the proposal was written is shown in Figure 16. The requirement was for a sealed electrostatic image-inverting tube, with a complex thermally-controlled power supply and a multianode readout header. However, as discussed in Sect. 1.3, a different approach evolved, which dispensed with the need for a sealed tube with a cooling jacket and complex power supply.

COOLING FLANGE

To replace the sealed tube, a demountable device was designed which is an eight inch vacuum flange supplying active cooling of the ceramic substrate to which the MCP is bonded, and which is adaptable for either charged particle or UV photon inputs. Since this is a prototype device for test and characterization, it directly mounts onto an ultrahigh vacuum system containing an electron or ion gun, or a UV light source. Also, by mating it with another flange containing a UV-transparent window (MgF, LiF, or sapphire) and a port for an external vacuum pump, stand-alone operation is possible for testing with an external UV source.

The design includes liquid cooling of the ceramic substrate, and makes the substrate a vacuum header, with the anode pinouts directly feeding into external high-speed electronics. Other cooling methods such as thermoelectric coolers were considered (Figure 49). However, since we have had experience with vacuum flange liquid cooling, this method was chosen.

Figures 50 and 51, taken from artist renderings in the patent application "Conductively Cooled Microchannel Plates" [49], illustrate the MCP device flange design. The MCP (280) is bonded to the alumina substrate (282) by an indium alloy bonding layer (283). The MCP input bias ring (284) supplies the negative high voltage to the MCP input face, and is attached by mounting posts and hardware (286). Although not numbered, the high voltage feed

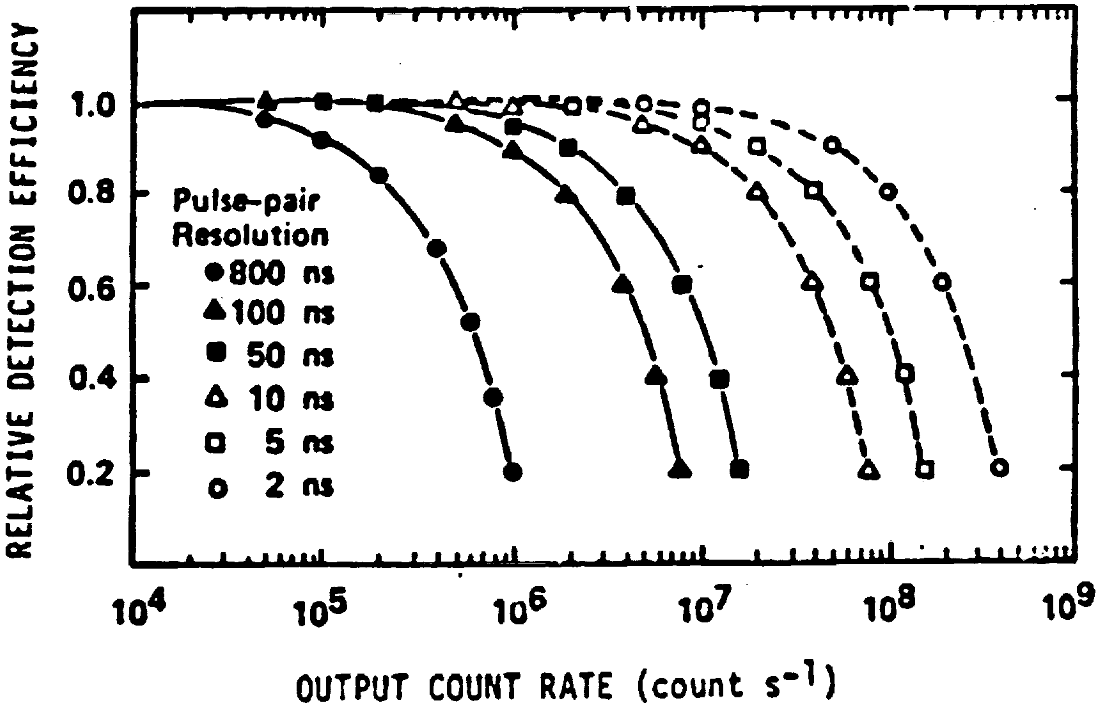

Figure 47. Effect of electronics pulse pair resolution on detection efficiency. [from Timothy]

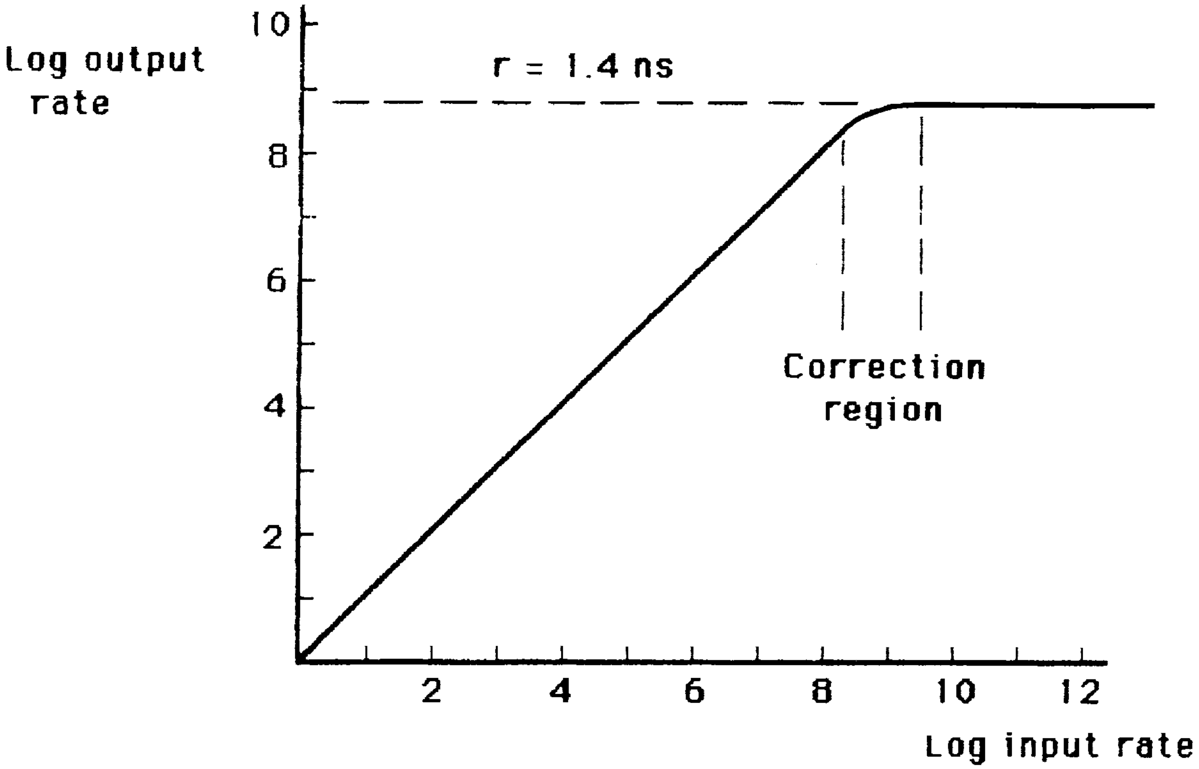

Figure 48. Electronics saturation due to pulse pair resolution.

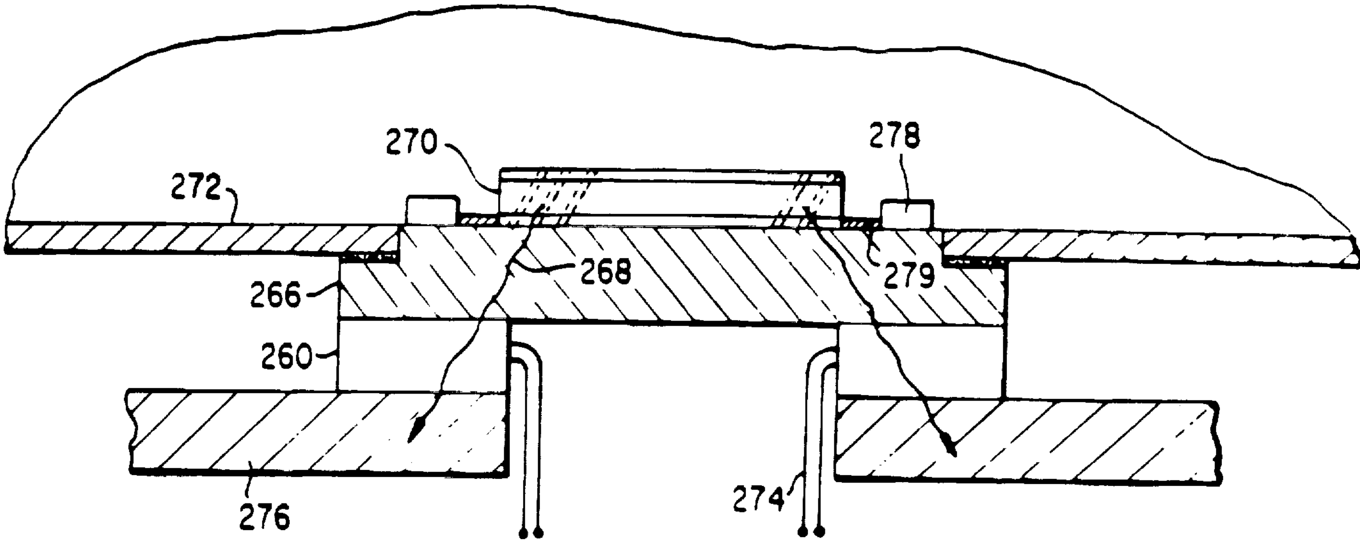

Figure 49. **Illustration of MCP thermoelectric cooling.**
[from Ref. 49]

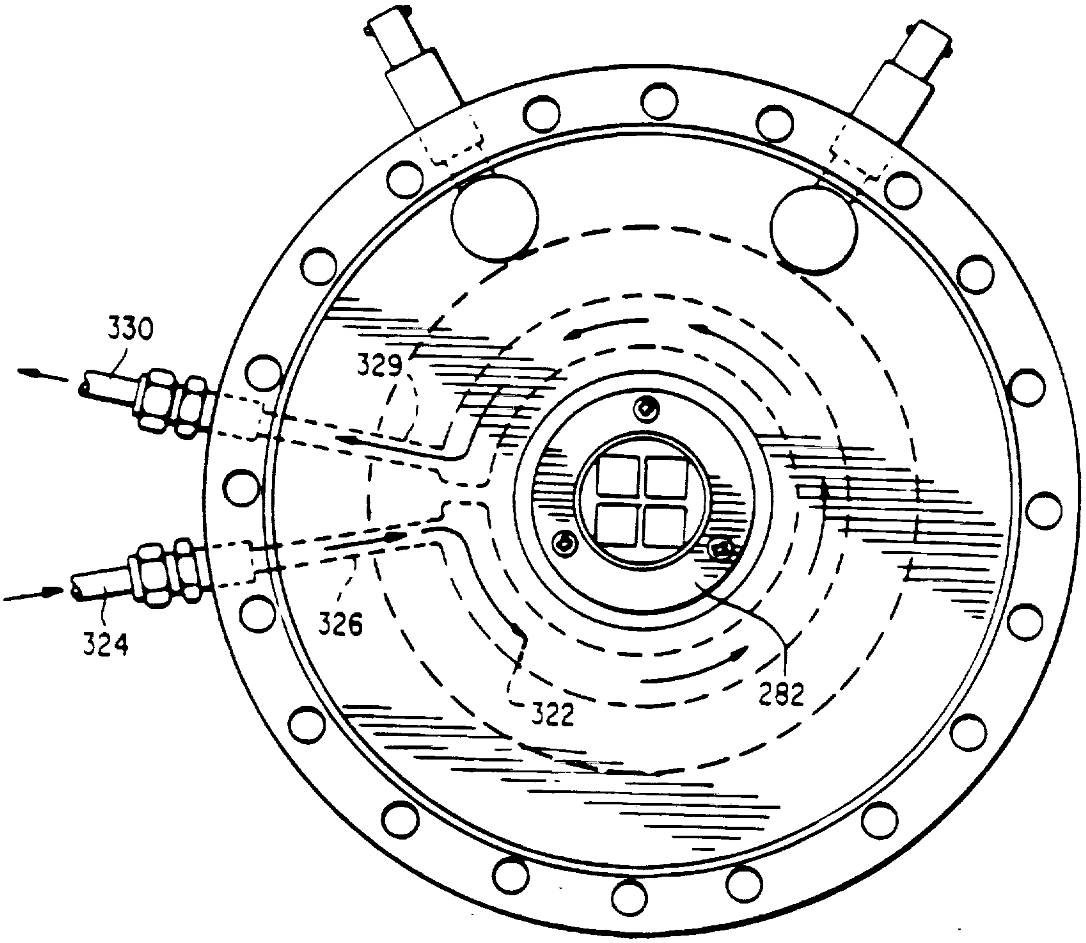

Figure 50. Top view of Phase II device cooling flange.
[from Ref. 49]

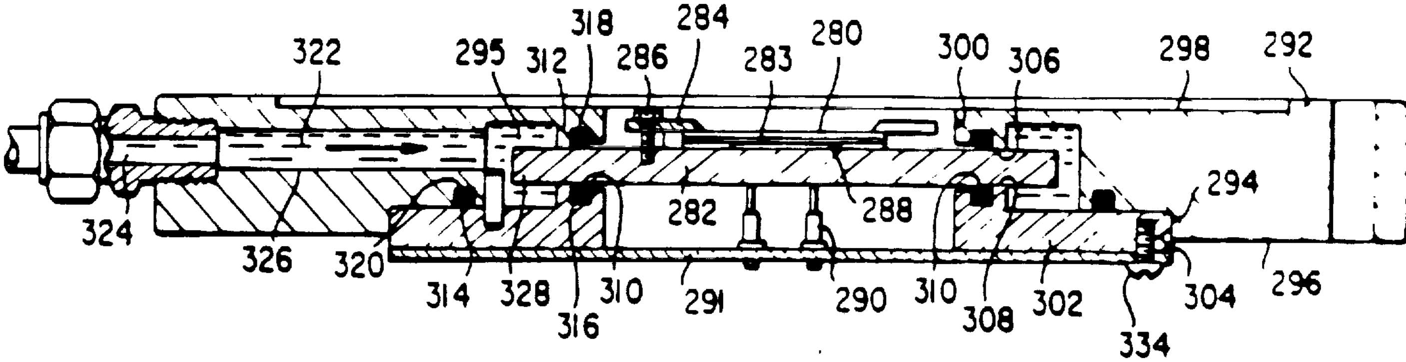

Figure 51. Side view of Phase II device cooling flange.
[from Ref. 49]

lines enter the flange though feedthroughs located at the 11 and 1 o'clock positions. The 2 x 2 anode array (288), to which the MCP is bonded, is integral with the substrate, and is continuous with pinout leads (290) which pass through hermetically sealed via holes. The four channel preamplifier electronics are carried on a circuit card (291) which is in close proximity to the anodes, to eliminate the need for transmission line design (necessary for leads longer than 10-15 cm). Although the rear face of the substrate is covered with a metal foil ground plane to minimize electrical interference and inductance, the circuit card also serves as a ground plane for additional protection.

Cooling of the MCP is accomplished by ethylene glycol flowing through the support flange (292); this fluid envelops the substrate perimeter. The fluid is sealed off using hermetic O-ring seals (310 and 312). The fluid enters into the flange through a radial inlet (324), and is maintained at the specified temperature by the external refrigeration unit, which is connected using flexible tubing. The cooling unit is a Neslab RTE-100 constant temperature bath ($\pm$ 0.1 °C), with a range of -30 to +100 °C.

For vacuum system mounting, the device flange is bolted onto a quick access vacuum door, which allows full access to both the vacuum and air side of the flange. The vacuum system is described in detail in Sect. 2.2.6 below.

2.2.6 COUNT RATE TESTS

EXPERIMENTAL APPARATUS

Vacuum System

Figure 52 shows a top view schematic of the vacuum system used for MCP count rate testing. The chamber tee was pumped using a 50 lpm Balzers turbomolecular pump. The relatively small chamber size, combined with the proximity of a large gate valve opening directly into the turbopump, insured very rapid pumpdown, to ~5 x 10^{-7} torr in 20 minutes. An eight inch rapid-access vacuum door with a Viton O-ring was at one end of the chamber, with the device flange mated to it. To monitor chamber pressure and to obtain mass scans, an Inficon Quadrex 200 RGA unit was used. A Kimball Physics E/IMG-16 electron/ion gun was mounted to the eight inch back flange, with a sophisticated power supply separate from the gun. This hybrid gun delivered a beam of either ions or electrons, at energies as low as 10 eV and as high as 3000 eV. A constant beam current (up to 0.1 μA) and spot size (1-10 mm) could be be maintained, giving a flux density at the MCP input of up to 10^{14} cm^{-2}s^{-1}.

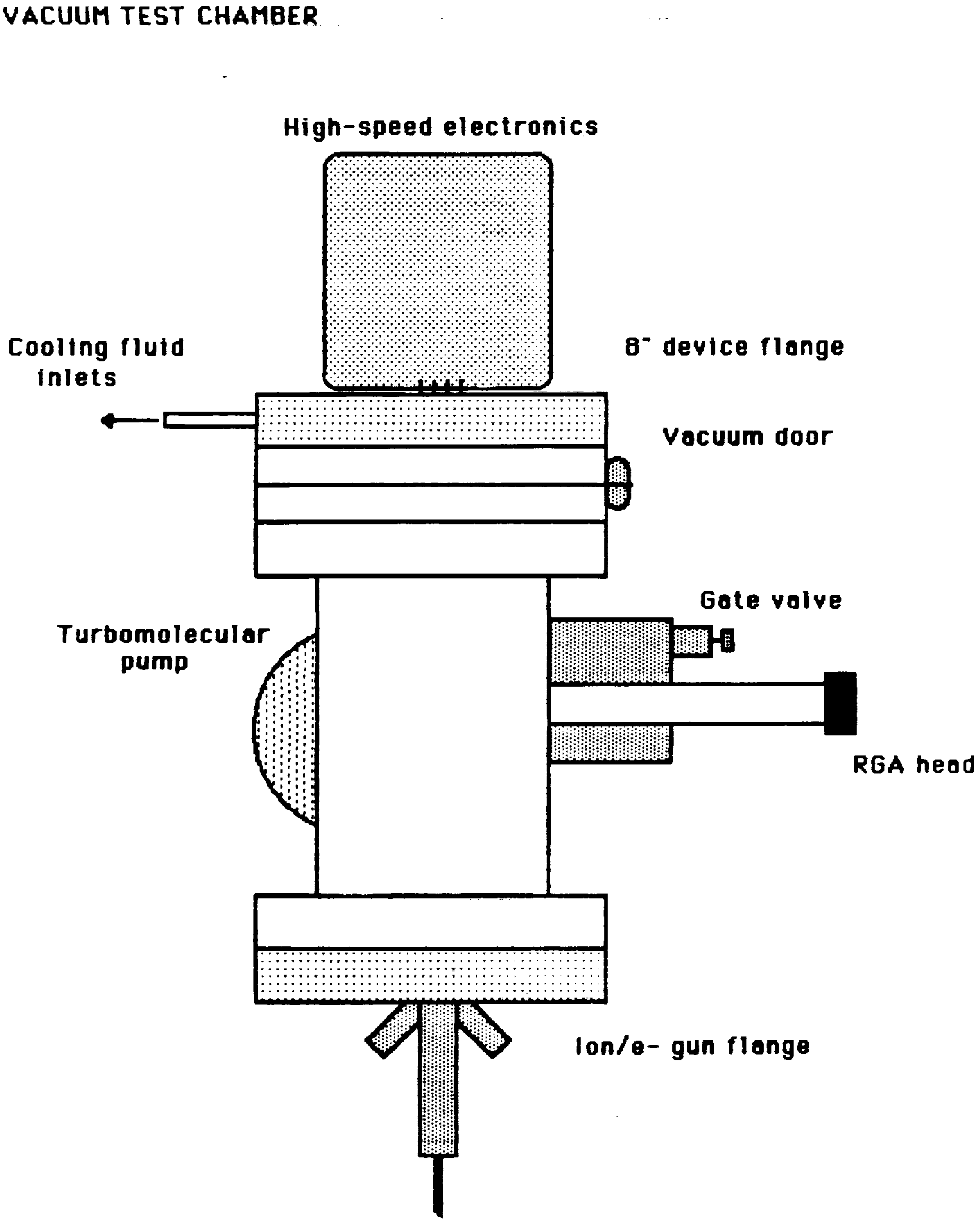

Figure 52. Schematic of Phase II vacuum test chamber.

Software

The control of the high speed electronics described earlier is carried out using an IBM AT-PC computer, with an internal parallel interface board linked to an external digital multiplexer board. The program for recording and processing data was written as a combined BASIC/assembly language routine. The display dialog and numerical data conversion routines were written in BASIC, with the assembly language module controlling the interface.

During recording of count data, the multiplexer transmits the count magnitude to the parallel port of the computer using 24-bit wide BCD words. This relatively large width allows relatively long shutter times. The BCD data are then immediately converted to decimal numbers and displayed on the monitor, and are also stored on disk.

MCP Selection

For a set of geometrically identical MCPs with identical preparation, variations will nevertheless be exhibited in gain, resistance, dark noise, quantum efficiency, and even spatial resolution. In serious scientific work, a selection process is normally used to identify those MCPs best suited to the application. For the 2 x 2 test device, a total of seven curved channel MCPs (80:1 L/D, 12 micron pores) were fabricated and electroded. After an ultrasonic alcohol wash and 105 °C air bake, an in vacuo resistance test was performed on each plate. Only MCPs falling within the 500-800 kilohm resistance range (@ 23 °C, total MCP active area equivalent) were selected, on the basis of the configuration constraints discussed in Sect. 2.2.3. Each plate passing this test was then visually inspected. Unusual markings such as scratches, dimples, and black spots were carefully noted.

The MCP which was finally bonded to the 2 x 2 substrate had an equivalent MCP resistance at 23 °C of 751 kilohms, higher than the 500 kilohm value originally specified (pg. 76). There were several reasons for this. First, it was one of only two plates which had no defects inside the MCP area which would be bonded to the 2 x 2 anode array. Second, the other plate had a room temperature resistance of 503 kilohms. Since time was limited, we chose the more conservative approach and used the higher resistance plate, simply because it would be less likely to suffer thermal failure (in actual operation, the Joule heating of the higher resistance plate would bring its resistance down into the 500-600 kilohm range.)

EXPERIMENTAL RESULTS

MCP Preconditioning

A thorough MCP cleaning and preconditioning process was carried out prior to conducting count rate tests. This is considered essential to obtaining desirable and reproducible operating characteristics. For example, trapped gases can introduce localized high background rates; however, proper cleanup will remove these. If not cleaned up, an unaged C-plate will typically have a very broad PHD (> 100% FWHM), and will have unusually high gain. On the other hand, if MCP channels are excessively dirty, secondary emission can be suppressed, such that the gain will be unusually low.

The MCP fabrication process can result in water adsorption on channel walls, and crystalline deposits can also form. Therefore, an ultrasonic bath in a 50/50 solution of isopropyl and methyl alcohol was carried out for 15 minutes. Following this, an air bake at 105 °C was performed for 30 minutes. Initially it was felt that the MCP should be cleaned once again after bonding to the alumina substrate, in case any debris or small particles lodged in the narrow gap between the unelectroded MCP output face and the substrate. However, the unknown effect of alcohol on the solder alloy, and the danger of temperature excursions in the drying oven above the indium melting point (118 °C) ruled this out. Instead, a careful cleaning with a directed jet of nitrogen together with a fine hair brush was used to remove any debris.

After bonding the MCP to the substrate, the 2 x 2 device was then mounted onto the demountable cooling flange. After attaching the flange to the vacuum system door, the chamber was pumped down using the turbo pump. A vacuum of $< 1 \times 10^{-7}$ torr was reached in less than an hour, indicating that the MCP was relatively clean. The system was held overnight at this pressure. Next, bake-out of the vacuum chamber walls was performed, by wrapping heating collars around the main chamber and heating to 250 °C for 8 hours. During this period the chamber pressure was monitored, together with the RGA mass spectrum. Initially the pressure rose as outgassing of the walls took place, but then fell to a stable level of 6×10^{-8} torr. The indium-bonded MCP was not allowed to heat up much over 100 °C, because of the melting point of the indium alloy. Therefore, the MCP and substrate were actively held at 30 °C by the cooling system while the chamber bake-out was taking place. The MCP resistance was monitored as a further check to insure that MCP heating was not occurring due to radiation from the walls. After the chamber bake-out, the heating collars were removed, and the chamber was allowed to cool slowly to room temperature.

The MCP itself was next heated through the ceramic substrate, by raising the temperature of the cooling/heating fluid to 70 °C. This temperature was maintained for two days to accelerate residual outgassing from the MCP, with the outgassing being monitored using an RGA. When the partial pressure of H_2O fell to a stable plateau of around 5 x 10^{-7} torr, this portion of the preconditioning treatment was terminated.

MCP outgassing

MCP outgassing is usually done to eliminate the short-term gain decay instability attributed to adsorption and desorption of gas molecules loosely bound onto channel walls. To remove this instability, a combination of vacuum bakeout at high temperatures (500 °C) and electron "scrubbing" is normally used. The scrubbing process requires operating the MCP at high gains with a low to moderate input flux for considerable time periods, to remove gas from channel walls through prolonged electron cascade bombardment. In the past, the bake and scrub combination has been found to largely eliminate subsequent outgassing of H_2, H_2O, CO_2, and N_2, to levels low enough to be removed by a getter during the lifetime of sealed intensifier tubes.

The separate effects of bake and scrub treatments on MCP stabilization have only recently been studied in detail [50]. In this study, it was found that during bakeout the outgassing products are primarily H_2, N_2, H_2O, and CO_2. During scrub, the outgassing products are H_2, N_2, and CO_2. It thus appears that bakeout is necessary but insufficient - necessary to remove water, but insufficient to fully desorb the other outgassing products. Electron scrubbing, conversely, is required to fully clean up the H_2, N_2, and CO_2, but by itself cannot fully remove H_2O.

MCP outgasssing can possibly also be accomplished by resistive self-heating of channel walls under high voltages. The extremely thin (2000 Å) semiconducting layer comprising the inner channel wall will undergo localized Joule heating which, given sufficient time due to the considerably lower surface temperatures (< 100 °C), may perform basically the same function as the vacuum bake. The drawback of this approach is that several days are required for outgassing of MCPs of moderate resistance (~30 megohms). Subsequent electron scrubbing will then remove the remaining adsorbed gases, such that the MCP is brought into the plateau region of stable gain, where gain is not artificially enhanced by ion feedback effects.

An experiment was therefore done to see if outgassing from a very low resistance 25 mm MCP (200 kilohms over 4.9 cm^2 @ 23 °C) using resistive self-heating could be monitored. This had never been tried before in standard mounting configurations, since an MCP of this type would quickly overheat and be destroyed. We deliberately chose an MCP having a resistance somewhat lower than what would be used in the 2 x 2 test device, to exaggerate the degree of wall heating. The MCP output face was electroded only within a single square .76 cm^2 area, and then bonded to a single anode. To prevent the indium bonding alloy from melting, we continually checked the operational MCP resistance (by monitoring V_{mcp}/bias current), and compared it with a passive heating/resistance calibration (below).

For standard MCPs, the initial application of bias voltages must proceed slowly since a relatively large load of adsorbed gas is being removed. If careful control is not exercised, intense ion feedback and intermittent catastrophic gas bursts can result. This may quickly lead to premature gain fatigue or severe damage to groups of channels [51]. For very low resistance MCPs, this precaution was felt to be especially important.

The voltage was ramped up from zero volts in 10 volt increments, with an RGA monitoring the mass peaks at each step. If no increase in the partial pressures of H_2, H_2O, N, CO, or O was noted, the voltage was further increased. (It should also be noted that the charge state could not be determined from cracking patterns.) Occasionally, vigorous outgassing could be seen, causing the partial pressure to increase over an order of magnitude. This consisted of H_2, and to a lesser extent, H_2O and OH (Figures 53 and 54). These gas bursts began to occur at about 1100 V, somewhat below the saturation voltage for 80:1 MCPs, yet with a predicted gain of roughly 10^4 [9] - conceivably high enough to dislodge adsorbed gas through electron scrubbing. Thus we could not determine whether resistive heating, electron scrubbing, or some combination of the two was facilitating the gas removal. Whenever a gas burst occurred, the voltage was quickly lowered to its former value to prevent damage to the MCP. If the pressure increase was less than a factor of ten, the higher voltage would be maintained, usually for a minute or two, until the pressure returned to its former level.

Interestingly, the MCP bias current would increase 20-30% simultaneously with the outgassing bursts; it would then return to its equilibrium value as outgassing diminished. This was presumably due to the saturation phenomenon noted in Sect. 1.2.1, where very high output currents, greater than roughly 10% of the bias current, may cause an effective lowering of the channel resistance. The outgassing burst would result in a level of ion feedback sufficient to drive the MCP into hard saturation. A correlation could also be seen between these outgassing events and a dramatic increase in the count rate registered by the electronics. After a minute or so, when the partial pressures returned to their earlier levels, the bias current and the count rate would also diminish. These desorption phenomena observed during preconditioning were very interesting in their own right, and are crucial to understanding the origin of ion feedback in MCPs. Further work is planned in this area, outside the scope of this program.

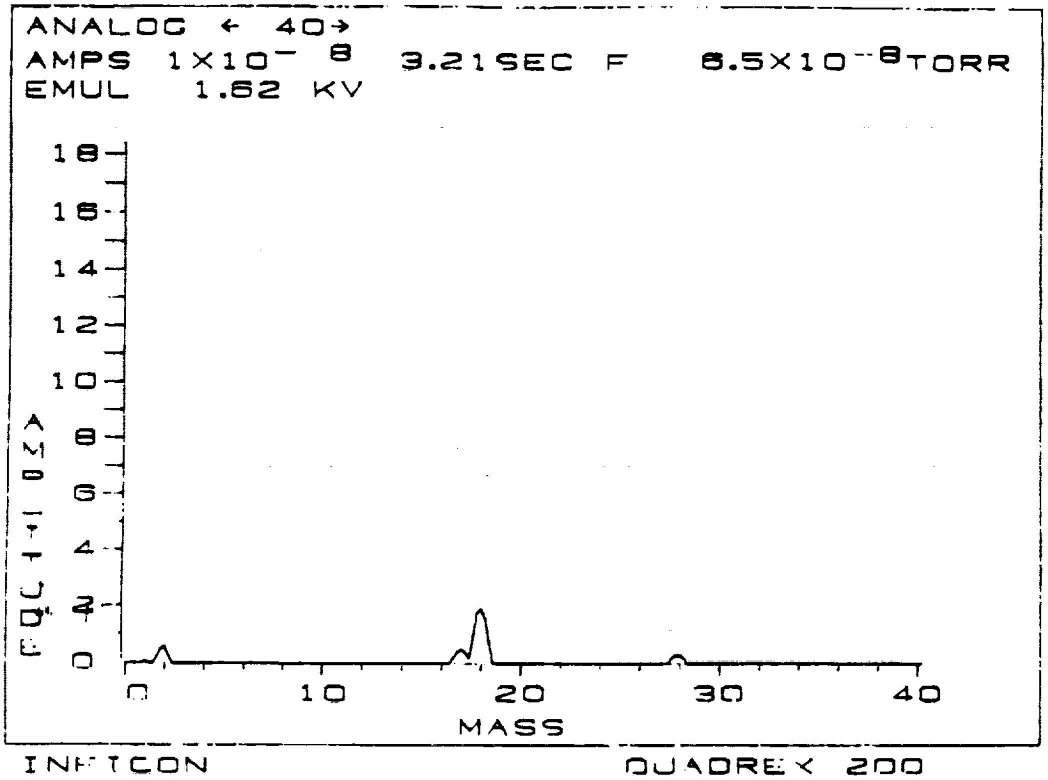

Figure 53. RGA plot of quiescent MCP outgassing condition.

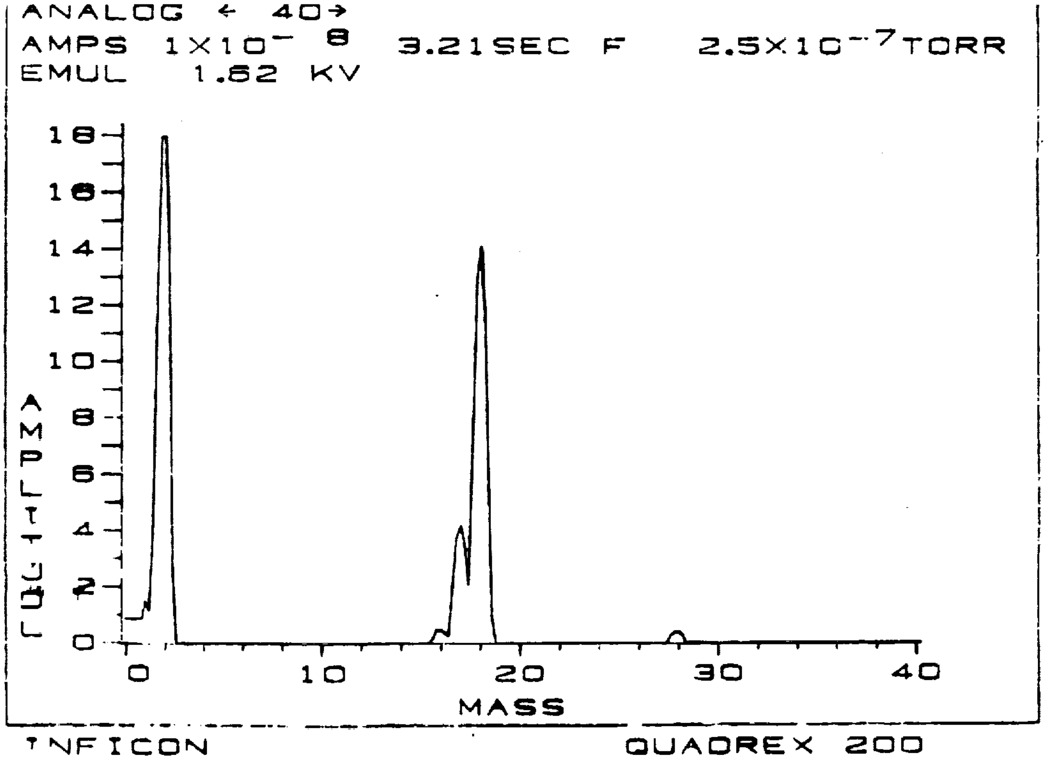

Figure 54. RGA plot of MCP outgassing after 10 V bias increase.

Resistance vs. temperature (2 x 2 device)

Since MCPs have a negative temperature coefficient of resistance, MCP heating due to the flow of bias current can be monitored through the drop in plate resistance. It is useful to know what the MCP operating temperature is, to allow comparison with the predictions of the thermal models discussed in Sect. 2.2.2, to insure that the indium bonding alloy melting point is not being exceeded, and also to see if a substantial lowering of gain might be anticipated (Fig. 33). As shown in Figs. 19-21, a nonuniform temperature profile will result when a very low resistance MCP is operated in thermal contact with a heat sink. The MCP input surface will run tens of degrees warmer than the output surface. Although it is impractical to directly monitor this temperature differential using thermocouples, an average MCP temperature can be determined from the drop in overall plate resistance.

A resistance vs. temperature calibration was done by monitoring the resistance of the 2 x 2 device, by connecting all four anodes in parallel (3.04 cm^2 total anode area). The substrate was heated by gradually increasing the temperature of the fluid bath, and the MCP temperature was assumed to have reached equilibrium with the substrate temperature after one hour. The parallel resistance of the anodes was then measured over the temperature range +20 °C to +70°C. A temperature coefficient α of -.008 was derived using the formula $R(T) = R_0(1+\alpha.dT)$, and the curve was extrapolated to +120 °C, just above the indium melting point, and shown in Fig. 55. (It is interesting to note that this temperature coefficient for very low resistance MCPs is somewhat smaller than the value of -.015 typically reported for standard resistance MCPs [11].)

The average MCP temperature rise was next derived using the resistance-temperature calibration curve. As the MCP voltage was raised, the total bias current through all four anodes was monitored, and the resistance calculated. The resistance-voltage curve is shown in Fig. 56, with the corresponding average MCP temperature shown in Fig. 57. Since the curvature accelerates above 1600 V, a voltage limit of 1750 V was set.

Thermal model experiment

An experiment was conducted to check the analytical thermal models discussed in Sect. 2.2.2. Combining the results for the substrate temperature profile with the MCP web temperature profile, a comparison with experiment was possible. The controllable parameters were the substrate perimeter temperature and the MCP voltage. By clamping the perimeter at a known temperature (the cooling fluid), and by monitoring the bias current while raising the voltage to a level where Joule heating was 10 watts, a direct comparison with the model was possible.

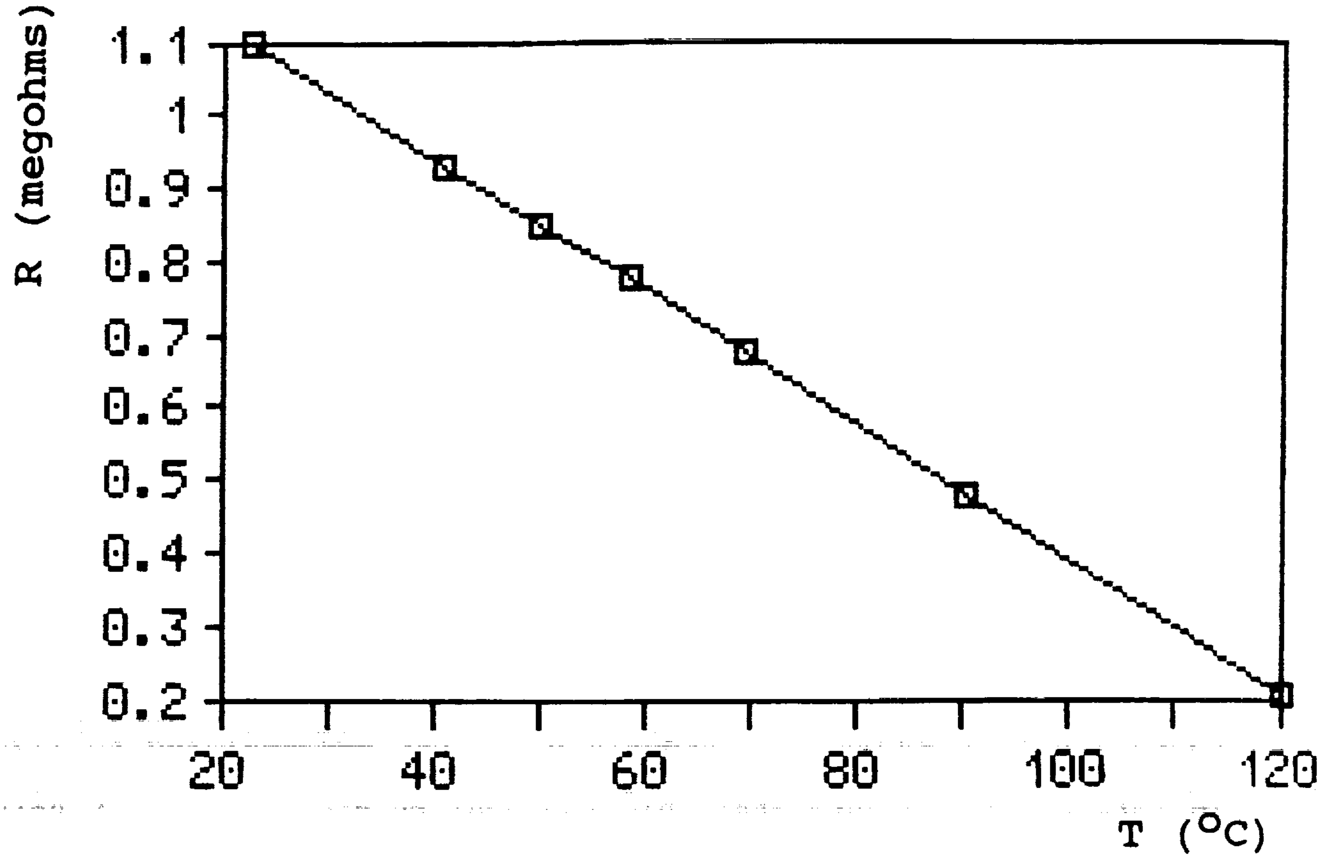

Figure 55. MCP resistance vs. temperature calibration.

Resistance of 3.05 cm^2 bonded active area
(values beyond 70 °C extrapolated)

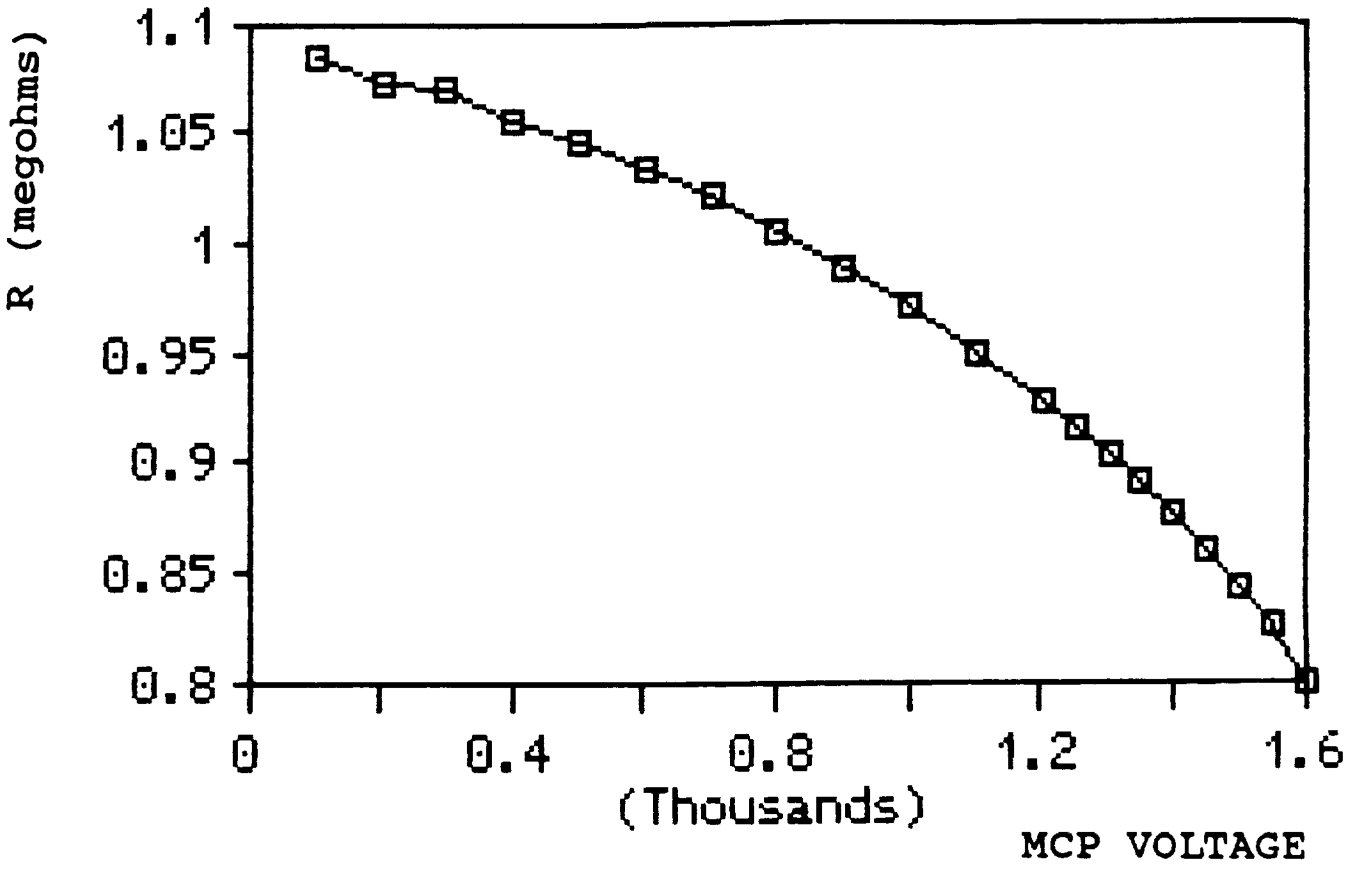

Figure 56. MCP resistance vs. bias voltage calibration. Resistance of 3.05 cm^2 bonded active area

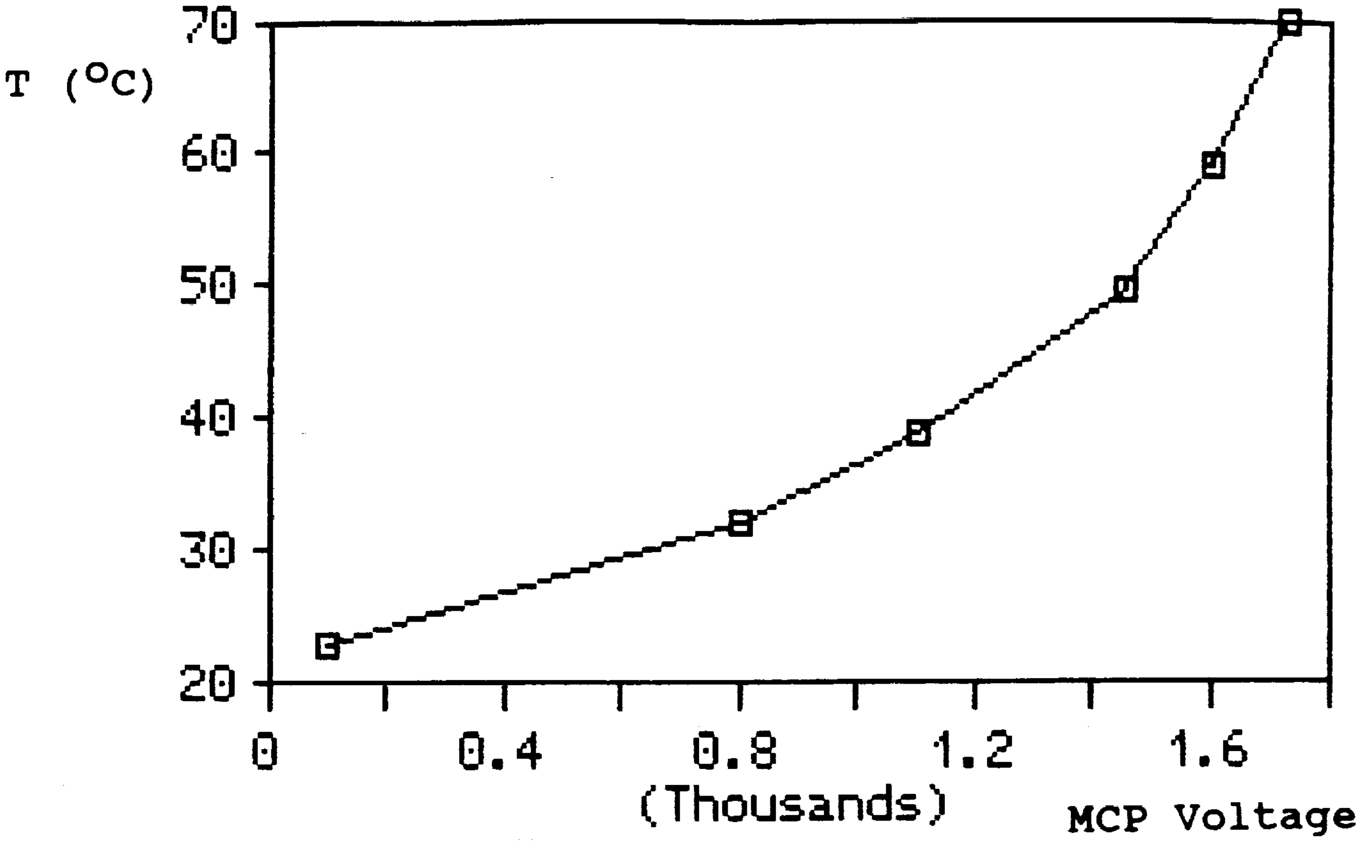

Figure 57. MCP temperature vs. bias voltage

Derived from data shown in Figs. 55 and 56

At 9 watts, for an 80:1, 12 micron MCP the models predicted an effective temperature increase of 27 °C as compared with the top surface of the heat sink. At this power level, the substrate surface would be about 15 °C warmer than the perimeter, so that the effective (average) MCP temperature was predicted to be 42 °C above the cooling fluid temperature.

To do the experiment, the cooling fluid was held at 5 °C, and the MCP voltage was adjusted to give a power dissipation of 10 watts. The drop in MCP resistance corresponded to an effective MCP temperature of 63 ± 2 °C, compared with the predicted value of 47 °C. This was considered in reasonable agreement with the model, considering the assumptions made (zero temperature coefficient of resistance, with no thermal contact resistance at the MCP/substrate interface.)

Positive ion count rate tests

MCP detection efficiency

The MCP detection efficiency for positive ions depends mainly on the ion energy and incident angle. There is also a minor dependence on the ion mass and charge state. For normally directed input particles, the incident angle is simply the MCP channel bias angle (typically 5-11°), which is set to give the maximum detection efficiency. The MCP efficiency for most ions follows a curve that rises from about 30% at 1 keV, with a peak appearing at a few keV of 65-80%, and a falloff beyond 100 keV (Figure 58). Generally, the efficiency for an ion and its neutral particle are about the same. For the same energy, light particles have a somewhat higher QDE than heavier ones. Also, negative ions have a higher QDE than positive ions. For the count rate tests, we used positive ions of He and N.

Count rate test

After the 2 x 2 device preconditioning and resistance calibration was completed, an output count rate test was finally conducted. To prevent the electronics pulse pair resolution from placing a ceiling on the measured count rate, we installed a stainless steel aperture plate with a 0.07 cm^2 circular aperture in proximity with the MCP input face, such that ions would strike well inside one of the four MCP active areas (each of four bonded anodes activates the MCP area to which it is attached). Ions would then either pass through the aperture, striking the MCP input face (Fig. 59), or else would strike the aperture plate, biased 10 V negative with respect to the MCP input (-HV). This slight negative bias helped repel secondary electrons from the interchannel web back into the MCP, preventing them from being lost to the grounded surroundings, which would lower detection efficiency.

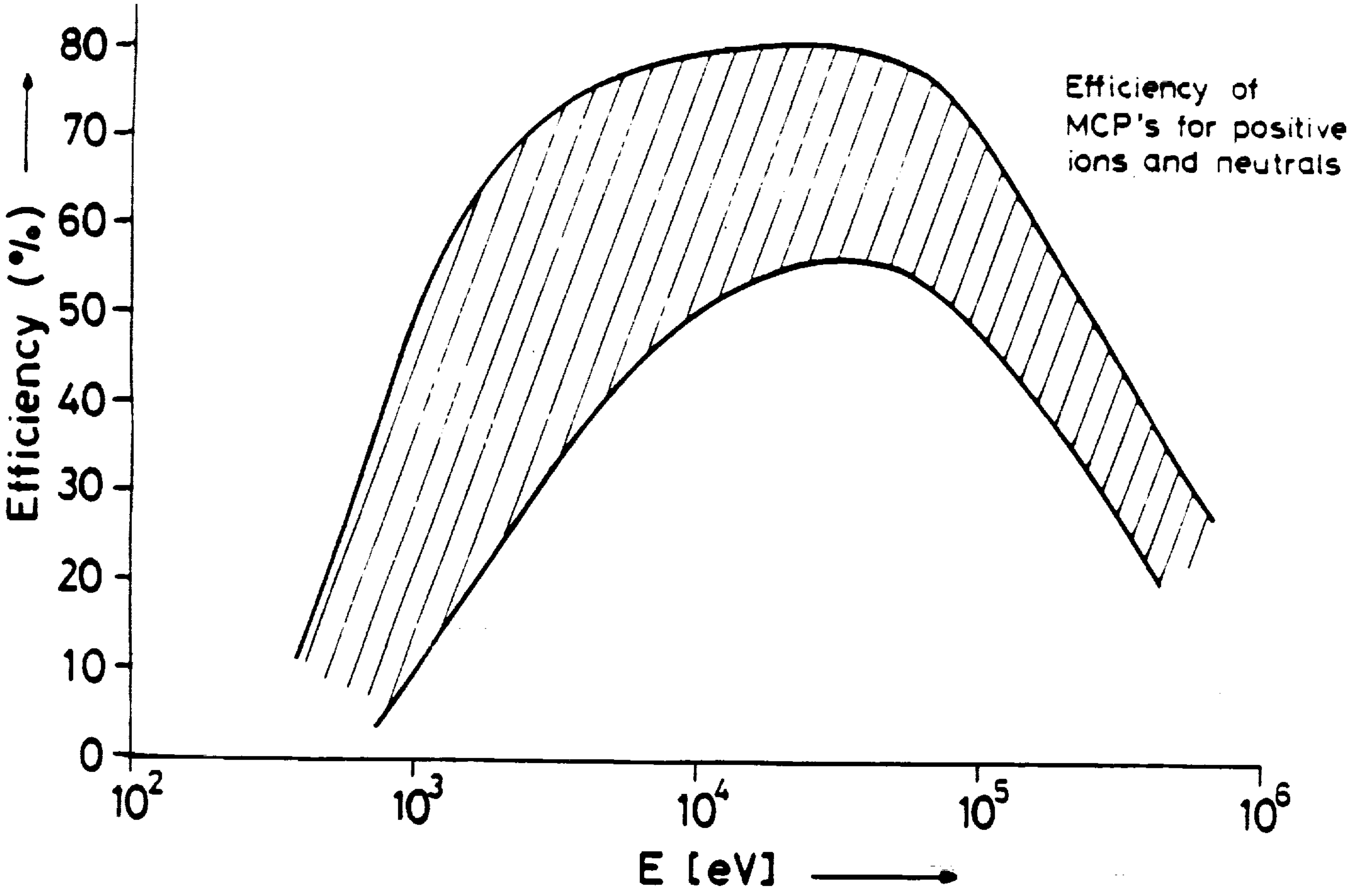

Figure 58. Detection efficiency of MCPs for positive ions. [from "MCP Report" (1982), FOM, Netherlands]

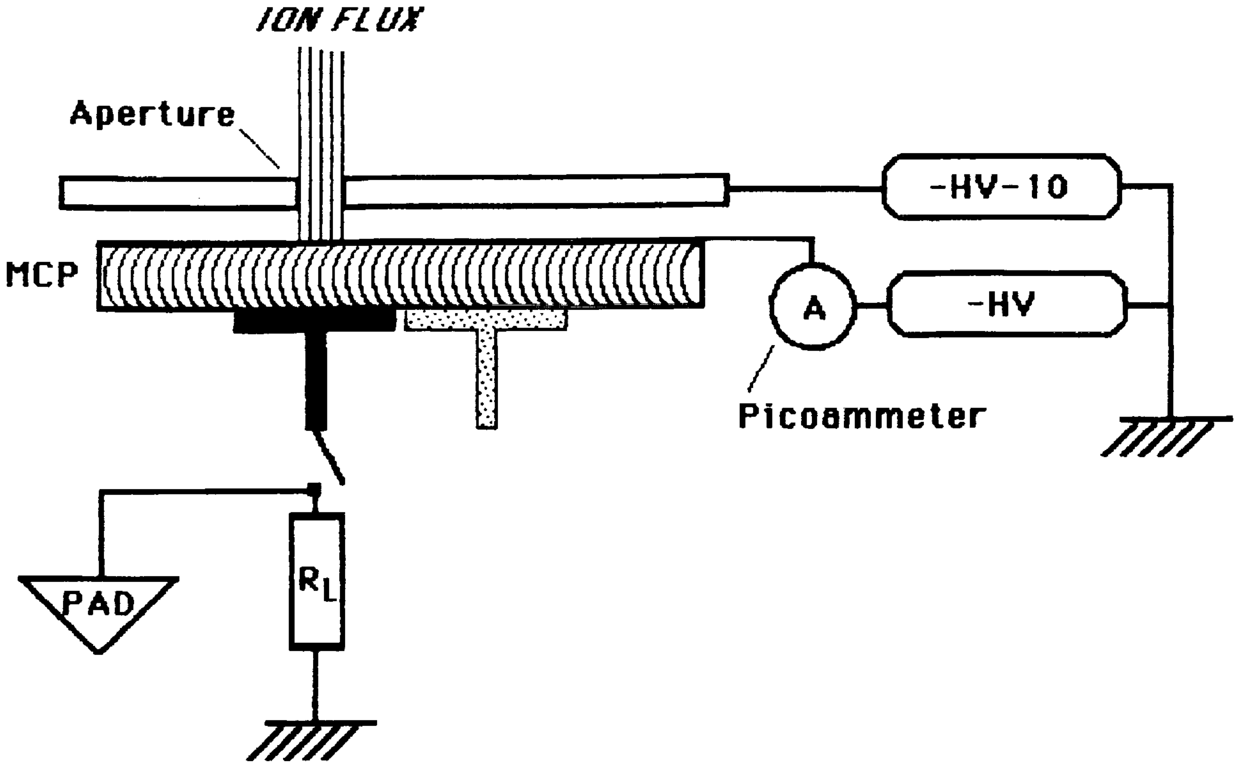

Figure 59. Ion input current calibration.

The ion beam focus was set to give the maximum flux through the aperture for a given filament current. The ion energy was set by maximizing the count rate for a given source current. The optimum ion source bias relative to ground was found to be +1990 V, giving an ion energy at the MCP of 1990+HV eV (adding the negative high voltage at the MCP). A control grid inside the ion gun afforded some control over the ion flux, allowing it to be turned on and off, as well as allowing a degree of modulation.

The ion beam current was measured for given settings of the control grid, by monitoring the current through a picoammeter. Although a Faraday cup may have been more accurate, use of the latter was attempted and was found to introduce undue complications in the test procedure. Precise calibration of the input was not needed for this particular experiment (although it will later be necessary in plots of input vs. output count rate). The main requirement for this experiment was to have an input flux roughly an order of magnitude greater than the expected maximum MCP output count rate (10^9-10^{10} $cm^{-2}s^{-1}$ for a 500-600 kilohm 80:1 MCP). A lower input flux would not drive the MCP to its maximum count rate, while a much higher input might cause the MCP to output simultaneous pulses, giving a proportional output current rather than a proportional output count rate (resulting in a fractional power law dependence [35]).

The ion current through the 0.07 cm^2 aperture was set at 1.2 nA, corresponding to an input flux of roughly 10^{11} $cm^{-2}s^{-1}$, and the discriminator threshold on the PAD (40 dB gain) was set at 75 mV, corresponding to a charge pulse of 1×10^5 e-. The substrate temperature was maintained at 23 °C. As the MCP voltage was raised to 1350 V, no counts above the discriminator level were seen. Beyond this the count rate rapidly increased (this initial rapid increase in count rate characteristically occurs as pulse amplitudes exceed the discriminator level), passing into the MHz cm^{-2} region above 1450 V, into the GHz cm^{-2} region around 1650 V, finally reaching a plateau at around 1700 V (Figure 60), with an output count rate of 6.3×10^9 $cm^{-2}s^{-1}$. The voltage was not raised above 1750, to keep the MCP temperature well below the indium melting point.

An approximate channel recharge time of 127 μs was derived from this measured count rate, given that the channel packing density was 8×10^7 D^{-2} channels cm^{-2}, with D being the channel diameter in microns. From an MCP resistance-temperature curve (Fig. 61), the 25 mm MCP used in this experiment had an equivalent operational resistance across the total 4.9 cm^2 active area of 550-600 kilohms. By comparing this experimental recharge time with Table 6, which gives values for an MCP having roughly this resistance, one can derive a gain in the neighborhood of 5×10^5 at 1700 V - although this is of course no substitute for a direct modal gain measurement from the PHD.

Therefore, a PHD measurement was attempted at 1650 V. Available multichannel analyzers were not fast enough to process the pulse rates our test device delivered, because of pulse pileup at the preamplifier input. An accurate PHD could not be obtained, since superposition of closely spaced pulses would severely distort the recorded amplitude spectrum. Even if a pulse pileup rejector were to be used, quantitative losses would still remain. However, our high-speed electronics were capable of handling the high pulse rates; thus we were able to obtain a (differential) PHD by obtaining the integral PHD (consisting of a histogram of the number of pulses whose amplitude exceeds a given discriminator setting). The discriminator level was initially set at a high value (for example, 400 mV), where the measured count rate was essentially zero. As the discriminator setting was systematically lowered, the count rate increased, and a histogram of counts versus threshold setting was plotted. The differential PHD obtained from this is shown in Fig. 62, displaying a peak at an approximate discriminator setting of 60 mV, corresponding to a modal gain of 1×10^5 (from Table 8, including 40 dB PAD gain), somewhat lower than the value derived above. This measurement was crude at best, since it involved manually adjusting the discriminator and then making a count rate measurement at each data point; the input current was observed to drift somewhat during the measurements, and occasionally had to be corrected. Thus, judging from the gain derived from the channel recharge calculation, and this crude gain measurement, it appears that the modal gain was somewhere in the vicinity of $2\text{-}4 \times 10^5$. Although the PHD had appearance characteristic of a weakly saturated 80:1 curved-channel MCP, further tests are in order before any definitive conclusions can be drawn.

Small apertures

Since high resolution mass spectrometers as well as other imaging spectrographs do not give uniform illumination at the focal plane, the spatially averaged count rate may be orders of magnitude less than the local count rate [28]. Usually, when MCP count rate capabilities are tested and published, it is with diffuse illumination not characteristic of the high level of intraspecular contrast found in spectrometers, and may give inaccurate information on the actual MCP count rate for the strongest spectral lines. Moreover, as discussed earlier (Sect. 1.2.1), capacitive coupling among large active groups of channels may increase the average dead time as compared with activation of only a few channels. It is therefore important to test the count rate capability of small localized areas directly.

We therefore attempted to test the count rate capability across very small areas, using two precision apertures of 10 and 100 microns diameter. These apertures were fabricated from 1 mil thick stainless steel and were attached to somewhat thicker stainless steel backing plates, held at the MCP input potential (-HV). Unfortunately, when the test was carried out, the output count rate was essentially zero even when the input flux was substantially

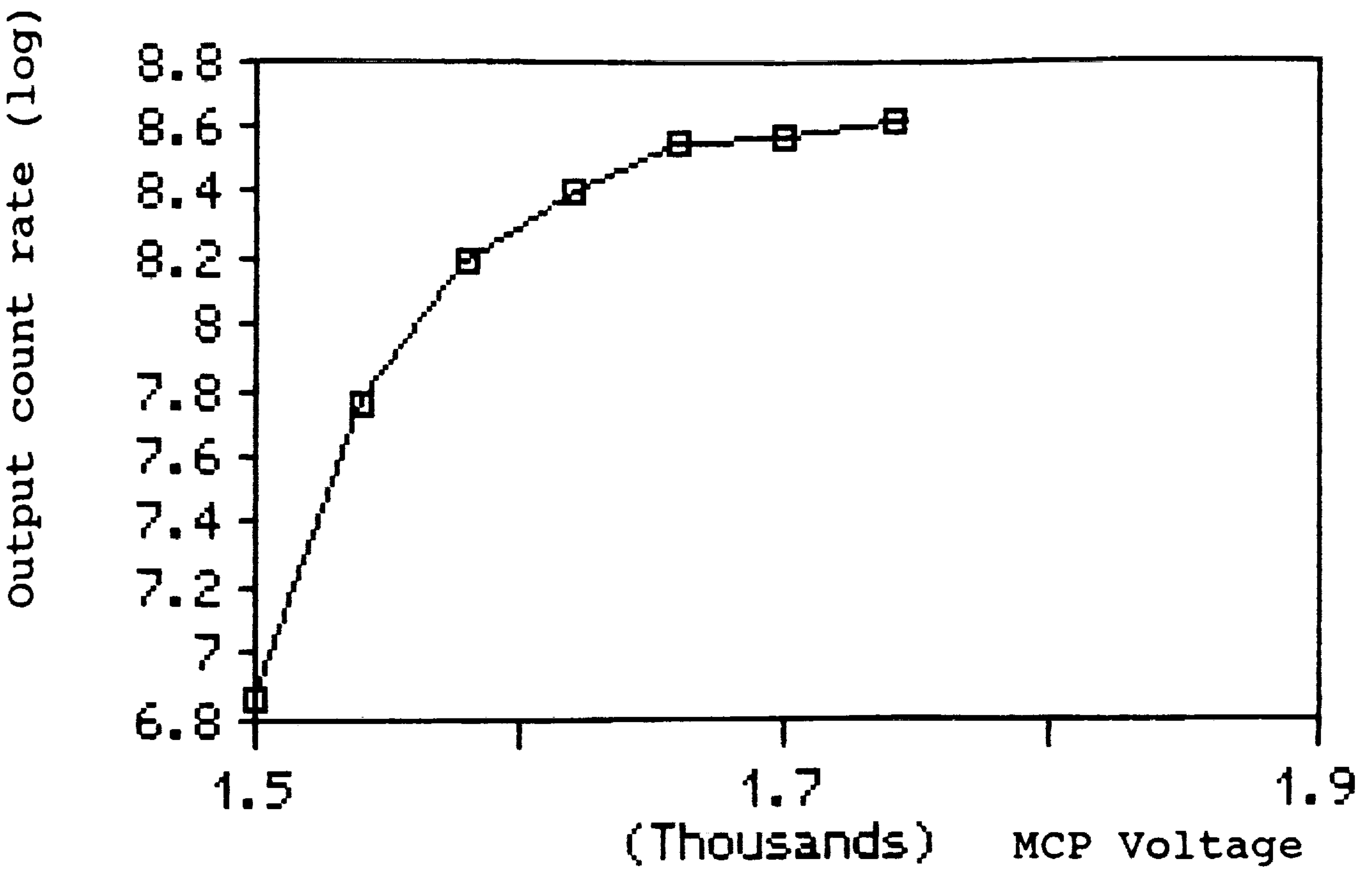

Figure 60. MCP output count rate vs. applied voltage

N_2 ions, 1.2 nA, .070 cm^2 aperture
substrate perimeter temp. = 23 °C

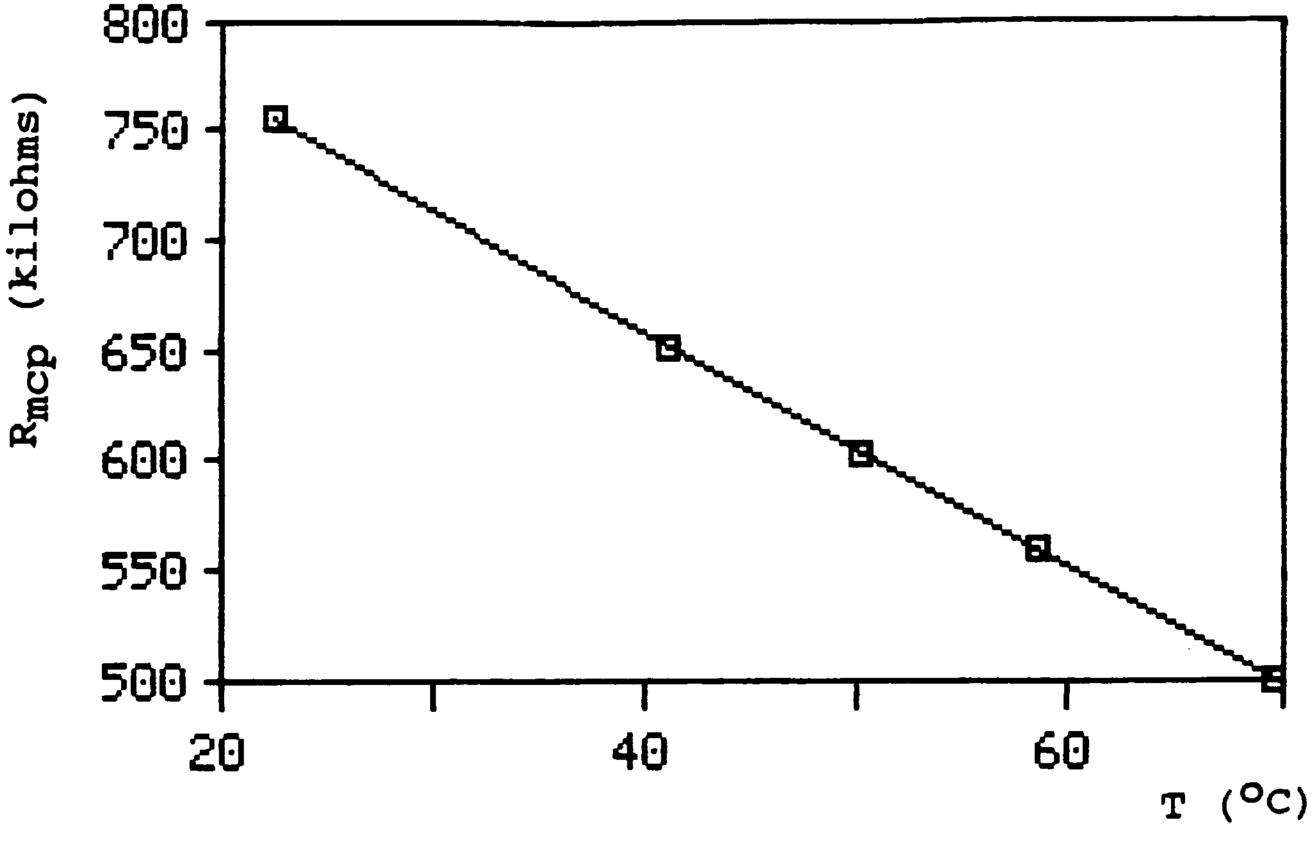

Figure 61. MCP resistance vs. temperature calibration

Equivalent resistance of 25mm MCP (4.9 cm^2)
(external heating)

increased. Electrical isolation of the aperture plate and biasing it 10 V negative with respect to the MCP input (-HV-10) had no effect. Time limitations precluded further work on this problem, although charging phenomena which prevented input ions from reaching the MCP are suspected.

Bias current increase

As a supplementary test to verify saturated MCP operation (with peaked PHDs being the primary test), one can make use of the saturation phenomenon mentioned in the section on outgassing and depicted in Fig.1 - the bias current increase in the saturation regime. Although this increase is usually plotted as a function of increasing input current at a fixed voltage, it can also be plotted with increasing voltage, using fixed input. In either case, the mechanism is presumably the same: the fraction of channel length possessing unity gain (the saturated region) expands up the channel, resulting in a progressively longer parallel resistive path, with an effective lowering in resistance. Using a nulling bridge at the anode we were able to accurately measure a change in bias current of 0.1 μA, as the ion input current of 100 pA cm^{-2} was gated on and off. As shown in Fig. 63, at progressively higher voltages, larger changes in bias current were noted as the input was gated. Each time the voltage was increased, the bias current would again be nulled at zero input, eliminating any chance that the measured increase was merely due to a voltage drop. Although one could argue that such an unorthodox test does not really give any useful information, it did give us increased confidence that the bonded anode MCP was behaving in a more or less predictable way.

ADDITIONAL TESTS

The count rate test described above gives an indication of the count rate capability of very low resistance MCPs. Nevertheless, additional tests should be carried out to fully understand the implications of the conductive cooling approach. Curves of input flux vs. PHD modal gain and FWHM as well as input flux vs. output count rate, covering an input range from 10^4 to 10^{11} $cm^{-2}s^{-1}$, need to be obtained at the optimum MCP operating voltage (where the maximum detection efficiency occurs).

These tests can be conducted in situ at NASA, using either charged particles or UV photons. Since an input range from low to high flux levels (10^4 to 10^{11} $cm^{-2}s^{-1}$)is relatively straightforward to attain with a UV source and neutral density filters, a UV window flange with vac-ion pump appendages is being provided by Galileo to allow stand-alone operation. In the coming months and independently of this contract, test and characterization efforts on high input flux, conductively cooled single anode MCP devices are also planned at Galileo.

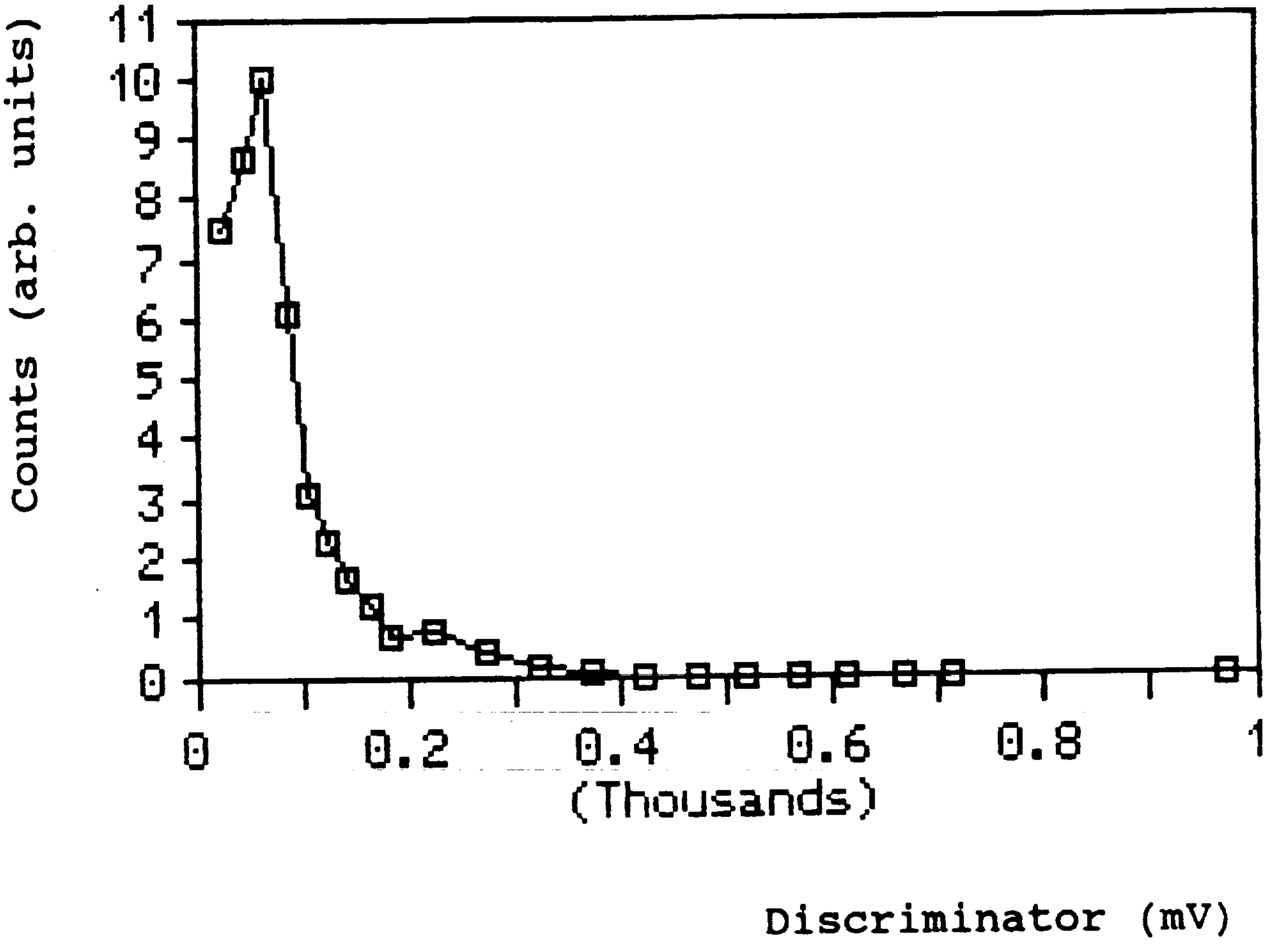

Figure 62. MCP pulse height distribution (PHD) at 1650 V
80:1 curved channel MCP, conductively cooled

The results achieved to date suggest that pulse-counting channel recharge times of 10 μs or less may be feasible with only a minor reduction in MCP thickness. One could conceivably use smaller pore curved-channel MCPs (for example, 6 micron pores, 120:1 L/D [8]), or alternatively smaller aspect ratio plates (for example, 60:1) with 10 or 12 micron pores.

2.2.7 MCP LIFETIME

For the new regime of high output current MCP operation which this program has achieved, greater demands will be placed on MCPs to maintain stable gain over extended time periods. The amplification properties of MCPs have always been observed to progressively degrade with long-term usage, limiting their operational lifetime, and MCP gain degradation has been correlated with total accumulated output charge. Long-term gain decay occurs to such a degree that MCPs can be rendered useless, usually after thousands of hours of continuous operation under low to moderate input currents. Curves depicting this are often cited in the literature, with a representative selection shown in Figure 64. These curves all demonstrate a progressive decrease in gain which inevitably sets in after a period of operation, with the length of time depending on various factors such as vacuum environment, glass composition, as well as glass thermal history; other undefined variables may also play a role. No perfectly flat plateau of gain stability has ever been demonstrated with any known type of channel multiplier device. Clearly, any time-dependent deterioration of the gain properties of radiation detecting devices is undesirable, leading to measurement uncertainty as well as system downtime when devices need to be replaced.

Both short-term and long-term gain instabilities occur, with the former being reversible while the latter is irreversible. Short-term decay is due to adsorption and desorption of loosely bound gas on the channel walls, which can be eliminated during tube processing by a process of either a vacuum bake treatment or an electron scrub. Residual gases in the vacuum system and in the MCP glass itself can be adsorbed onto channel walls, which can then be desorbed by both bake and scrub. When gases are present, the channel gain will increase due to the creation of positive ions, which are accelerated and which initiate secondary electron avalanches upon collision with the channel wall.

Long-term gain decay is different than short-term decay. It usually becomes significant after several thousands of hours of continuous MCP operation (at relatively low input currents). It is irreversible, monotonic, and correlates strongly with accumulated output charge. It has also been found to be independent of output count rate and applied voltage. Chemical and physical changes to the secondary emitting surface at the output end of the channel have been implicated in irreversible gain decay. These changes progressively lower the secondary yield, which in turn reduces multiplier gain. Although various mechanisms have

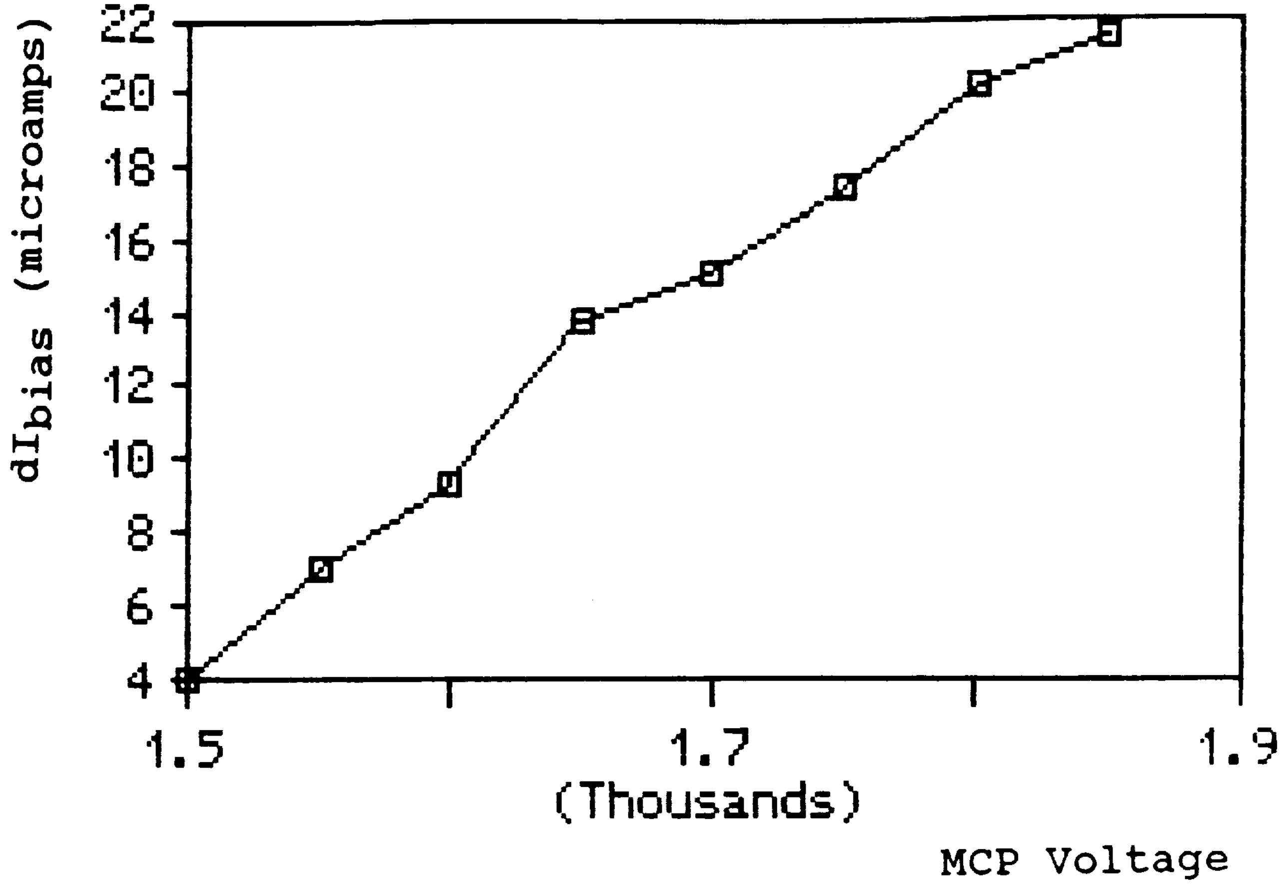

Figure 63. MCP operational bias current increase
80:1 curved channel MCP, 100 pA cm^{-2} input

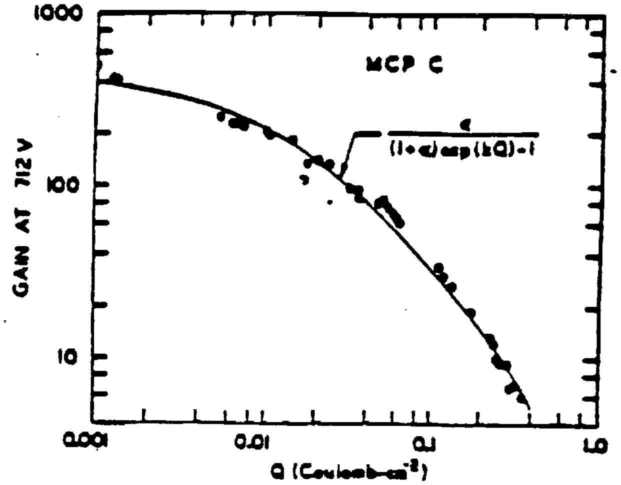

[Sandel et al.,'77]

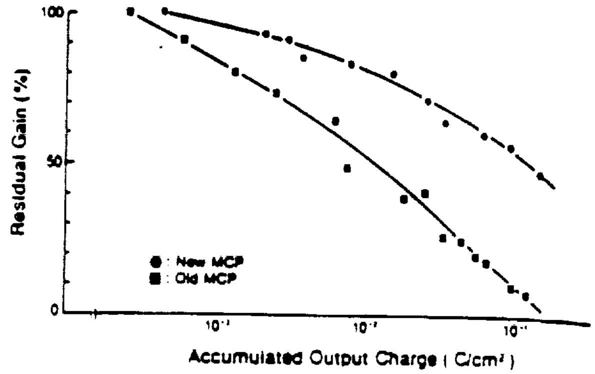

[Oba et al., '85]

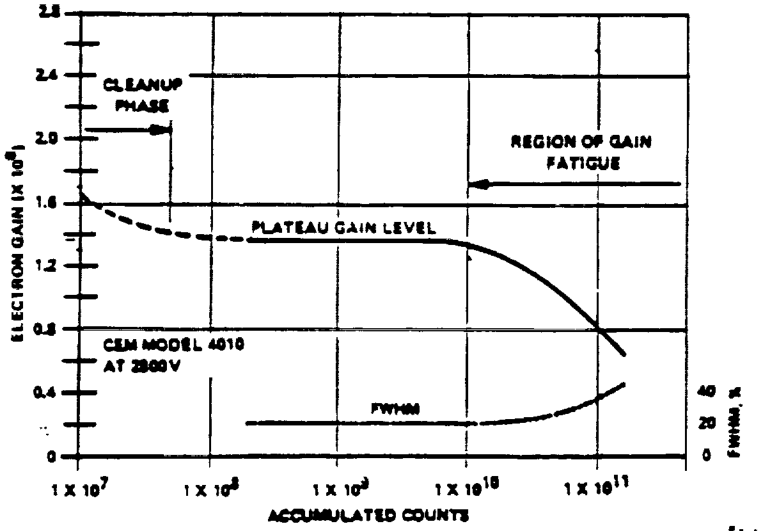

[Klettke et al., '69]

Figure 64. MCP gain degradation as function of total output charge. [from Refs. 65,66,67]

been proposed, there is increasing evidence that one key factor is a decrease in the surface concentration of alkali species (Cs, Rb, or K) from electron irradiation, which raises the surface work function and lowers the secondary yield (cf., A. Then, M.Sc. Thesis, Penn. State Univ., 1990).

For very high current MCPs capable of continuous duty cycle operation, the lifetime issue will become especially important. Consider Table 9 showing the operating time required to reach an accumulated charge of 1 C/cm^2 on the channel wall material near the MCP output.

This level of accumulated charge is often mentioned as an order of magnitude benchmark for surface changes in glass due to electron bombardment [52]. It correlates well with gain reduction in 40:1 unsaturated Long Life™ MCPs, and reasonably well with saturated MCPs having an L/D of 80:1 or greater [18]. Obviously, operation at very high flux rates will accelerate MCP gain degradation (although these high levels may in practice be only intermittent). If high input flux detectors utilizing high bias current MCPs are to be practical, renewed attention may need to be given to further extending MCP lifetime.

Table 9

MCP useful life (hours) vs. input flux density (continuous)

	Input flux density (cm^{-2}s^{-1})		
MCP Gain	10^8	10^9	10^{10}
10^3	3E4 hrs	3E3	300
10^4	3E3	300	30
10^5	300	30	3
10^6	30	3	.3

(based on 50% gain decay at 1 C/cm^2 accumulated output charge, Galileo 40:1 MCP-10 data)

MCP LIFE TEST

An accelerated lifetest was attempted on the bonded single anode MCP device. The input current (N_2 ions) was set at about 500 pA cm^{-2}, corresponding to an input flux of 6 x 10^8 cm^{-2}s^{-1}; the MCP voltage was set at 1650 V, using the PHD data taken earlier and giving an estimated gain of 2-4 x 10^5. After 5 hours into the lifetest, difficulties were encountered in obtaining a PHD with a clearly identifiable peak, preventing us from measuring the drop in modal gain. Presumably, the modal gain had moved below the discriminator threshold at some point in the test. Therefore, no conclusions can yet be drawn regarding the relative pulse-counting gain stability of very low resistance 80:1 MCPs and standard MCPs manufactured from the same glass. (However, the analog 40:1 MCP lifetest discussed on pg. 41 gives a preliminary indication that the very low resistance MCP gain decay behavior may be quite similar.)

The 2 x 2 device was not subjected to a lifetest, since it must have the full MCP gain capability upon delivery at program completion. However, if it is found that the modal gain of the 2 x 2 device has not significantly diminished at the conclusion of tests at NASA, we recommend that a lifetest be attempted at that time. In any case, continuing characterization work on bonded anode, low resistance MCPs at Galileo should provide this information in the reasonably near future.

3. SUMMARY

3.1 PHASE II ACCOMPLISHMENTS

The overall objective of this program was to increase the MCP dynamic range by three to four orders of magnitude. In support of this objective, we have accomplished the following primary goals:

- The MCP background noise has been reduced almost two orders of magnitude, to the cosmic ray limit.

- The MCP input count rate capability has been increased by two orders of magnitude, at temperatures < 70 °C.

In support of these primary goals, we have accomplished the following subsidiary goals:

-A new low noise MCP glass system was developed, patent applied for.

-Complete dark noise testing and documentation of low noise MCPs was carried out.

-A very high bias current MCP was developed. The gain performance, resistance stability, and mechanical stability were demonstrated.

-An unorthodox mounting configuration allowing very high bias current MCP operation was conceived (conductive cooling), patent applied for.

-Detailed thermal models of the interior of an MCP were constructed and tested.

-Bonding of an MCP to a hybrid readout array/heat sink was demonstrated.

-The feasibility of an MCP contact anode/electrode was studied in detail and demonstrated.

-High-speed pulse counting electronics to match the improved MCP performance were designed, fabricated, and tested, for this and for future bonded anode devices.

-A demountable device incorporating a very low resistance curved channel MCP with active cooling and multianodes was successfully constructed. This device is currently undergoing high input flux and other characterization tests.

Unexpected advances were made which were not part of the original proposal such as:

- -Proximity photocathode heating from low resistance MCPs and resultant thermionic noise has been eliminated. For example, conductive cooling of low resistance MCPs (as opposed to radiative cooling) will allow UV or visible photocathodes to be either proximity focused or directly deposited onto the MCP input face, without being heated by the MCP.

- -MCP electronic readout with distortionless imaging in very strong magnetic fields has been made possible. This is due to the removal of the electron cloud drift region, the gap between MCP output and the anode plane. This gap can cause image distortion or displacement as Lorentz forces act on MCP output charge pulses. Recent work has shown that MCPs can be operated in fields as strong as 3 T while maintaining narrow peaked pulse height distributions, if considerably higher bias voltages and defect-free MCPs are used [53].

- -MCP operation at cryogenic temperatures using standard mounting configurations may now be possible. Very low resistance MCPs (at room temperature) will attain standard MCP resistance and bias current levels when cooled to such low temperatures.

3.2 ANTICIPATED BENEFITS

Applications outlined in the Phase II proposal, as well as others requiring very low detector background noise and/or very high MCP frequency response will benefit from the work carried out in this program.

Specifically, the dark noise reduction, which was carried out relatively early in the program, is already being used by researchers to redesign and characterize spaceflight-qualified soft X-ray detectors [54]. These MCPs have had an immediate impact on X-ray astronomy, where very low signal count rates ($<1\ \mathrm{cm^{-2}s^{-1}}$) are often encountered from extremely distant or diffuse objects which may have low surface brightness. A 1989 IR&D-100 Award was presented in recognition of this work.

As the scientific community becomes more aware of ultralow-noise MCPs, their use will become more widespread, especially in the various spectroscopies. For mass spectrometry in general, the low signal levels obtained with very small samples are often masked by detector noise, so that any noise reduction will allow smaller levels of trace isotopes to be detected. One example of this is high sensitivity radioisotope dating using compact accelerator mass spectrometers (AMS) [55]. Using ion conversion methods, these machines are now capable of holding the cyclotron background to levels at or below the detector background.

Another example of a spectroscopy which will benefit is Conversion Electron Mossbauer Spectroscopy (CEMS), where weak conversion electron signals require MCP background to be as low as possible [56]. These examples represent only a few of the conceivable uses of ultralow-noise MCPs in scientific instruments.

The work on the high input flux problem has proved to be complex and challenging, and is now at the advanced proof-of-concept stage. It is anticipated that single anode and linear array multianode detectors (non-imaging) for high frequency application will be designed and built within the next six to twelve months and in service soon thereafter.

A number of scientific applications will benefit, several are of immediate interest to NASA for wind tunnel studies. Improved wind tunnel detectors incorporating higher frequency MCPs will be used for: 1) observation of laser beam interactions, in the measurement of combustion products in high enthalpy wind tunnels; 2) improved time-of-flight measurement of gases in shock waves, allowing monitoring of very high temperatures in hypersonic flow regimes; and 3) improved ion sensing for real-time mass spectrometry of boundary layer gases. Mass Spectroscopy/Time-of-Flight is a candidate for either improved mass resolution or shorter (more compact) flight tubes if a higher frequency detector were available. In other spectroscopies, improvements in accuracy could result from faster detectors, allowing either more counts per sample time, or more samples per unit time. Improved framing rates of high speed sensors could separate closely spaced events or increase the speed at which an event is identified.

Some techniques or disciplines which will benefit from very high frequency MCP-based detectors include plasma diagnostics, surface analysis (spin polarization, SIMS, XPS, ESCA, EELS, LIMS, etc.), solar astronomy, non-destructive evaluation (NDE), as well as photon spectroscopies (UV and visible), pattern recognition, optical computing, and spatial light modulators - in general, any area in which high input flux rates need to be linearly detected.

3.3 FUTURE DIRECTIONS

This work has highlighted several areas of future development. These include imaging readout with heat sinking capability, better sensitivities of high speed pulse counting electronics, and thinner MCPs with uniform and stable pulse counting characteristics.

As regards simultaneous MCP heat sinking and imaging readout, much work needs to be done to achieve a MCP contact anode array with both high resolution imaging capability and heat sinking properties. (Galileo has taken a preliminary step in this direction; cf., NASA Report L-518-17-C, June 1989.) Possibly, some of the work done in recent years in the general area of microelectronic packaging may be relevant. In designing hardware for increasingly fast computers, for example, the thermal control of densely packed IC chips as well as proper conductor topography have been a primary concern of design engineers. For conductively cooled MCPs, the Joule heat removal problem as well as the placement and interconnection of readout circuit conductors will now become key issues. An example can be given from an already mature semiconductor technology, that of multilayer ceramic substrates.

Suppose one has a 1000 x 1000 array of anode pixels (the precise topography is not important here), with individual pixels multiplexed so that relatively few amplifier channels are required for registering and assigning event locations (Figure 65). Multiplexing a million pixels would be difficult at best on a single plane, assuming that large numbers of conductors must be physically isolated from one another. Instead, the multiplexing could be implemented on several different physical levels (substrate layers), with vertical pathways or vias connecting the different layers as is done with VLSI. Multilayer substrates are currently fabricated from thermally conductive materials such as alumina, beryllia, and most recently, aluminum nitride. The heat dissipation ability of these substrates is now over 30 W/cm^2, an order of magnitude greater than required for very low resistance MCPs. Also, non-ceramic materials such as graphite fluoride composites (being developed at NASA Lewis) with thermal conductivities even higher than copper, are currently under development. Consequently, a very low resistance MCP could be mated to a multilayer substrate, which would perform the necessary heat sinking and multiplexing functions.

Also in progress at Galileo are efforts to improve the sensitivity of high speed pulse counting electronics, allowing discriminator levels approaching 10^4 to be set. The lower saturated gain levels attained by thinner MCPs (or smaller pore MCPs) will be able to be electronically registered without substantial signal-to-noise degradation. The combination of thinner saturated MCPs and more sensitive electronics enhances the prospects for even higher frequency response devices, based on higher bias current MCPs.

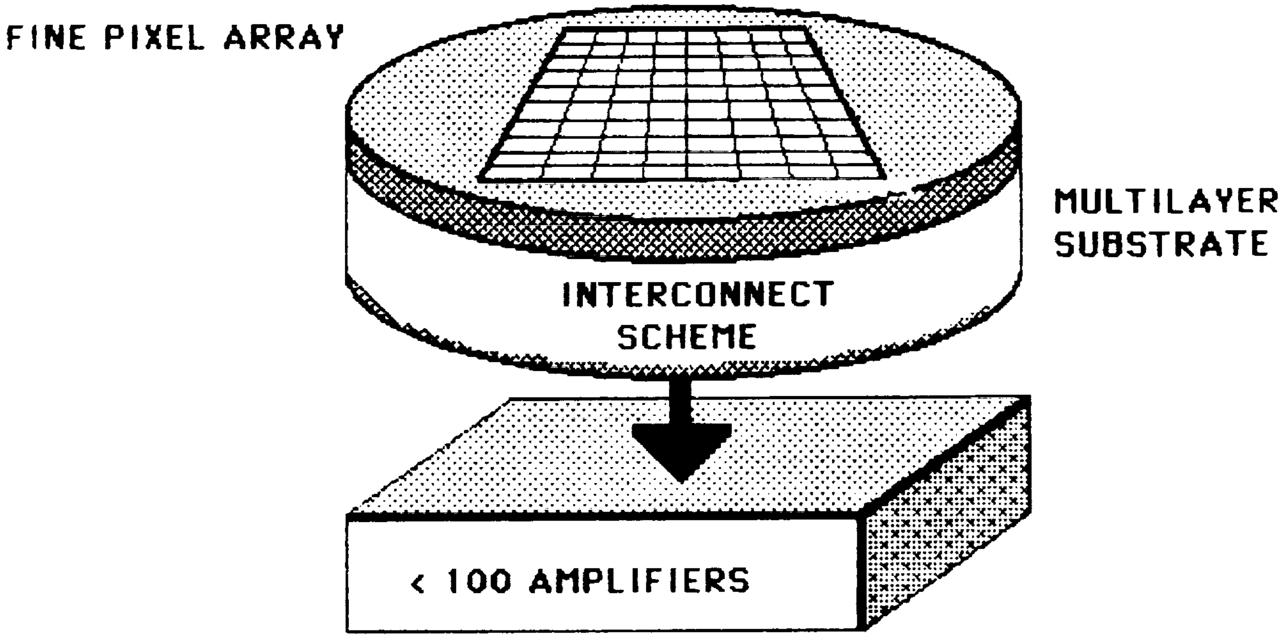

Figure 65 High speed fine pixel array.

The third development area is the fabrication of thinner saturable MCPs. Thinner MCPs reduce the thermal conductive path length from the front surface of the MCP to the heat sink. However this implies smaller L/D ratios, a higher secondary yield or higher field strengths to produce narrow peaked PHDs, and reduced or nonexistent ion feedback. One approach now being studied at Galileo and using proprietary techniques, has produced a 40:1 MCP which will operate in the saturated pulse counting mode. In addition, other internal programs are addressing gain improvement as well as ion feedback reduction.

4. ACKNOWLEDGEMENTS

Those of us who were part of the NASA "Wind Tunnel" Team wish to thank all those who assisted with the technical effort. Specifically, we wish to thank:

-individuals or companies who closely collaborated with Galileo at various points in the program:

Gordon Chu, Danvers, MA
George Fraser, Univ. of Leicester (UK)
Michael Garcia, Harvard Univ. and Smithsonian Astrophysical Observatory
Steve Murray " " " "
Frederick White, Rensselaer Polytechnic Institute
Ceramic-to-Metal Seals, Inc., Melrose, MA

-people at Galileo who contributed their time and effort at various points:

Martin Blum
Patty Carville
Lee Cook
Hector Delgado
Glenn Ellis
Maddie Goodall
John Gray
Jerry Horton
Bruce Laprade
Scott Reinhart
Bill Tasker
Chris Tosswill
Bob White
...as well as many others.

The principal author of the Final Report (B.F.) also wishes to thank Mike Corbett, Don Corey, and Galen Powers for assistance with the manuscript, as well as Carol Borowiec for her usual diligence.

REFERENCES

1. Richter, L. and Ho, W., "Position-sensitive detector performance and relevance to time-resolved electron energy-loss spectroscopy", Rev. Sci. Instr. 57 (1986) 1469.

2. Loty, C., "Saturation effects in channel electron multipliers", Acta Electronica 14-1 (1971) 107.

3. Koshida, N., "Effects of electrode structure on output energy distribution of microchannel plates", Rev. Sci. Instr. 57 (1986) 354.

4. Shyutte, N. et al., "Some operating characteristics of herringbone microchannel amplifiers", Instr. Exp. Tech. 30 (1987) 191.

5. Pearson, J. et al., "Operating characteristics of sandwich microchannel plates", IEEE Trans. Nucl. Sci. NS-35 (1988) 520.

6. Cho, D. and Morris, M., "Local deadtime effects in microchannel plate imaging multipliers", Proc. SPIE 976 (1988).

7. Eberhardt, E., "An operational model for microchannel plate devices", IEEE Trans. Nucl. Sci. NS-28 (1981) 712.

8. Laprade, B. and Reinhart, S., "Recent advances in small pore microchannel plate technology", Proc. SPIE 1072 (1989) 119.

9. Fraser, G. et al., "The gain characteristics of microchannel plates for for X-ray photon counting", IEEE Trans. Nucl. Sci. NS-30 (1983) 455.

10. Soul, P., "Operational properties of channel-plate electron multipliers", Nucl. Instr. Meth. 97 (1971) 555.

11. Pearson, J. et al., "Variation of microchannel plate resistance with temperature and applied voltage", Nucl. Instr. Meth. A258 (1987) 270.

12. Laprade, B., Proc. "The high output technology microchannel plate", SPIE 1072 (1989) 109.

13. Wiza, J., "Microchannel plate detectors", Nucl. Instr. Meth. 162 (1979) 587.

14. Henry, J. et al., "High-resolution imaging X-ray detector for astronomical mesurements", Proc. SPIE 106 (1977) 163.

15. Tosswill, C., "Microchannel plates in low-light level high-speed imaging systems", Proc. SPIE 424 (1983) 125.

16. Siegmund, O. et al., "Investigation of large format microchannel plate Z configurations", IEEE Trans. Nucl. Sci. NS-32 (1985) 443.

17. Van der Ziel, A., Solid State Physical Electronics, Prentice-Hall (1976).

18. Fraser, G. et al., "Evaluation of long-life (L^2) microchannel plates for X-ray photon counting", IEEE Trans. Nucl. Sci. NS-35 (1988) 529.

19. Fraser, G. et al., "Developments in microchannel plate detectors for imaging X-ray astronomy", Proc. SPIE 597 (1985) 343.

20. Fraser, G. et al., "Dark noise in microchannel plate X-ray detectors", Nucl. Instr. Meth. A257 (1987) 447.

21. Siegmund, O. et al., "Background events in microchannel plates", IEEE Trans. Nucl. Sci. NS-35 (1988) 524.

22. Feller, B. et al., "Low noise microchannel plates", Proc. SPIE 1072 (1989) 138.

23. Fraser, G. et al., "Advances in microchannel plate detectors", Proc. SPIE 982 (1988) 98.

24. Petrovskii, G., et al., "Structure and properties of reduced layers on the surface of lead silicate glasses", Fiz. Khim. Stekla 7 (1981) 457.

25. Trap, H., "Electronic conductivity in oxide glasses", Acta Electronica 14 (1971) 41.

26. Blodgett, K. and Green, R., "Electrically conducting glasses", Jour. Amer. Ceram. Soc. 31 (1948) 89.

27. Timothy, J. and Bybee, R., "Preliminary results with microchannel plates employing curved channels to inhibit ion feedback", Rev. Sci. Instr. 48 (1977) 292.

28. Liptak, M. et al., "Microchannel plate electron multiplier for mass spectrometer applications", IEEE Trans. Nucl. Sci. NS-31 (1984) 780.

29. Borom, M., "Electron microprobe study of field-assisted bonding of glasses to metals", Jour. Amer. Ceram. Soc. 56 (1973) 254.

30. Anthony, T., "Anodic bonding of imperfect surfaces", Jour. Appl. Phys. 54 (1983) 2419.

31. Murray, S. et al., "Advanced X-Ray Astrophysics Facility High Resolution Camera", Proc. SPIE 597 (1985) 274.

32. Audier, M. et al., Revue Phys. Appl. 13 (1978) 93.

33. Adams, J. and Manley, B., "The mechanism of channel electron multiplication", IEEE Trans. Nucl. Sci. NS-13 (1966) 88.

34. Gatti, E. et al., "Study of the electric field inside microchannel plate multipliers", IEEE Trans. Nucl. Sci. NS-30 (1983) 461.

35. Nicoli, A., "Dynamic range of microchannel plate photon multipliers", M.Sc. Thesis, MIT (1985).

36. Lampton, M. and Bixler, J., "Counting efficiency of systems having both paralyzable and nonparalyzable elements", Rev. Sci. Instr. 56 (1985) 164.

37. Martin, C. et al., "Wedge and strip anodes for centroid finding position-sensitive photon and particle detectors", Rev. Sci. Instr. 52 (1981) 1067.

38. Timothy, J., "Performance characteristics of multianode microchannel array detectors", Proc. SPIE 501 (1984) 89.

39. Timothy, J., and Bybee, R., "Multianode microchannel array detector for space shuttle imaging applications", Proc. SPIE 265 (1981) 93.

40. Morgan, J., et al., "Centroid position measurements and sub-pixel sensitivity variations with the MAMA detector", Applied Optics 28 (1989) 1178.

41. Timothy, J. and Bybee R., "High resolution pulse-counting array detectors for for imaging and spectroscopy at ultraviolet wavelengths", Proc. SPIE 687 (1986) 109.

42. McClintock, W. et al., "Rocket-borne instrument with a high-resolution MCP detector for planetary UV spectroscopy", Appl. Optics 21 (1982) 3071.

43. Turner, L. et al., "Development and characterization of a charge-coupled device detection system for ion microscopy", Rev. Sci. Instr. 60 (1989) 886.

44. Timothy, J. et al., "Detector arrays for photometric measurements at soft X-ray, ultraviolet and visible wavelengths", Proc. SPIE 183 (1979).

45. Shockley, W., "Currents to conductors induced by a moving point charge", Jour. Appl. Phys. 9 (1938) 1095.

46. Beck, G., "Photodiode and holder with 60 ps response time",

Rev. Sci. Instr. 47 (1976) 849.

47. Armentrout, C., "Large area triple-layer microchannel plate arrays", Rev. Sci. Instr. 56 (1985).

48. Timothy, J., and Bybee, R., "One dimensional photon-counting detector array", Applied Optics 14 (1975) 1632.

49. Feller, B., "Conductively cooled microchannel plates", U.S. Patent Applic. No. 309,195 (1989).

50. Siegmund, O., "Preconditioning of microchannel plate stacks", Proc. SPIE 1072 (1989) 111.

51. Timothy, J., "Curved channel microchannel array plates", Rev. Sci. Instr. 52 (1981) 1131.

52. Pantano, C. and Madey, T., "Electron beam damage in auger electron spectroscopy", Appl. Surf. Sci. 7 (1981) 115.

53. Morezoni, E. et al., "Performance of microchannel plates in high magnetic fields", Nucl. Instr. Meth. A26 (1988) 397

54. Garcia, M. et al., "Low noise microchannel plate detectors for X-ray astronomy", Proc. SPIE 1140 (1989) 101.

55. Friedman, P. et al., "Low background-rate detector for 40-keV ions using a conversion dynode and a microchannel plate electron multiplier to reject low-energy ions, electrons and photons", Rev. Sci. Instr. 59 (1988) 98.

56. Klingelhoefer, G. et al., "Measurement of the detection efficiency of MCPs for 1-15 keV electrons", Nucl. Instr. Meth. A247 (1986) 379.

57. Stearns, D. and Wiedwald, J., "Response of charge-coupled devices to direct electron bombardment", Rev. Sci. Instr. 60 (1989) 1095.

58. Watton, R. et al., "Thermal imaging with a pyroelectric/CCD hybrid array", Proc. SPIE 588 (1986) 52.

59. Milton, A., "Readout mechanisms for infrared focal plane arrays", Proc. SPIE 443 (1984) 112.

60. Fraser, G., "X-ray detectors: A review", Proc. SPIE 1140 (1989) 50.

61. Guest, A., "A computer model of channel multiplier plate performance", Acta Electronica 14 (1971) 79.

62. Matsuura, S. et al., "Current status of the microchannel plate", IEEE Trans. Nucl. Sci. NS-31 (1984) 399.

63. Kurz, E., "Channel electron multipliers", American Laboratory (March 1979).

64. Feller, B. and Cook, L., "Low noise, long lifetime, high gain microchannel plate glass", U.S. Patent Applic. No. 234,325 (1988).

65. Sandel, B. et al., "Statistical performance of the intensified charge-coupled device", Applied Optics 16 (1977) 4135.

66. Oba, K. et al., "Characteristics of the newly developed MCP and its assembly", IEEE Trans. Nucl. Sci. NS-32 (1985) 350.

67. Klettke, B. et al., "Long-term stability characteristics of commonly used channel electron multipliers", 16th Nuclear Science Symposium, IEEE, (Oct., 1969).

National Aeronautics and Space Administration

Report Documentation Page

1. Report No. NASA CR - 181947	2. Government Accession No.	3. Recipient's Catalog No.

4. Title and Subtitle

Development of Microchannel Plates in
Advanced Wind-Tunnel Instrumentation

5. Report Date
February, 1990

6. Performing Organization Code

7. Author(s)

W. Bruce Feller

8. Performing Organization Report No.

10. Work Unit No.
506-43-31-05

9. Performing Organization Name and Address

Galileo Electro-Optics Corp.
P.O. Box 550
Sturbridge, MA 01566

11. Contract or Grant No.
NAS1-18482

13. Type of Report and Period Covered
Contractor Report

12. Sponsoring Agency Name and Address

National Aeronautics and Space Administration
Langley Research Center
Hampton, VA 23665-5225

14. Sponsoring Agency Code

15. Supplementary Notes

Langley Technical Monitor: Dr. Jag Singh
Final Report - SBIR Phase II

16. Abstract

Microchannel plate (MCP) electron multiplier dynamic range has been increased 3 to 4 orders of magnitude at ambient temperatures, through enhanced input count rate capability and reduced background or "dark" noise. The previous upper limit of roughly 10^{7}-10^{8} cm $^{-2}$s^{-1} at ambient has been extended to levels approaching 10^{10} cm^{-2}s^{-1} under continuous d.c. operation. The lower limit, previously set by an irreducible background component (approximately 0.6 cm^{-2}s^{-1}), has been lowered to the cosmic ray limit of .01 cm^{-2}s^{-1}. The high end improvement was achieved by conductively cooling a very low resistance MCP by bonding it to a heat sink, while maintaining pulse-counting operation with multianode readouts. The low-end improvement was achieved by removing all radioisotopes from the MCP matrix glass. The detectors will benefit optical and mass spectrometry, flow visualization, plasma diagnostics, magnetometry, and other high signal flux applications. Very low MCP background noise will benefit X-ray and UV astronomy, medical imaging, trace isotope mass spectrometry, and other applications where the signal flux is often extremely low.

17. Key Words (Suggested by Author(s)) Microchannel plates, detector, dynamic range, dark noise, radiation, high flux	18. Distribution Statement Unclassified - Unlimited Subject Category 35

19. Security Classif. (of this report) Unclassified	20. Security Classif. (of this page) Unclassified	21. No. of pages 150	22. Price

NASA FORM 1626 OCT 86

PRECEDING PAGE BLANK NOT FILMED

BLANK PAGE